PROCESS DEVELOPMENTS
IN
ELECTROCHEMICAL ARC MACHINING

A K De Silva

Ph D

University of Edinburgh

1988

ACKNOWLEDGEMENTS

I wish to express my sincere thanks to Professor J A McGeough for his supervision and constant guidance throughout this project.

Many thanks are due to my colleagues Drs M Barker, A B Khayry, the late Dr I M Crichton, Messers C Spencer and A Wood for their advice in various parts of this project.

The support given by the staff of the Mechanical Engineering Workshop is greatly acknowledged. Special thanks are due to Messers D Anderson and R Gustart for their help in the design and construction of the portable drilling apparatus.

I also wish to thank Mrs I Duncan, Miss M McLeod and Ms D McCluskey for their assistance in typing this thesis.

I wish to thank my husband Alan, for not only proof reading the thesis but also for being a constant source of support and encouragement.

Finally, the financial support given by the South of Scotland Electricity Board is greatly appreciated.

ABSTRACT

Electrochemical arc machining (ECAM) utilises pulsed power across a cathode-tool and an anode-workpiece, separated by a gap filled with electrolyte, in order to achieve both electrochemical dissolution (ECD) and electrodischarge erosion (EDE) of the workpiece. This thesis describes some further developments made in the ECAM process.

The feasibility of using ECAM to drill holes in several alloys of industrial interest, which are difficult to machine by conventional methods, was investigated. The effects of the machining variables on the process parameters were evaluated and the optimum machining conditions established for each of the five materials drilled: chrome steel, cobalt alloy, nickel alloy, titanium and low alloy steel. The surface effects on the alloys drilled by ECAM were analysed by means of optical and scanning electron microscopy and microhardness testing. These revealed that for most of the alloys, the heat induced damage due to EDE phase can be eliminated by the ECD phase, leaving smooth, damage free surfaces. However, the last few millimeters of the hole exhibited EDE induced damage due to lack of electrolyte at the exit, which prevented the ECD action. One exception was titanium, which showed typical EDE damage consistently along the hole. This is because of the oxide film which develops in water based, salt electrolytes, inhibiting the the ECD action.

Occasionally, some localised areas were found to exhibit extensive surface damage in the form of large craters, grain boundary cracking and microcracking. This type of damage was attributed to abnormal discharges. These are the prolonged discharges which occur in the same location causing severe damage to both the workpiece and the tool.

In order to prevent these undesirable abnormal discharges an analysis into the gap phenomena in ECAM was undertaken. The radio frequency emission from the gap was used to differentiate between the normal and the abnormal discharges, since the RF level was found to be considerably higher for normal discharges than for abnormal ones. The monitoring of the RF signal together with the current or voltage can give a clear indication of the gap situation ; whether it is electrochemical action, a normal discharge, an abnormal arc or a short circuit.

A theoretical model has been developed for the RF emission from the gap, assuming the discharge to be a small Hertzian dipole antenna.

Finally, as an industrial application of the ECAM process, a portable ECAM drilling apparatus was designed and built. This can be used successfully to drill holes of high depth/diameter ratio in large steel structures. One specific application for the Electricity Generating Industry is the drilling of holes in boilers to insert thermocouples.

ABBREVIATIONS & SYMBOLS

A	Magnetic vector potential, $Wb\ m^{-1}$
B	Magnetic flux density, $Wb\ m^{-2}$
C	Coulomb
$d\mathbf{l}$	Element of length (vector), m
dV	Element of volume (scalar), m^3
$d\mathbf{S}$	Element of surface (vector), m^2
ε_0	Permittivitiy of free space, $F\ m^{-1}$
E	Electric field intensity, $V\ m^{-1}$
ECAM	Electrochemical arc machining
ECD	Electrochemical dissolution
ECM	Electrochemical Machining
EDE	Electrodischarge erosion
EDM	Electrodischarge machining
emf	electromotive force, V
F	Faraday's Constant, 96500 C
g	Inter-electrode gap length, m
H	magnetic field, Am^{-1}
I	current, A
J	current density, Am^{-2}
k_e	Electrolyte conductivity, $\Omega^{-1}\ m^{-1}$
LMRR	Linear metal removal rate, $mm\ \text{min}^{-1}$
$\dot{m}$	Metal removal rate, $g\ s^{-1}$
μ_0	permeability of free space, $H\ m^{-1}$
N	Atomic weight, $g\ mole^{-1}$

n	Valency
η	Current efficiency
ω	frequency, $rad\ s^{-1}$
ρ	charge density, C m^{-3}
RF	Radio frequency
SMRR	Specific metal removal rate, mm^3 min^{-1}
V	Scalar potential, V

1 : INTRODUCTION

1.1 Nontraditional Machining Processes

The so-called "nontraditional machining processes" are the ones which emerged after World War II in response to the changing machining requirements made by industry. Electrochemical machining (ECM) and electrodischarge machining (EDM) are two such processes which were developed primarily to :

a) machine hard, tough materials which are difficult to machine by conventional methods.

b) produce intricate and complex geometries to close dimensional tolerances which are beyond the capabilities of the traditional processes.

Both ECM and EDM, although different in their metal removal mechanisms, are widely used in similar applications such as die sinking and fine hole drilling, especially in the aerospace industry.

1.1.1 Electrochemical Machining

Although the application of electrolytic dissolution as a metal removal tool is relatively new, the basic principles are not. During the period 1818-1827, Michael Faraday(**1**) showed that when two electrodes were immersed in an electrolyte with a potential difference applied across them, the cathode would deposit metal on to it and the anode would dissolve into the solution. The rate of metal dissolution/deposition is a function of the electrochemical equivalent of the material and the current passed.

In the electrochemical machining process, the anodic workpiece and the cathodic tool is connected to a low voltage DC supply. The inter-electrode gap is flushed

with an electrolyte, which, as well as being the essential medium for the electrolytic process, carries the by-products away from the machining gap. In order to maintain the gap at equilibrium, one of the electrodes is fed towards the other at a speed determined by the metal removal rate.

The typical reaction at the cathode is the the evolution of hydrogen gas . At the anode, the anode metal dissolves, atom by atom, into the electrolyte solution releasing electrons. The theoretical rate of metal removal is given by Faraday's Laws of Electrolysis. The actual rate at which metal is removed depends upon the current density and this, in turn, depends not only upon the conductance of the electrolyte and the voltage applied across the electrodes but also upon the shape of the electrodes and their distance apart. Typical current densities are in the range 150 - 200 A mm^{-2} and the gap sizes vary from 0.025 -0.750 mm (**2**).

Modern developments in ECM machines such as adaptive control systems and silicon controlled rectifier power sources enable ECM to be used in a wide variety of industrial applications. It is mostly used to machine very hard metal that would be less economical to work in other ways. Die sinking, fine and multiple hole drilling, trepanning, deburring and grinding are some of the many applications of ECM (**3**).

The major advantages of the process are the absence of tool wear as well as any thermal load on the workpiece. Furthermore, the surface finish can be smooth and free from residual stresses. However, there are disadvantages such as the poor dimensional accuracy and the inability to produce sharp contours.

1.1.2 Electrodischarge Machining

The work done in the early 1940's by two separate groups of people with different objectives led to the development of the EDM process. The studies

done by B.R. and N.I. Lazerenko (**4**) into the erosion of electrical contacts led to the development of the basic method for shaping metals in 1943. They developed the R-C generator for EDM. At about same time, the investigations by another group of people (H.L. Stork, H.V. Harding and J. Beam) into removing broken taps and drills from hydraulic valve bodies, made them develop an electrical circuit that produced a spark after the electrode had made physical contact with the workpiece (**5**).

The EDM process is effectively a thermal one, which removes metal by the erosive effects of discharges. The tool and the workpiece (which can be of either polarity) is connected to a pulsed DC supply and the inter-electrode gap is flushed with a dielectric. The voltage across the gap is high enough to cause the dielectric to breakdown resulting in electric discharges. These discharges occur randomly over the machining area and the high temperatures of the discharges cause tiny craters to be removed from both electrodes by melting and evaporation. Erosion of the electrodes is asymmetric. By choosing appropriate tool material and controlling the discharge, varying its duration, intensity and polarity, a significant asymmetry can be obtained : for instance, 99.5% of erosion of the workpiece to 0.5% erosion of the tool (**6**). The metal removal rate is determined by the frequency of the discharges and the energy available to them, which is proportional to the product of the current and the pulse duration. Although the higher energy discharges yield faster machining rates, they also increase the surface roughness and the overcut, due to the larger crater sizes produced.

EDM machining has evolved to be an accurate machining process due to the advances made in transistorised power supplies, adaptive control systems, electrode materials and dielectric fluids. The orbiting technique and computer control has further enhanced its capabilities in many modern machining applications

(7,8). Latest developments include computer aided process planning packages for EDM (9). Nevertheless, the principal disadvantage of EDM still remains, that it is rather a slow process.

1.2 Electrochemical Arc Machining (ECAM)

Although ECM and EDM differ in their principles of metal removal, the many similarities in their machine configuration (tool and workpiece separated by a small gap containing a liquid medium) has led to the development of combined processes. Electrochemical arc machining (ECAM) is such a process which combines features of ECM and EDM, by having a cathodic tool and an anodic workpiece, which are separated by a gap filled with electrolyte, and pulsed DC power applied between them. This leads to discharges in electrolytes, thus achieving both electrochemical dissolution and electrodischarge erosion of the workpiece. One of the major advantages of ECAM, over ECM or EDM, is that the combined metal removal mechanisms in ECAM, yield a much higher machining rate (**10**).

Furthermore, in EDM, discharge energies are limited to avoid poor surface finish. In ECAM however, much higher energy discharges can be used because the craters produced by the erosive nature of discharges are smoothed out by the electrolytic dissolution process. In order to distinguish the high energy ECAM discharges from the EDM ones, they are referred to as "arcs", hence the name Electrochemical arc machining. It is obvious therefore, that the metal removal rate of ECAM is much higher than EDM because the combination of high energy discharges and the electrolytic dissolution, remove a far greater amount of material from the workpiece.

The rate of metal removal is also higher than ECM. This is because that in ECM the generation of hydrogen gas at the cathode causes a choking effect, which

prevents the electrochemical dissolution action (**11**). Furthermore, the anodic films produced under some conditions are also responsible for the reduction in metal removal. In ECAM, the gas bubbles have the opposite effect, that of increasing the metal removal. This is due to the fact that discharges in ECAM occur through these gas bubbles, therefore, instead of having a blocking effect on the metal removal, they actually enhance it by facilitating the discharge erosion action. Moreover, the discharges help to breakdown the anodic films, which also contribute to the increase in metal removal.

In ECM, sparking between the electrodes is a major problem. Obviously, this problem is nonexistent in ECAM. Furthermore, the ECAM machining gap is larger than the EDM one. Thus the clearance of debris from the gap is much easier in ECAM than in EDM.

1.3 Review of Literature

Despite the many potential advantages a process combining features of EDM and ECM has to offer, very few published papers can be found on the subject.

The early work on the combined electrochemical - electrodischarge processes used separate ECM and EDM flow systems and power sources. Inoe and Shibuya (**12**) have investigated such a machine which performed the roughing operation, firstly by ECM to get the faster machining rate, then by EDM to obtain the dimensional accuracy and finally, finishing by ECM. Another form of the combined process was the electrochemical discharge grinding process developed by Inoe et al (**13**). This used a graphite wheel electrode and a pulsed power supply giving electric discharges which broke down the passivation layer thus assisting the electrochemical grinding process. Later progress of this process has led to the development of a triplex combined process : electro-chemical-discharge

mechanical grinding, as reported by Kubota (**14**). Kimoto (**15**), investigated EDM in very dilute electrolytes and found that it increased the erosion rate and decreased the wear ratio.

All the processes above are biased towards either EDM or ECM and therefore do not contribute much to the understanding of a truly combined process. Dimensional electrochemical machining, reported by Lazarenko (**16**) and also by Glaskov (**17**) can be regarded as a truly combined process. They have reported the occurrence of a significant discharge phase in electrochemical machining. Kubota (**18**) has developed a combined process called Electrochemical discharge machining (ECDM) for sinking holes. From his several publications on ECDM (**18,19,20**) a significant amount of insight into the workings of a combined process is gained. Zaytev and Polyanin (**21**) have also developed a spark- electrochemical machine for piercing small holes, which utilises an EDM type power supply. Saushkin et al (**22**) have investigated a combined electrochemical- electroerosion process (named EECP) for machining elongated surfaces. They recorded that when large areas (18.5 cm^2) were present only electrochemical machining occurred in certain zones, while in the other areas combination of discharge erosion and anodic dissolution occurred. The areas where electric discharges occurred were the downstream regions where the strongest concentration of gas bubbles were present.

The literature on the ECAM process includes some fundamental aspects of the mechanisms involved and the feasibility studies of its various applications. Crichton et al (**23**) have carried out a comparative analysis of the metal removal mechanisms an the applications of ECM, EDM and the combined process ECAM. The fundamental study of single discharges in electrolytes by Crichton (**24**) has given some insight into the process, although conditions are much more compli-

cated in full scale ECAM.

Satisfactory results have been obtained by Drake (**25**) and also Khayry (**26**) into hole drilling by ECAM. The ECAM drilling differed from the previously recorded ECDM hole sinking by Kubota, because it employed vibration of one of the electrodes. This gave it an added controlling dimension. El Hofy (**27**) has investigated the feasibility of wire cutting by ECAM. Munro (**28**) applied the ECAM process to remove irregularities from machined components. All the above feasibility studies have given valuable knowledge about the ECAM process. However, much more research is still required before ECAM can be established as a machining process in the same level of EDM and ECM.

The success of EDM and ECM has been based mainly on the ability to control the process effectively. EDM and ECM both employ sophisticated "in-process" evaluation systems in order to achieve process optimisation. Since the metal removal mechanisms of both processes are well understood, and the gap situation is correlated to either the machining current or the voltage, the usual feedback signals are easily derived from the time averaged current or voltage. The problem of stationary arcs in EDM has been overcome by monitoring various other signals such as the radio frequency emission from the gap. A survey of various control techniques in EDM is given in Snoey (**29**).

The complex nature of ECAM requires further analysis of the gap situation in order to employ some form of feedback control. The analysis of the ECAM gap may be done by monitoring signals such as current, voltage and the radio frequency emission.

1.4 Objectives of the thesis

The purpose of the present thesis is to investigate the ECAM process further in order to gain more insight into the underlying mechanisms of the process and also to help its establishment as an industrially viable machining technique. Specifically, the study has the following objectives:

1. Investigate the electrochemical arc drilling of different alloys which are difficult to machine by conventional methods.
2. Study the surface effects on the alloys produced as a result of ECAM drilling.
3. Analyse the gap phenomena which occur in ECAM, with the practical monitoring of the gap using the radio frequency emission signal.
4. Develop a theoretical model for the discharges using the RF emission.
5. Design and develop a portable electrochemical arc drilling machine as an industrial application of the process.

1.5 Thesis Organisation

Chapter 2: An experimental investigation into the electrochemical arc drilling of five different alloys of industrial interest is presented. The analysis shows how the machining variables such as gap voltage, vibration amplitude and phase angle influence the metal removal mechanisms of electrochemical dissolution and electrodischarge erosion. The correlations between the process parameters (metal removal rate, tool wear, overcut) and the machining variables are established together with optimum machining conditions which yield the best hole for each material.

Chapter 3: The surface effects produced by ECAM drilling on the alloys are examined in this chapter. The investigation is based on optical and scanning electron microscope examinations and microhardness testing. The results presented show how the electrodischarge erosion and electrochemical dissolution actions have affected the drilled surface and the sub-surface layers of the materials.

Chapter 4: An analysis of the gap phenomena in ECAM is presented in this chapter. The mechanism for the electric discharge occurrence in electrolytes is explained. The ECAM discharge types are classified into "normal" and "abnormal" discharges or arcs and comparison is made with the EDM discharges. The abnormal arcs are undesirable as they tend to occur in one location causing damage to workpiece and tool. In order to differentiate between the normal and abnormal discharges, radio frequency emission from the gap is monitored. The RF waveforms together with the current or voltage waveforms are presented for square pulsed power experiments. From these waveforms, the different gap phenomena can be identified.

Chapter 5: A mathematical model relating the charge behaviour within, and radio frequency emission from, the gap is developed for ECAM discharges. Assuming the discharges to be small radiating dipoles, the electromagnetic radiation from the discharges are calculated and compared with the measured values.

Chapter 6: An industrial application of the ECAM process is considered in Chapter 6. The design and development of a portable ECAM device for in-situ hole drilling of large steel structures is described. One

possible use of it is to drill holes to insert thermocouples in large steam boilers in the electricity generating industry.

Chapter 7: This chapter gives the conclusions with recommendations for further developments.

The published material on the surface effects on alloys drilled by ECAM is given in the Appendix.

2 : ELECTROCHEMICAL ARC DRILLING OF ALLOYS

2.1 Introduction

Electrochemical arc machining is particularly useful in applications for which conventional methods are not suitable. For instance, when tough, hard, heat and corrosion resistant materials are encountered and also when holes of large depth to diameter ratios (20:1 or more) are needed.

Previous research by Drake (**25**) and Khayry (**26**) into ECAM has proved that it can be used successfully to drill holes at rates much faster than the comparable processes of ECM and EDM. They have done extensive experimental work in electrochemical arc drilling of mild steel material, relating the process parameters with the machining variables. Although metal removal of ECAM is independent of the mechanical properties of the workpiece material, the composition and the material properties such as the thermal conductivity can affect the process parameters. Therefore, further experimental study is necessary to establish the relationships between the machining variables (feed rate, gap voltage, amplitude and phase of vibration, electrolyte pressure) and the process parameters (linear metal removal rate, specific metal removal rate, relative tool wear, overcut and taper) for other different metals and alloys.

This chapter is concerned with an experimental investigation into the feasibility of producing fast and accurate holes in five different alloys by ECAM. All the alloys are of potential industrial interest, four of which are widely used in the aerospace industry, and the fifth in the electricity generating industry. The alloys investigated are low carbon chrome steel, cobalt alloy steel, nickel alloy, titanium and low alloy steel.

2.2 ECAM Drilling

In the course of ECAM, electrochemical dissolution (ECD) and electrodischarge erosion (EDE) can occur simultaneously in different regions of the gap, or in succession in the same area. In ECAM drilling, the inter-electrode machining gap can be divided into two main zones: the frontal gap and the side gap (Figure 2.1). In the frontal gap the main contribution to material removal comes from the EDE action, whereas, in the side gap it is predominantly ECD which removes metal. In the intermediate region where the two zones overlap, both ECD and EDE are possible. The front gap tends to favour discharges because the rapid advancement of the tool towards the workpiece keeps the gap relatively small. Furthermore, the accumulation of machining by-products such as gas bubbles and metal particles encourage electric discharges.

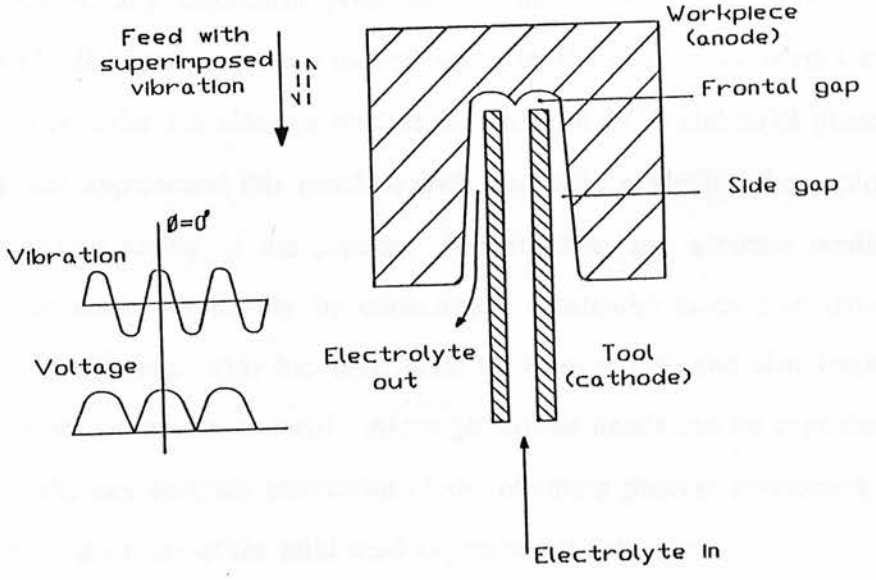

FIGURE 2.1 Machining gap in electrochemical arc drilling

The reactions in the machining gap cause the metal dissolution and thermal erosion processes to act randomly. It is the proportion of the intensity and duration of ECD to EDE phase which determines the end results for the drilling operation.

In ECM the theoretical metal removal rate can easily be predicted using Faraday's Laws of electrolysis. However, in EDM this is not very easy. Extensive studies (**30,31,32**) have been carried out to correlate the erosion rate of EDM with the physical properties of the electrodes and the machining variables. The useful conclusions drawn from these studies are :

a) the volume of the craters eroded increases as the applied energy is increased

b) the optimum erosion occurs at a certain pulse width irrespective of the pulse energy.

Obviously the thermal properties of the material determines how much material is removed per discharge.

In ECAM, any theoretical prediction of the metal removal rate is extremely difficult. It is not only the random nature of the electric discharges that ECAM has to consider but also the relative durations of ECD and EDE phases. Khayry (**26**), has approached this problem with stochastic modelling thus accounting for the random nature of the process. Nevertheless, any accurate predictions can only be made empirically by collecting a substantial amount of data from the actual machining. This has been done by Khayry (**26**) and also Drake (**25**) for mild steel workpiece material. Although similar trends can be expected for other materials, any accurate estimation of the optimum process parameters cannot be made on the basis of the mild steel experimental data, alone.

The primary objectives of this chapter are to investigate how some machining variables affect the process parameters and to establish the optimum conditions which yield the best hole for each of the five materials. The best hole is defined

as the one that has the highest drilling rate, the least overcut and taper and the minimum tool wear. The materials investigated and their composition are given in Table 2.1.

TABLE 2.1 Composition of the alloys

Alloy	Composition per cent											
	Cr	Ni	Mo	V	Co	Ti	C	Si	Mn	Cu	Al	Fe
Jethete	12.00	2.00	2.00	0.30	-	-	0.10	-	-	-	-	bal.
Rex535	10.00	-	0.08	-	6.00	-	-	-	-	-	-	bal.
Inco901	12.00	42.00	6.00	-	1.00	2.80	0.05	0.40	0.50	-	0.20	bal.
Low alloy steel	1.08	0.14	0.51	0.02	-	-	0.10	0.28	0.44	0.02	0.15	bal.
Titanium	commercially pure											

2.3 Experimental Apparatus

The salient features of the prototype ECAM drilling apparatus are shown in the schematic diagram in Figure 2.2. The four main aspects of the apparatus are:

(1) the main machine unit which locates the tool and the workpiece and provides the controlled movement of the workpiece.

(2) the power supply.

(3) the electrolyte supply system.

(4) the instrumentation for monitoring the process.

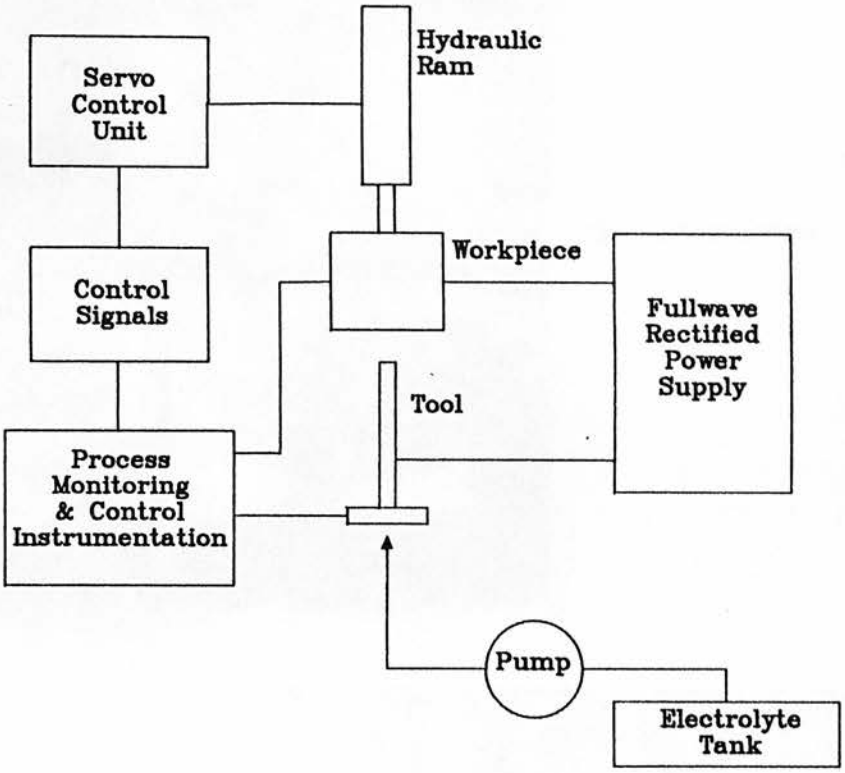

FIGURE 2.2 Schematic diagram of the ECAM drilling apparatus

2.3.1 The Main Machine Unit

A general view of the prototype ECAM apparatus is shown in Figure 2.3(a). The workpiece was located above the tool and was given a linear feed movement, superimposed with a sinusoidal vibration. A hydraulic cylinder was used to provide both the feed and the vibration. The uniform feeding motion of the hydraulic ram was obtained by using a ramp voltage generator. The signals from the ramp voltage generator, fed via a differential amplifier to the servo unit, controlled the feed motion.

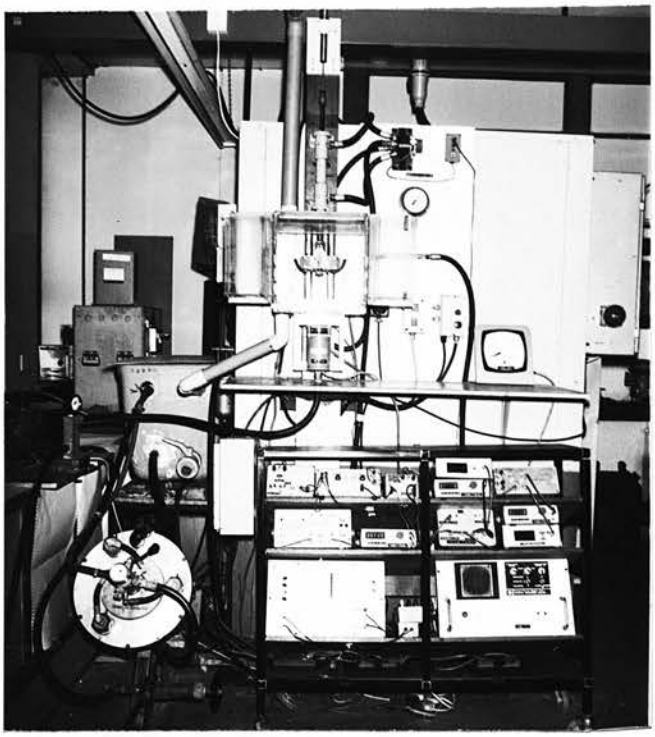

(a) a general view

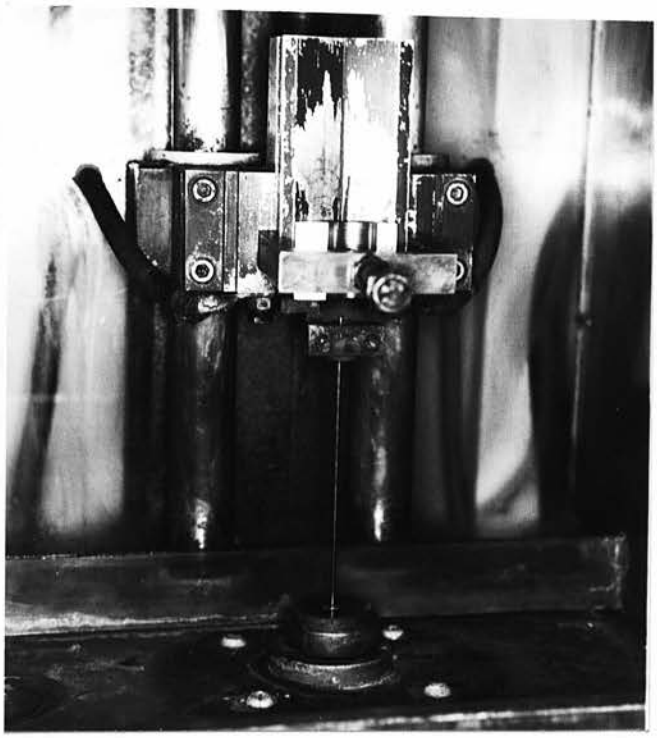

(b) tool and workpiece arrangement

FIGURE 2.3 The prototype ECAM drilling apparatus

The amplitude and the frequency of the vibration were controlled by a sinusoidal signal from a variable phase function generator to the differential amplifier unit. The generator was triggered from a full-wave rectified mains signal, enabling the output to be locked with the trigger input. In this way, the phase relationship between the vibration and the machining voltage waveforms can be varied from 180° lag to 180° lead. A linear variable differential transformer provided the feedback element.

The tool was kept stationary, except for the optional rotational movement which was provided by a stepper motor. The tool was fixed in place by a collet chuck arrangement as shown in Figure 2.3 (b).

2.3.2 The Power Supply

The power supply consisted of a variable transformer, a step-down transformer and a rectifying bridge. This provided a single phase, full-wave rectified voltage which was variable between 0 to 50 volts.

2.3.3 The Electrolyte Supply System

The electrolyte, maintained at the room temperature, was drawn from a 250 *litre* storage tank by means of a diaphragm pump capable of delivering 18 *litres* min^{-1} against a maximum back pressure of 127 bar. By means of a control valve fitted in the flow delivery line to the tool electrode, the electrolyte pressure could be preset in the range 13 to 120 bar.

2.3.4 The Process Monitoring Instrumentation

The machining voltage and the vibration waveforms were recorded in a two channel oscilloscope. This enabled the phase angle between the two waveforms to be preset accurately by adjustment of the phase shift control on the function generator.

To measure the current a Coulomb counter was used. This measured the total charge consumed within the machining period. By dividing the amount of charge recorded by the total machining time, the average machining current could be obtained. Similarly, the total electrical energy consumed was measured by a Joule counter.

2.4 Experimental Procedure

After recording the workpiece and tool weights and lengths, they were mounted in their respective positions in the ECAM apparatus. The initial inter-electrode gap was set to about 5 mm, while the process variables, such as amplitude and phase of vibration, voltage, feed rate and electrolyte pressure were set to their required values. The feed switch was now turned on to commence the machining. Each experiment was continued until the drill broke through the workpiece. Occasionally (about 1 in 25), the drilling process had to be abandoned due to severe short circuiting of the tool and the workpiece.

After each test the weight loss from both the tool and the workpiece was measured. The reduction in tool length was also noted. The diameter of the hole at drill entry and exit was measured using a microscope.

Experiments were performed for each of the materials using different combinations of process variables, until the best hole was achieved. Experiments were then repeated for the same conditions to ensure that these were the optimum process variables for the given material.

The electrolyte used throughout was 20% weight/volume aqueous sodium nitrate. Although it is appreciated that the electrolyte type can affect materials differently (2), it was too vast an experimental programme within this project to find out which electrolyte was the best for a given material. Sodium nitrate was chosen because this was found to be the most satisfactory electrolyte for mild steel by

Drake(**25**) who investigated a variety of electrolytes in ECAM.

The tools used for all the tests were copper tubes of inner and outer diameters 0.864 and 1.890 mm respectively. The workpieces were of various lengths ranging from 30 to 100 mm.

2.5 Results and Discussion

Different machining variables influence the process to different degrees. The effect of some machining variables on the process parameters are independent of the material properties. Therefore, in the optimisation of the process parameters for different alloys, these variables will have common optimum values. However, the effects of some variables are dependent on the material properties, thus giving differing optimum values. Nevertheless, similar trends can be expected in the relationships between the machining variables and the process parameters for all the materials.

The machining variables investigated are : the machining gap voltage, the vibration amplitude and phase, the feed rate and the electrolyte pressure. The process parameters are defined below.

1. *Linear Metal Removal Rate (LMRR)*

   This is the actual drilling rate which is less than the feed rate. The value of this was obtained by dividing the hole length by the machining time.

2. *Specific Metal Removal Rate (SMRR)*

   This indicates the rate of metal removal per unit electric charge. The volume (V) removed is obtained by dividing the workpiece weight loss by its density. The average machining current (I) is calculated from the of charge registered in the Coulomb counter. For a machining time T in minutes :

$$SMRR = \frac{V}{IT}\ mm^3A^{-1}\min^{-1}$$

3. *Volumetric Tool Wear Ratio*

This gives the volume of tool eroded as a percentage of the workpiece loss.

4. *Taper and Overcut*

Taper = [hole diameter at drill entry − hole diameter at drill exit] + 2

Maximum Overcut = [hole diameter at drill entry − tool diameter] + 2

2.5.1 Feed Rate

In order to minimise the number of experiments required to establish the optimum machining variables for each of the five materials, some variables were kept constant. Since the fastest drill rate is a criterion for determining the optimum performance, it was decided to carry out all the experiments at a feed rate of 20 mm min^{-1}, as this was found to be the maximum feed rate achievable without excessive short circuits, by Khayry (**26**)and also Drake (**25**). They have found that at low feed rates the metal removal rate was very low and was mainly due to ECD, because the machining gap was too large for any discharges to occur. Furthermore the ECD rate was well below the theoretical value due to low current densities resulting from larger gaps. As the feed rate was increased, the ECD rate increased. Consequently, more gas was generated in the gap. This increase in the amount of gas combined with the decrease in the gap produced electric discharges, thereby increasing the metal removal rate. Further increase in the feed rate resulted in short circuits.

2.5.2 Electrolyte Pressure

The electrolyte in the gap performs two essential tasks. Firstly it is the medium in which electrolysis occurs and secondly, it acts as a coolant and carries the debris away from the gap. The flow of electrolyte is controlled by the pressure

reading in the gauge in the inlet line.

The variation in electrolyte pressure does not influence the process parameters significantly (**25**). However, the pressure should be adequate to flush the debris from the gap, in order to sustain efficient machining. Although the variation in the flow pattern could affect the ECD phase, this is not critical for the overall performance. Preliminary tests were done at 20, 30 and 40 bar for one material (Jethete). No significant change in the process parameters was observed. Hence the rest of the experiments were performed at 30 bar pressure as this proved to be the most stable and provided adequate flushing of the gap.

2.5.3 Vibration Amplitude

In ECAM, vibration of one of the electrodes is necessary for the following reasons:

1) The vibration facilitates the removal of debris from the machining gap.
2) It allows the control of the amount of energy transmitted across the gap at any instant by varying the phase angle between the gap and the voltage waveforms.

From the preliminary experiments performed, it was found that the specific metal removal rate decreased very slightly with increasing vibration amplitude. Although larger vibration amplitudes mean better flushing of the machining debris from the gap, they also give rise to increased lateral movement of the tool. This causes more tool wear and less metal removal from the workpiece. However, with the tool penetrating further into the workpiece, especially at higher vibration amplitudes, machining along the side walls of the hole is increased. This is accompanied by efficient expulsion of the machining products from the inter-electrode gap by increase in turbulence of the convective flow. For such conditions, the decrease in specific metal removal is expected to be smaller at greater

vibration amplitudes.

On the whole, varying the vibration amplitude did not have a significant effect on the process parameters, hence it did not warrant a detailed investigation. The two limits for the vibration amplitude were that it should be large enough for the debris to be flushed away and small enough for no lateral vibration which tended to cause short circuits. This was found to be between 0.10 to 0.15 mm peak-peak.

2.5.4 Phase Angle between Vibration and Voltage Waveforms

The phase angle between vibration and voltage waveforms determines the instantaneous relationship between the inter-electrode gap width and the amount of power transmitted across it. This, therefore can be used to control the relative intensities and durations of electrochemical and electrodischarge phases in ECAM.

Since the effect of the phase angle on the process parameters is independent of the properties of the materials, the optimum value of the phase angle would be the same for any material.

Previous researchers explorations in to phase angle influence on process parameters is not fully clear. Khayry (**26**) has reported a slight increase in specific metal removal rate (SMRR) with phase angle increase from 30° lag to 20° lead. Whereas, Drake (**25**) observed a slight decrease in SMRR in the same range, using the same conditions of machining.

From the experiments carried out the most stable machining was achieved when the phase difference was 0°. When the phase angle was 180° lead or lag, intermittent periods of very intense sparking and quiet periods were noted. Table 2.2 gives the process parameters for three different phase angles (0°, 30°, 180°) for one of the materials (Jethete - the chrome alloy). The values given in the table were obtained by taking the average of three experimental data values.

TABLE 2.2 Process Parameters for Different Phase Angles

Phase Angle	LMRR mm min^{-1}	SMRR mm^3 $A^{-1}min^{-1}$	Drill Wear Ratio	Taper mm/100mm
0°	16.2	8.11	11%	0.32
30°	13.4	12.67	16.5%	1.56
180°	12.4	14.57	20%	3.42

From the table it is apparent that the optimum conditions were obtained when the phase angle was 0°, i.e., the fastest drill rate, the least tool wear and the smallest taper. This can be explained with the aid of graphical illustrations in Figure 2.4. Figure 2.4(a) shows the case when phase angle is 0°. This gives the condition, that at instant *x* in time, the voltage is maximum when the gap is maximum. As the gap decreases, so does the voltage, giving minimum voltage at minimum gap at instant *y*. It can be assumed that at equilibrium gap (i.e. when the feed rate equals to the sum of linear metal removal rate and the tool wear rate), the variation in electric field strength across the gap is minimal, giving very stable machining conditions. As illustrated in Figure 2.4(a) the actual machining voltage waveform shows ECD occurring at low values of the voltage giving rise to low intensity EDE as the peak value of the voltage is reached.

In Fig. 2.4(b), the case is illustrated when the phase angle is 180°. This gives minimum voltage at maximum gap at instant *x* to maximum voltage at minimum gap at instant *y*. When the gap is at equilibrium, the electric field strength would vary from a minimum to a maximum, giving unstable machining. As depicted in Figure 2.4(b), actual machining voltage had very spiky peaks indicating high a intensity discharge phase. The severity of the discharge phase caused large craters to be removed giving high SMRR but low LMRR.

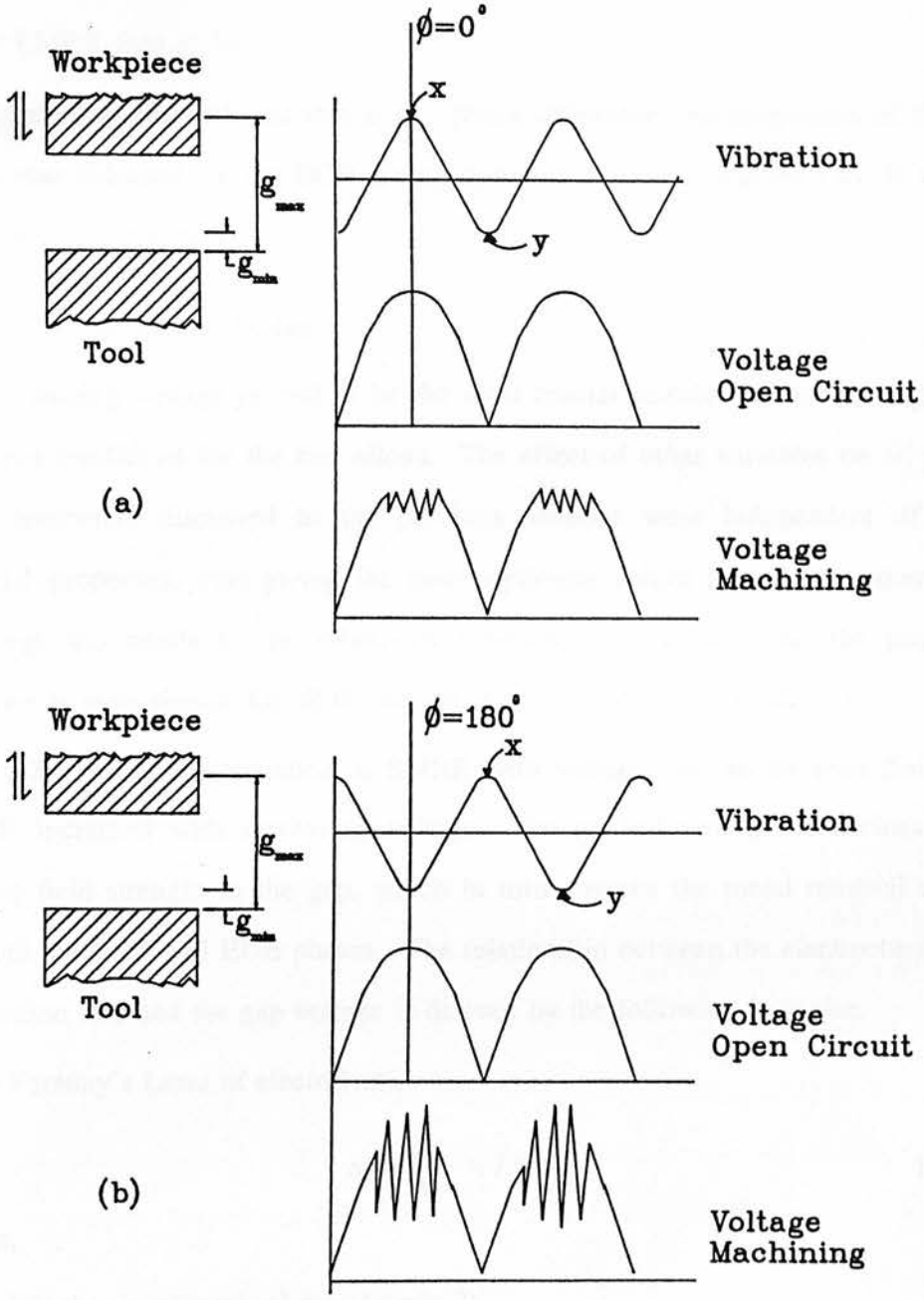

FIGURE 2.4 The effect of phase angle on the gap - voltage relationship

The intermediate phase angle of 30°, gave gap conditions which were more stable than 180° but not as stable as at 0°. This is evident from table 2.2, as 0° has higher LMRR than at 30°.

The conclusion reached was that at 0 ° phase difference, the proportion of EDE action was balanced by the ECD giving optimum results of highest LMRR with least tool wear and taper.

2.5.5 The Machining Voltage

The machining voltage proved to be the most crucial variable in determining the optimum conditions for the five alloys. The effect of other variables on all process parameters discussed in the previous sections were independent of the material properties, thus giving the same optimum values for all the materials. Although the trends in the relationship between the voltage and the process parameters were similar for all the materials, the optimum values differed.

Figure 2.5 shows the variation in SMRR with voltage. It can be seen that the SMRR increased with increasing voltage. The applied voltage determines the electric field strength in the gap, which in turn governs the metal removal rates by both the ECD and EDE phases. The relationship between the electrochemical dissolution rate and the gap voltage is derived by the following formulae.

From Faraday's Laws of electrolysis,

$$\dot{m} = \frac{N}{nF} \times I \times \eta \qquad [2.1]$$

where,

$\dot{m}$ is the metal removal rate (g min^{-1})

N is the atomic weight (g $mole^{-1}$)

n is the valency

F is Faraday's Constant (96500)

I is the current

η is the current efficiency

From Ohm's Law, the current I is related to the voltage V and the gap resistance R by

$$I = \frac{V}{R} \qquad [2.2]$$

and for an electrolytic gap width g, current path area A and electrolyte conductivity k_e

$$R = \frac{g}{k_e \times A} \qquad [2.3]$$

the current density J is given by

$$J = \frac{V \times k_e}{g} \qquad [2.4]$$

therefore,

$$\dot{m} = \frac{N}{nF} \times \frac{V \times A \times k_e}{g} \times \eta \qquad [2.5]$$

From equation 2.5 above, it can be seen that the voltage is directly proportional to the metal removal rate. At higher voltages, the enhanced ECD rate will produce more hydrogen gas, which will lead to more discharges. Furthermore, the discharges have more energy at higher voltages owing to the increased ionisation which occurs as a result of high field strengths. Consequently, the craters eroded will have larger volumes resulting in higher metal removal rates.

Although the SMRR increases with voltage the LMRR does not. This in fact can be seen from Figure 2.6. In effect, what the voltage increase does is to remove larger volumes of material at a given instant, resulting in increased SMRR and large overcuts.

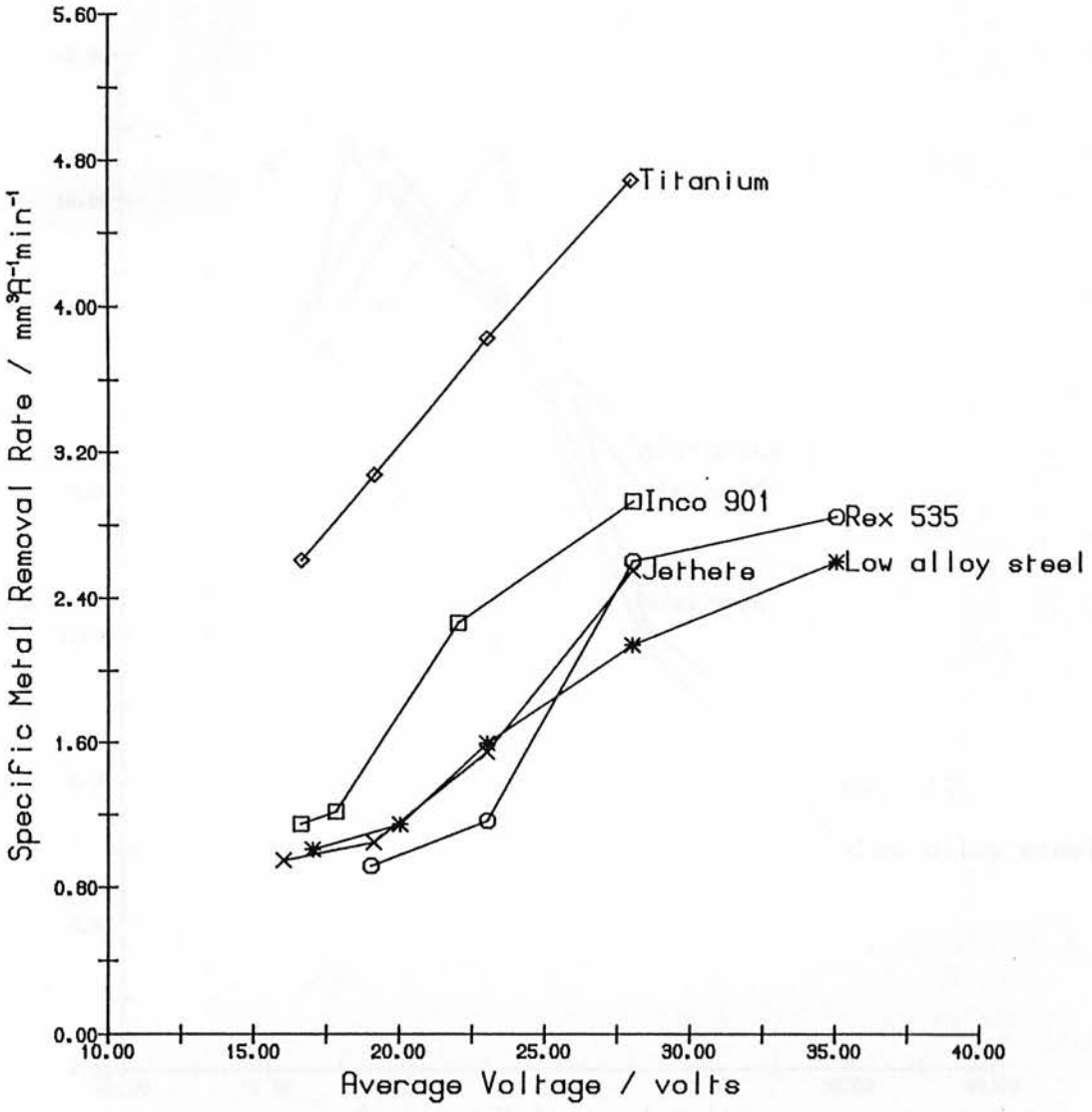

$feedrate = 20\ mm.min^{-1}$
$vib.amp. = 0.1\ mm$
$phase = 0^{0}$

FIGURE 2.5 Specific metal removal rate vs. voltage

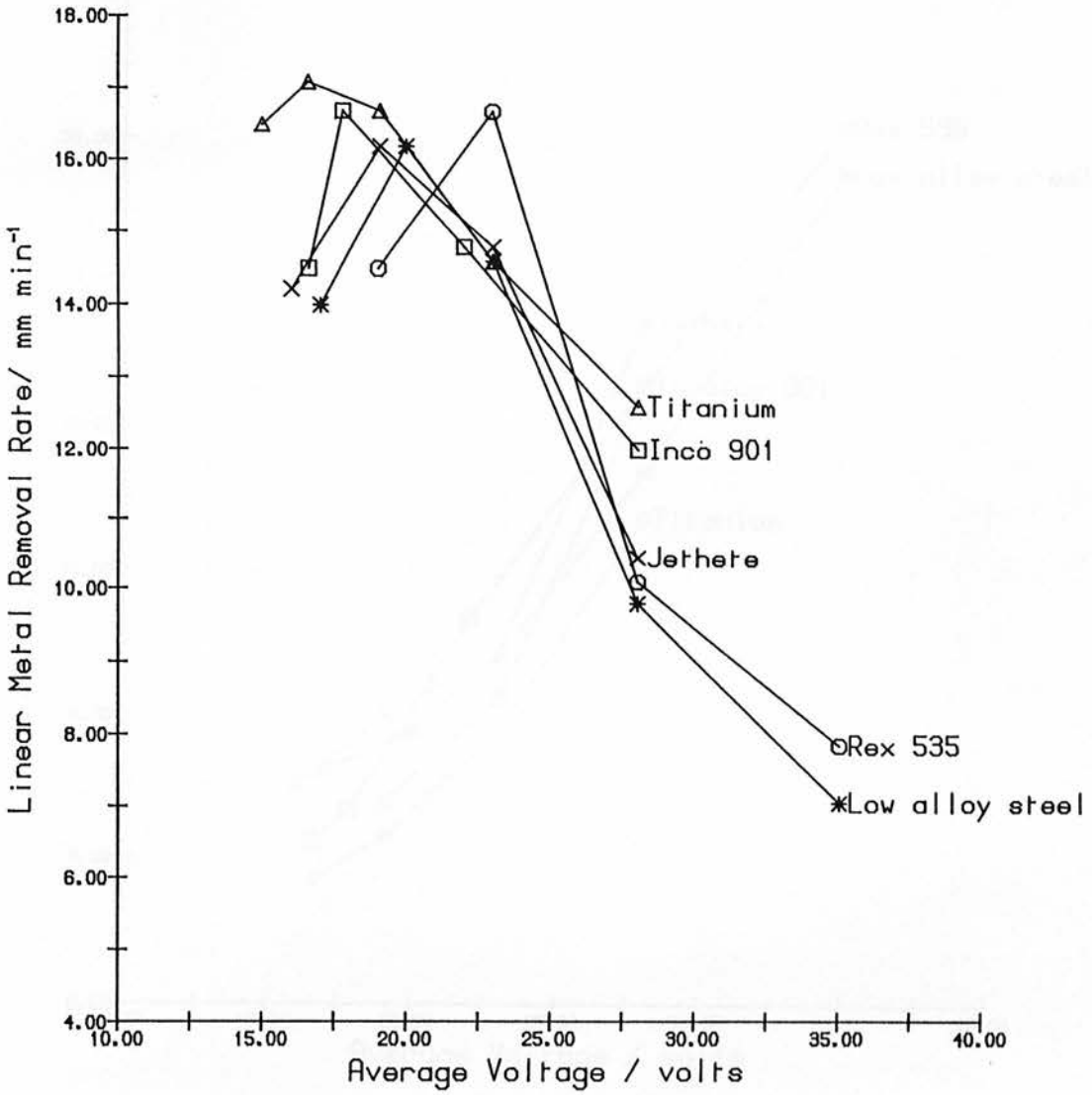

$feedrate = 20\ mm.min^{-1}$
$vib.amp. = 0.1\ mm$
$phase = 0^0$

FIGURE 2.6 Linear metal removal rate vs. voltage

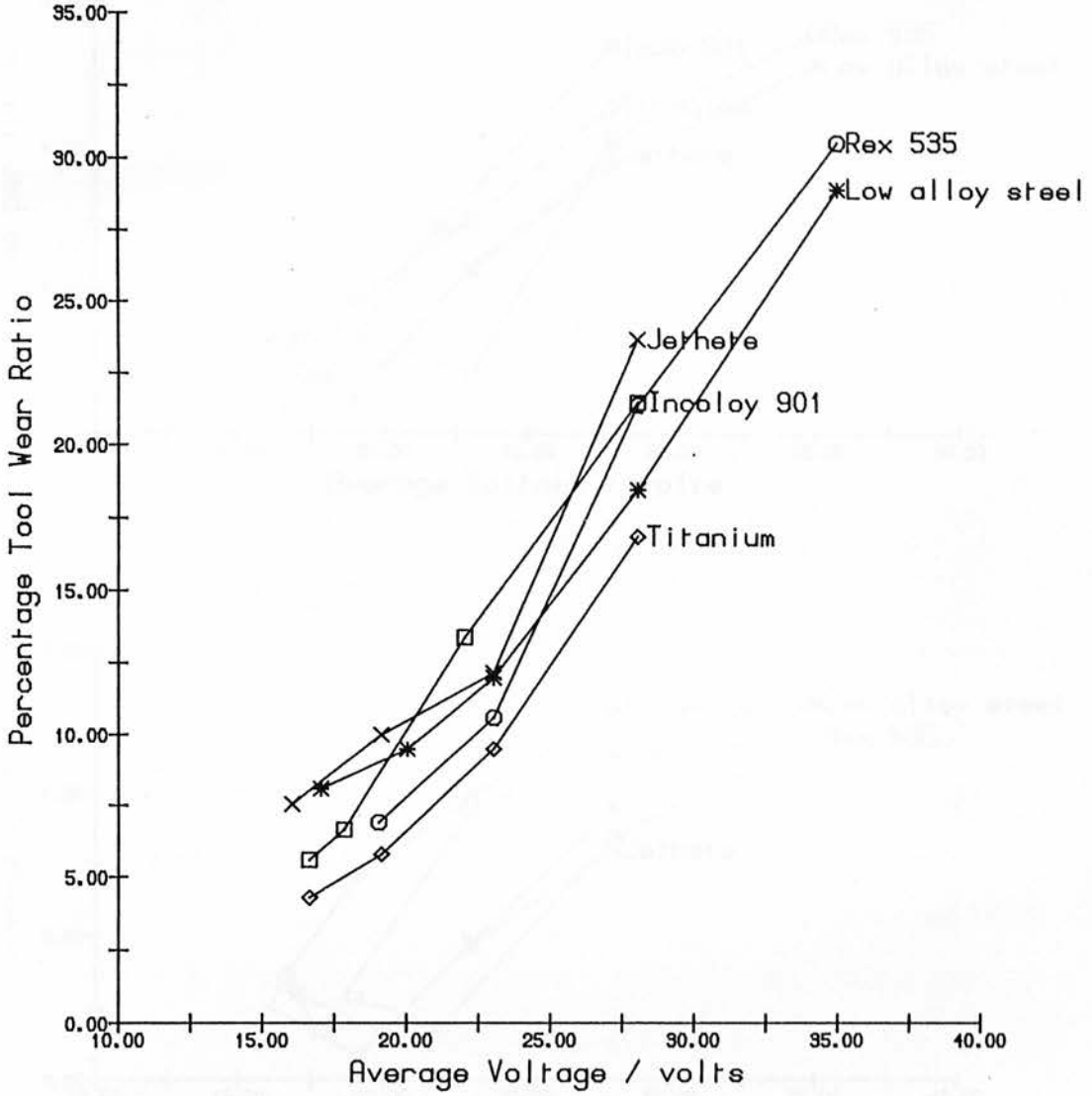

$feedrate = 20\ mm.min^{-1}$
$vib.amp. = 0.1\ mm$
$phase = 0^{o}$

FIGURE 2.7 Volumetric tool wear ratio vs. voltage

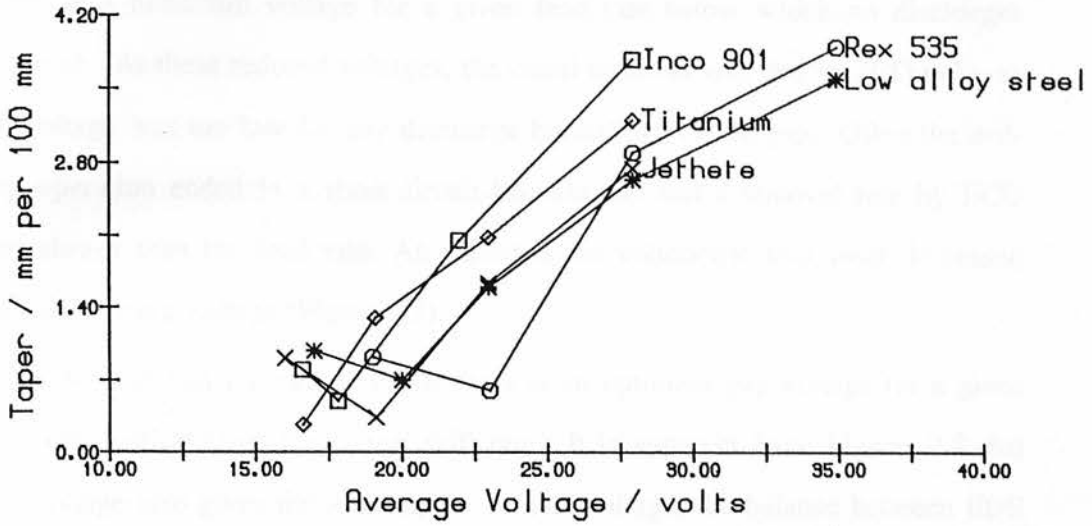

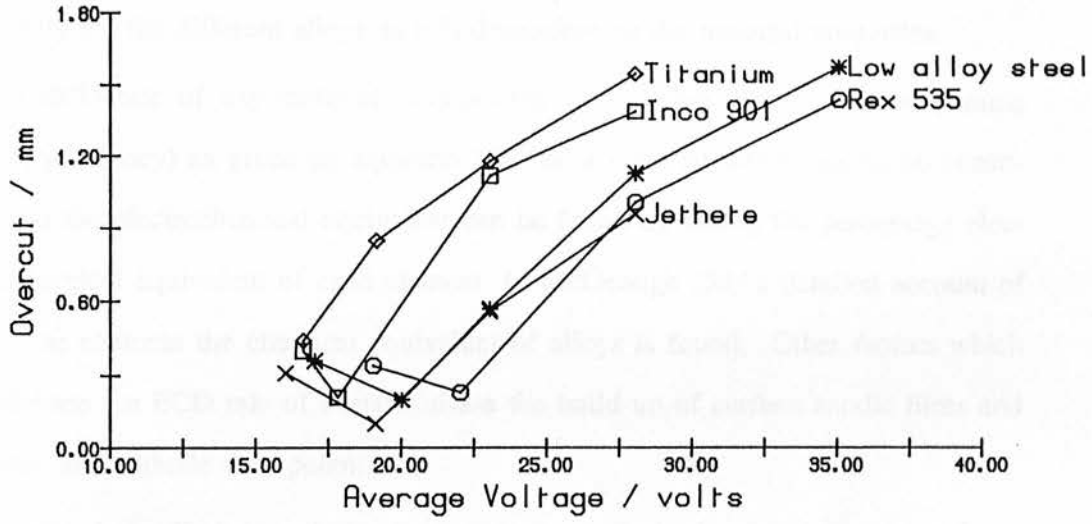

$feedrate = 20\ mm.min^{-1}$
$vib.amp. = 0.1\ mm$
$phase = 0^0$

FIGURE 2.8 Taper and overcut vs. voltage

There is a minimum voltage for a given feed rate below which no discharges occurred. At these reduced voltages, the metal removal was due to ECD only, as the voltage was too low for any discharge breakdown of the gap. Often the drilling operation ended in a short circuit because the metal removal rate by ECD was slower than the feed rate. As expected the volumetric tool wear decreased with decreasing voltage (Figure 2.7).

It can be said that for each material there is an optimum gap voltage for a given feed rate, which gives the fastest drill rate. It is apparent from Figure. 2.8 that this voltage also gives the least taper. At this voltage, the balance between EDE and ECD phases is achieved, giving high LMRR, low taper and overcut and low tool wear. The voltage where that right balance of EDE to ECD occurs, differs slightly for the different alloys as it is dependent on the material properties.

The ECD rate of any material is dependent on its chemical equivalent (atomic weight/valency) as given by equation 2.5. For a material which has many constituents the electrochemical equivalent can be found by taking the percentage electrochemical equivalent of each element. In McGeough (**33**) a detailed account of how to estimate the chemical equivalent of alloys is found. Other factors which influence the ECD rate of a material are the build up of surface anodic films and anode and cathode over-potentials.

For the electrodischarge phase, the metal removal rate depends upon the volume of metal removed by each discharge and the frequency of discharges. The volume of metal removed per discharge is a function of the discharge energy. A certain power density (heat flux) is necessary to sustain the boiling temperature at the centre of the plasma channel. Clearly this heat flux will depend on the rate at which heat is conducted into the electrodes from the surface heat source. This rate of heat flow will be dependent on the material properties such as thermal

conductivity, diffusivity and melting/boiling point. There are many theories based on heat conduction models to correlate the crater volume removed per discharge with the thermal properties of the material. Although it is very difficult to establish a definite relationship between the thermal properties and the metal removal rate, the following relationships established empirically by Berghausen (**34**) give a good indication of how metal removal rate is determined by the melting point.

$$R_w = 2.43\ M_w^{-1.23} \qquad [2.6]$$

and

$$V = 1.36\times10^{-4} M_w^{-1.43} \qquad [2.7]$$

where,

R_w is the average metal removal rate from workpiece ($in^3 amp^{-1}\text{min}^{-1}\times10^4$)

V is the average volume per discharge (in^3)

M_w melting point of workpiece (°C)

Table 2.3 gives the thermal properties of each material and also the electrochemical equivalent.

TABLE 2.3 Some physical properties of the materials

Material	Density Kg m^{-3}	Thermal Conductivity W m^{-1} $°C^{-1}$	Melting point °C	Electrochemical Equivalent g $mole^{-1}$
Jethete	7700	18.8	1470	26.28
Rex 535	7900	61	1321	26.94
Incoloy 901	8100	113	1365	29.80
Titanium	4500	17	1725	11.89
Low alloy steel	7800	21	1320	27.48

It can be seen from Figure 2.5 that SMRR for titanium was considerably higher than for the other materials. This is attributed to the low average current drawn while machining titanium in comparison to the others (table 2.4). This is also evidence, that in titanium very little ECD occurred, therefore all the energy applied was available to the EDE phase. Consequently, a larger volume of metal was removed per discharge. Although titanium has a high melting point, its very low thermal conductivity may have contributed to it undergoing thermal shock. This may have caused the grains to be ripped away from their boundaries. The LMRR for titanium was only slightly higher than for the other materials (Figure 2.6). The taper was found to be the least in titanium (Figure 2.7) again indicating the absence of ECD phase. However, as can be seen from Figure 2.8, the overcut endured by titanium was not any less than for the other materials. This supports the argument that with titanium, the high intensity discharges have caused whole grains to be eroded giving high rate of volumetric metal removal. For the other four materials, the SMRR differed only slightly. Since it is very difficult to estimate the relative intensities and durations of ECD and EDE phases, no analysis can be made on how material properties have affected the process conditions. From Figure 2.5 it can be seen that the nickel alloy (Inco 901) has slightly higher SMRR than the other three alloys. This may be due to the greater ECD rate resulting from the higher electrochemical equivalent.

What was achieved by varying machining conditions was the balanced ECD/EDE which gave optimum results for the five materials. The optimum machining variables together with their resulting process parameters are given in Table 2.4.

TABLE 2.4 Optimum Machining Variables and Process Parameters

Material	Average Voltage	Average Current	Volumetric M.R.R.	Linear M.R.R.	Volumetric Tool Wear	Hole Geometry		
	volts	amps	$mm^3 min^{-1}$	$mm\ min^{-1}$	Ratio	Diameter/mm entry	exit	Taper Angle
Jethete	19.1	66	61.2	16.2	11%	2.31	2.12	0.17°
Rex535	22.0	61	63.6	16.7	8%	2.45	2.13	0.28°
Incoloy901	17.8	63	76.2	16.7	9.1%	2.28	2.02	0.24°
Titanium	16.6	29	88.8	17.1	5.2%	2.20	2.08	0.10°
Low alloy steel	20.0	68	69.5	16.2	12%	2.46	2.11	0.31°

Process variables common to all the materials:

Tool Feedrate	- 20 $mm\ min^{-1}$
Vib. Amplitude	- 0.1 mm peak to peak
Phase Angle	- 0°
Elec. Pressure	- 30 bar

The values shown in the table are the average values of three sets of experimental data.

2.6 Summary

ECAM has been used successfully to drill holes in the five alloys (chrome alloy, cobalt alloy, nickel alloy, titanium and low alloy steel) investigated. The experiments performed examined how the machining variables influenced the process parameters and whether it was dependent on the material properties. For each of the materials, a set of optimum machining variables was established, which yielded the highest linear metal removal rate, the least taper and overcut and lowest tool wear. For most materials, this optimum performance was achieved when the EDE phase was balanced by the ECD phase. This meant that the energy

available to the discharges must have been such that it was directed at the frontal gap, removing craters which were small enough for the ECD action to smooth out completely. This way the highest drill rate was achieved with the least over-cut and taper.

In the case of titanium, however, the ECD rate was much less, therefore the optimum conditions were determined entirely by the energy available to the discharges.

3 : SURFACE EFFECTS ON ALLOYS DRILLED BY ECAM

3.1 Introduction

Electrochemical arc machining is a contactless machining process. Nevertheless the thermal and the electrochemical metal removal mechanisms in ECAM can affect the surface integrity of a machined component. The degree of alteration to the surface integrity of any material is determined by the material properties such as the thermal conductivity and the composition. It is of value therefore to investigate the effects of ECAM on different types of materials. The surface characteristics of machined parts are of great interest for two reasons:

(1) Higher surface-volume ratios are encountered as strength-weight ratios are increased.

(2) The extreme environments to which they may be subjected make them inherently more sensitive to their surface conditions.

This chapter investigates the surface effects produced by ECAM drilling on the five materials encountered in the previous chapter. The analysis of the surface quality is based on optical and scanning electron microscopic examination and microhardness testing.

Since the surface effects produced by ECAM are expected to have both EDM and ECM surface characteristics, a brief account of the EDM and ECM characteristics is given first.

3.2 EDM Surface Effects

Several publications can be found on surface characteristics of EDM components (**35, 36, 37**). It is well known, that when a discharge occurs the material is melted, or even evaporated, thus forming craters on the component surface. The heat of the discharge penetrates to the sub-surface layers inducing a heat affected zone. The amount of heat damage is dependent on the thermal conductivity of the material and the intensity of the discharge itself, which is governed by the process variables and the gap conditions. The craters produced by EDM are associated with fusion and plastic deformation due to molten liquid solidifying epitaxially when quenched by dielectric. Platanik et al (**38**) have reported that this in turn causes slip, twinning, cleavage and microcracks in the surface depending on the crystal structure, regardless of the ductility of the material. A review on the existing published work on the nature of electrodischarge machined surfaces can be found in Crookall and Khor (**35**). Typical surface defects and sub-surface layers which can be caused by EDM is shown in Figure 3.1.

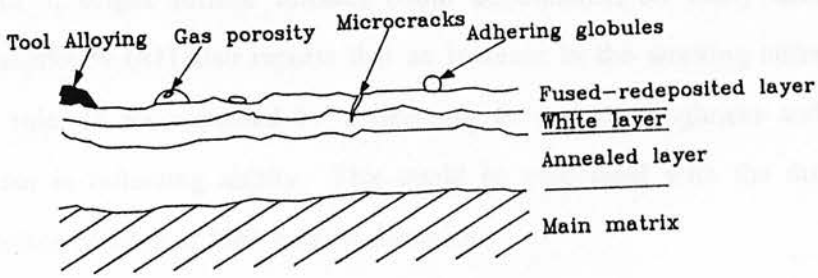

FIGURE 3.1 Typical EDM surface effects

3.3 ECM Surface Effects

The microfinish of an electrochemically machined surface is governed mainly by the type of electrolyte, the composition of the workpiece material and the machining conditions such as the current density and the electrolyte flow rate.

The main factors resulting in poor surface finish in ECM are pitting, preferential grain boundary attack, surface waviness and formation of oxide layers. These effects are illustrated in Figure 3.2. Pitting tends to occur in regions of low current density where the passivating layer would slow down dissolution of the majority of the surface. Grain boundary attack is an example of local recession and is very important because severe attack may reduce fatigue life by as much as 50%.

De Barr and Oliver (**2**) describe how current density, electrode potential and type of electrolyte can result in differential removal rates in inhomogeneous materials. Bannard (**39**) has investigated the surface finish of fine hole drilling using ECM. He has found that electrochemical drilling of multiphase alloys could present particular problems, where, if the correct dissolution-controlling anodic film is not generated, differential dissolution of the phases would occur resulting in a rough surface. However, Cole (**40**) claims that if the current density is sufficiently large (100 A cm^{-2}), bright surface finishes could be obtained on many metals and alloys. Kashthejev (**41**) also reports that an increase in the working current density, as a rule, is accompanied by a decrease in surface roughness and by an improvement in reflecting ability. This could be associated with the disappearance of surface etching at high current densities.

ECM surfaces are free from residual stresses and also from any heat affected zones or recast layers. Therefore smooth ECM surfaces are much preferable to EDM surfaces.

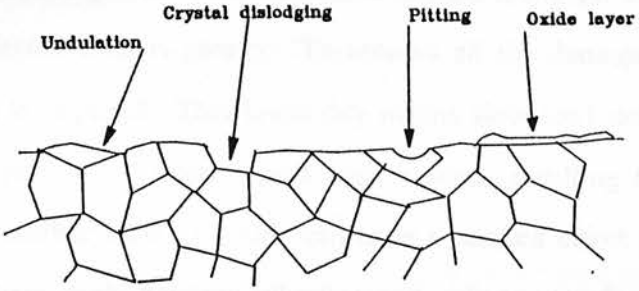

FIGURE 3.2 Typical ECM surface effects

3.4 Surface Effects of ECAM Drilling

In ECAM drilling the main mechanism responsible for material removal at the frontal gap is electrodischarge erosion (EDE) while at the side gap electrochemical dissolution (ECD) of the material occurs. The metallurgically damaged layers caused by the discharge erosion phase are wholly or partially removed by the electrochemical dissolution phase. Therefore, the main factor which determines the ECAM surface integrity is the proportion of EDE to ECD phase.

In McGeough et al (**42**) the factors which affect the surface quality produced by the ECD phase are given as: formation of anodic surface films, non-uniformity of the electrolyte flow pattern, change in bulk conductivity and effects of cathode and anode overpotentials. Likewise, the factors for the EDE phase are given as: the type and duration of the machining voltage, the frequency and distribution of discharges and the effect of electrolyte flow rate.

The proportion of EDE to ECD phase is determined mainly by the machining variables and the gap conditions. Machining voltage is the most crucial process variable where surface quality is concerned. At higher voltages, the intensities of the discharges are greater, thus the craters formed are larger and also the depth of the heat affected zone is greater. To remove all the damaged layers, prolonged ECD action is required. This invariably means slow feed rates. Prolonged ECD action will also cause larger tapers and overcuts, resulting in poor dimensional accuracy. Another variable which can have a marked effect on the surface quality is the phase angle between vibration and voltage waveforms. As discussed in Chapter 2, the instantaneous relationship between the machining gap and the power transmitted across it is determined by the phase angle. By varying the phase angle the relative intensity and duration of ECD and EDE phases can be changed.

3.5 Evaluation of Surface Integrity

Surface effects were analysed for the holes drilled using the optimum machining variables for each of the five materials. Normal illumination optical microscopy was used to examine the structures in the sub-surface layers of the specimens. Specimens were prepared by taking longitudinal sections through the drilled hole for each material. These were then polished and etched in the following etchants:

low carbon chrome steel (Jethete)	-	5% ferric chloride/nitric acid
cobalt alloy (Rex 535)	-	5% ferric chloride/nitric acid
nickel alloy (inco 901)	-	5% ferric chloride/nitric acid
low alloy steel	-	5% Nital
titanium	-	10% hydrofluoric acid/5% nitric Acid

The microstructure along the drilled hole was examined and photographed on a "Zeiss" photomicroscope. Microhardness readings were taken using a "Leitz" microhardness tester. Scanning electron microscopy was used to examine the ECAM drilled surface. This technique allows the identification of any craters and also gives some indication of the surface roughness due to its relatively high depth of field (1 mm).

3.6 Results and Discussion

The analysis of the surface integrity along the hole was divided into three areas of significance as shown in Figure 3.3.

(1) The first one to two millimetres near drill entry where it generally exhibited rounding-off effects due to stray electrochemical attack.

(2) The middle section which consisted of most of the hole length, where actual ECAM (combined ECM and EDM) surface effects were to be found.

(3) Finally the last two to three millimetres near the exit where it was expected to have mainly EDM surface effects.

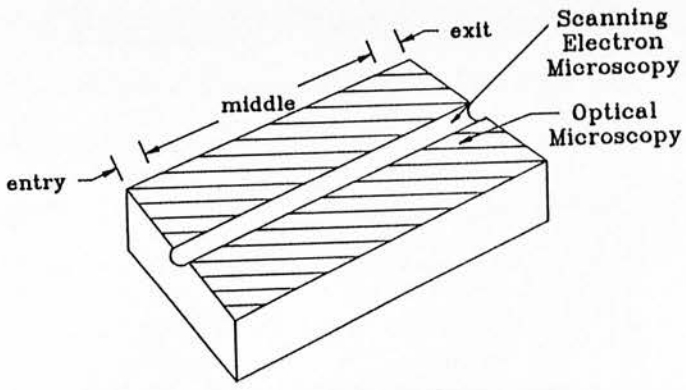

FIGURE 3.3 The three zones of the drilled surface

The microhardness readings in Table 3.1 were taken from the middle of the hole as this is where the true ECAM effects are represented.

TABLE 3.1 Variation of microhardness with depth

Depth from the drilled surface	Microhardness $Kg\ mm^{-2}$				
µm	Jethete	Rex535	Low alloy steel	Incoloy 901	Titanium
70	340	363	147	458	377
170	339	371	151	452	416
270	348	377	145	452	406
370	368	378	155	436	371
570	350	371	150	427	383
1000	357	370	155	433	394

3.6.1 Low Carbon Chrome Steel (Jethete)

Figure 3.4 shows photomicrographs of longitudinal sections taken from drill entry, middle and drill exit points of a typical ECAM specimen. Apart from near the drill exit end, the martensitic surface structure of the low carbon chrome steel appears to be regular with no sub-surface layers or microstructural change. At the exit, however, some damage is evident, a white layer of about 10 μm thickness can be seen (Figure 3.4(c)). This white layer extended to about 1.5 mm from the exit end. Table 3.1 shows the microhardness readings taken at various depths from the drilled surface. No significant variations in these readings can be detected, which indicates that there are no hardened layers left on the surface.

Scanning electron microscope photographs of the drilled surface are presented in Figure 3.5. Except for the exit end, the surface is smooth and crater-free. Some surface etching is visible in the middle area, at higher magnification as can be seen from Figure 3.6. This is because that the ECD phase was such that it left a highly polished surface which was subsequently etched by the etching solution. At the exit, a rough and irregular surface, similar to that of an EDM surface is apparent, with signs of surface melting and resolidification.

The smooth profile and the absence of surface layers up until the last 1-2 mm from the exit end, is taken as evidence that all the damage induced by the electrodischarge erosion action has been effectively removed by the following electrochemical dissolution action. At the drill exit end, electrolyte was lost in the machining gap, as a result of the drill breaking through the workpiece. This stops the electrochemical dissolution at the exit, leaving the damage caused by the discharge erosion action.

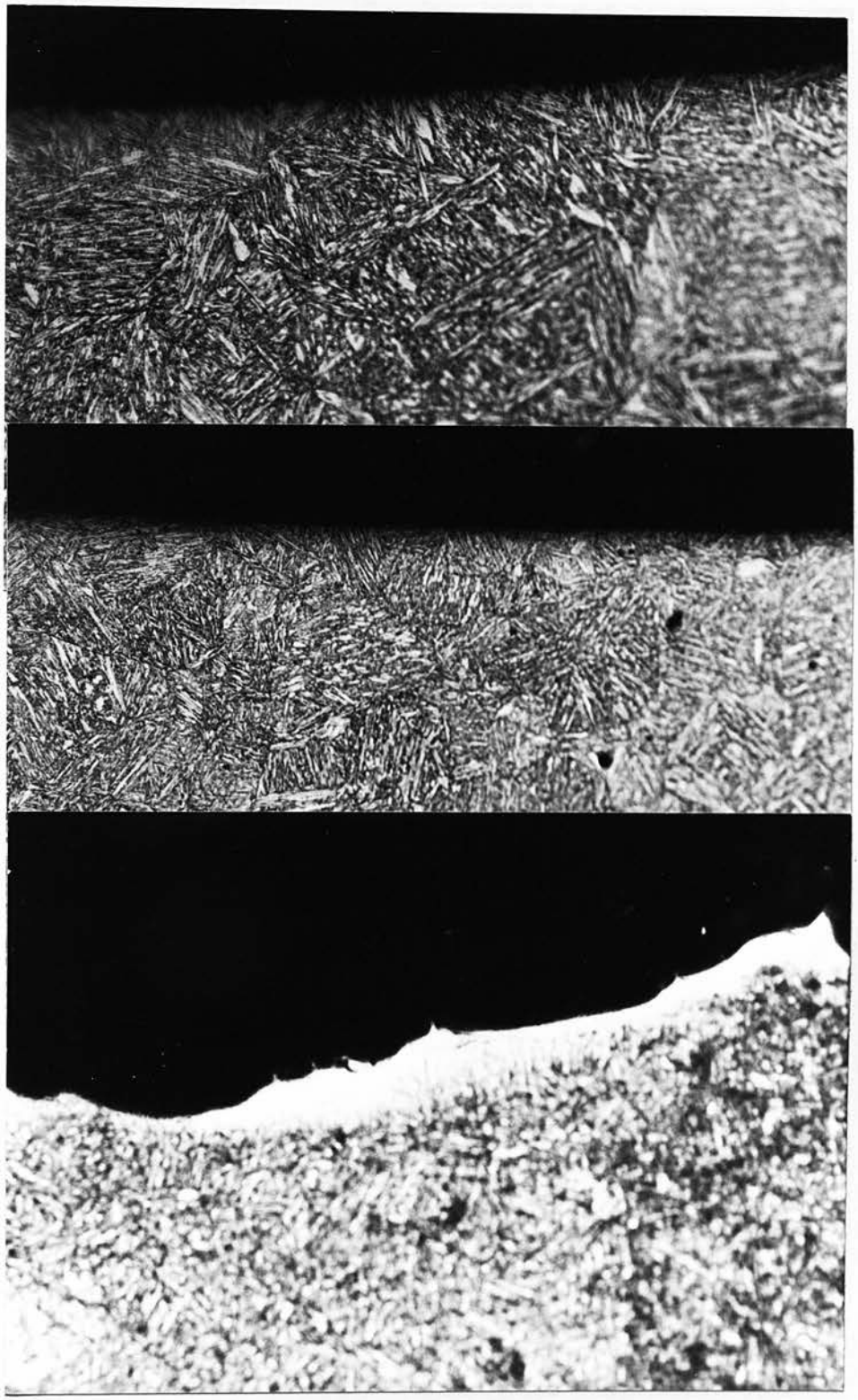

FIGURE 3.4 Photomicrographs of polished and etched Jethete specimens showing the subsurface region along the hole. (a)near drill entry × 640, (b) middle × 640, (c) near exit × 640

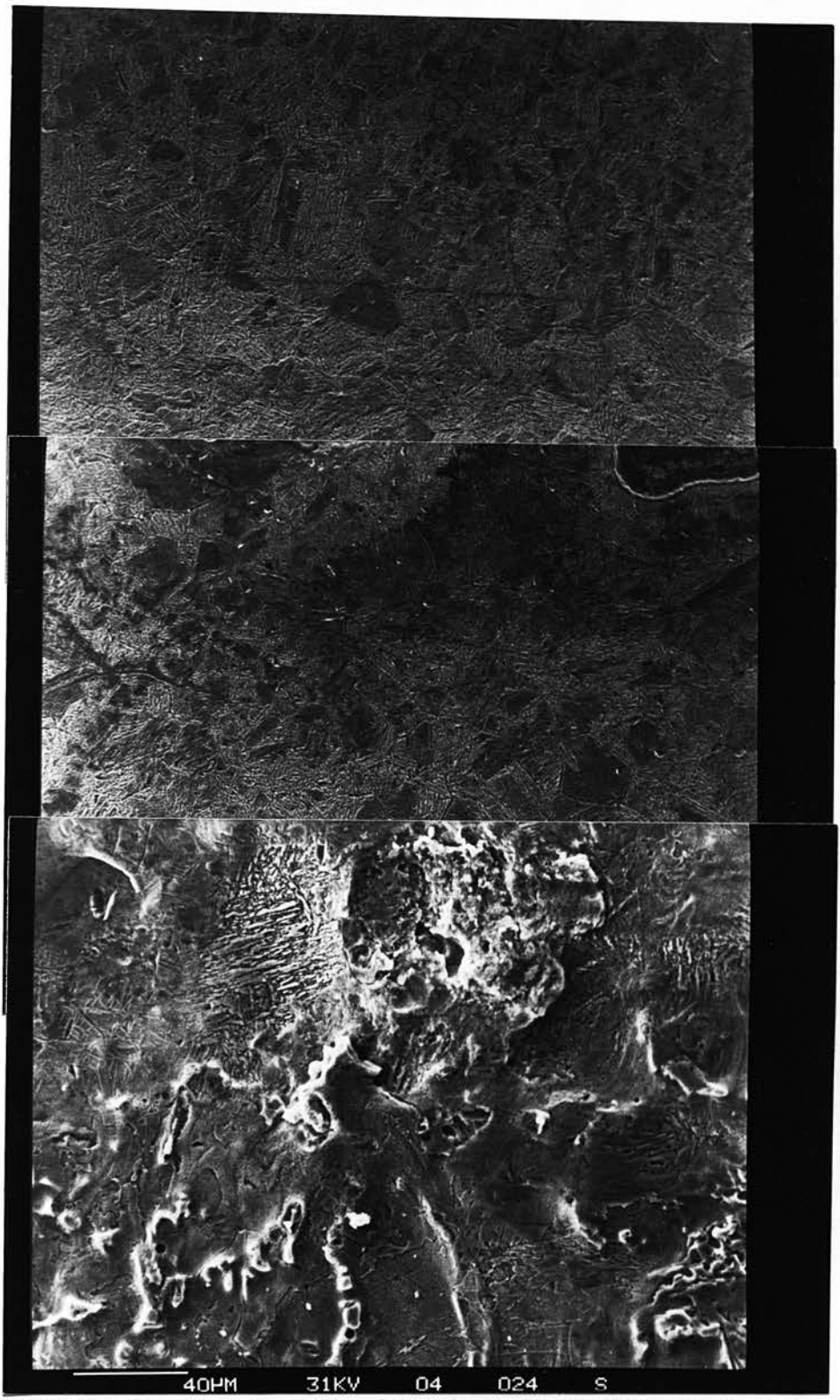

FIGURE 3.5 Scanning electron micrographs of Jethete specimens showing the drilled surface along the hole. (a)near drill entry × 100, (b) middle × 100, (c) near exit × 500

(a)

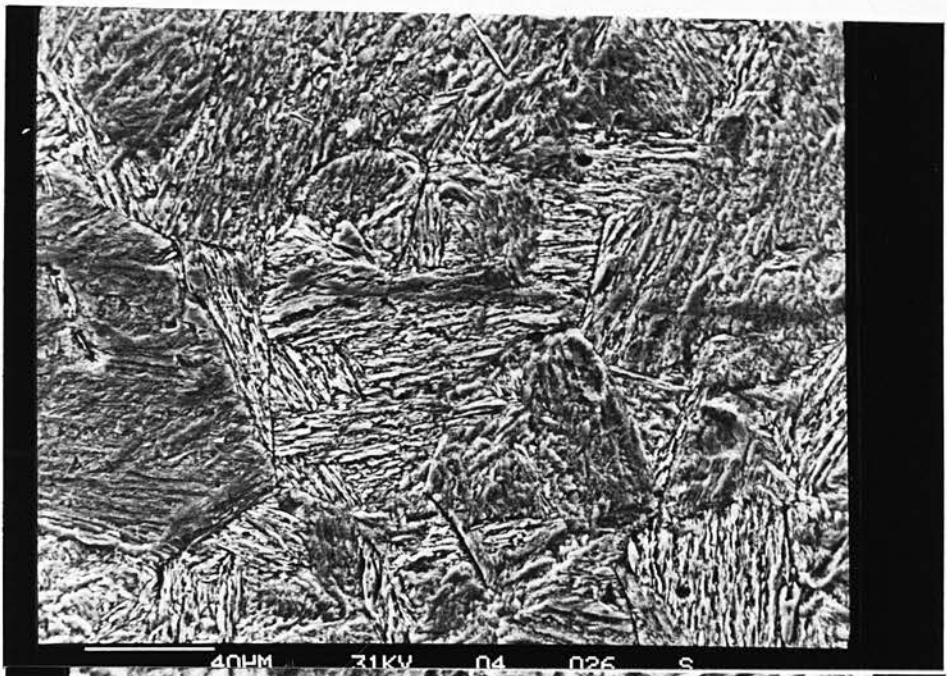

(b)

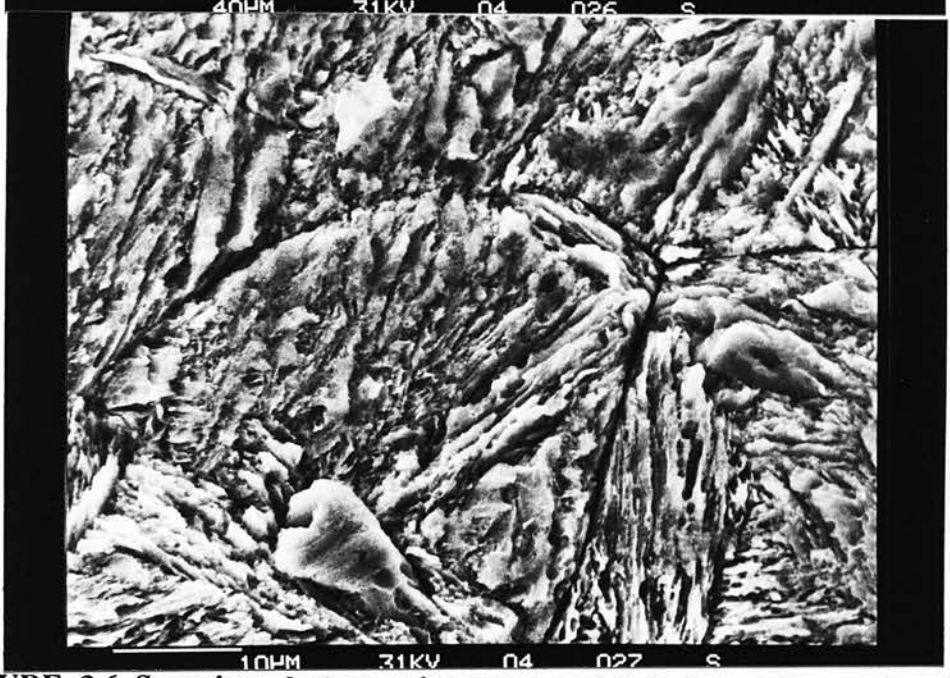

FIGURE 3.6 Scanning electron micrographs of Jethete specimens showing the drilled surface along the hole. (a)near drill entry × 500, (b) middle × 2000

3.6.2 Cobalt Alloy Steel (Rex 535)

As seen from the photomicrographs of Rex 535 in Figure 3.7, no significant or measurable effects on the microstructure can be detected. Even at the exit end, the sub-surface region appears to be unaffected. Nevertheless the scanning electron microscope (SEM) photograph of the exit end in Figure 3.8 shows signs of splashing during the ejection and resolidification due to discharges. A few pock marks, caused by the entrapped gas bubbles reaching the surface, are also visible. This damage is limited to the final length (last mm) of the hole as the SEM photographs on entry and middle sections show a very smooth bright surface. This indicates that ECD occurring along the side gap has effectively removed the surface damage produced by the erosive effects of discharges. In the final mm of length of the hole the damage remains because the electrochemical action is lost due to lack of electrolyte. Microhardness readings in Table 3 do not vary significantly with depth from the machined surface. This is further evidence that there are no hardened layers left on the surface.

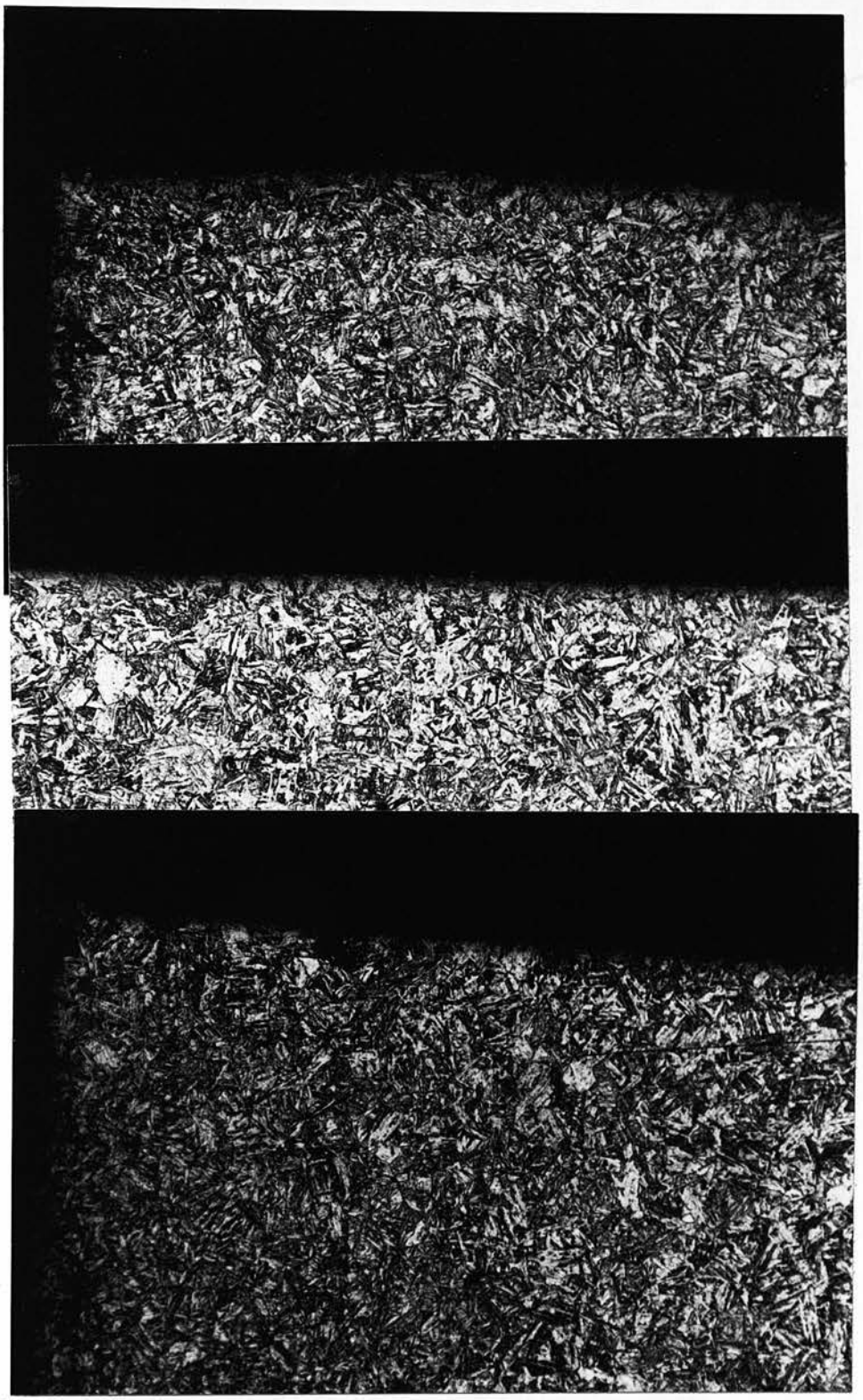

FIGURE 3.7 Photomicrographs of polished and etched Rex 535 specimens showing the subsurface region along the hole. (a)near drill entry × 320, (b) middle × 320, (c) near exit × 320

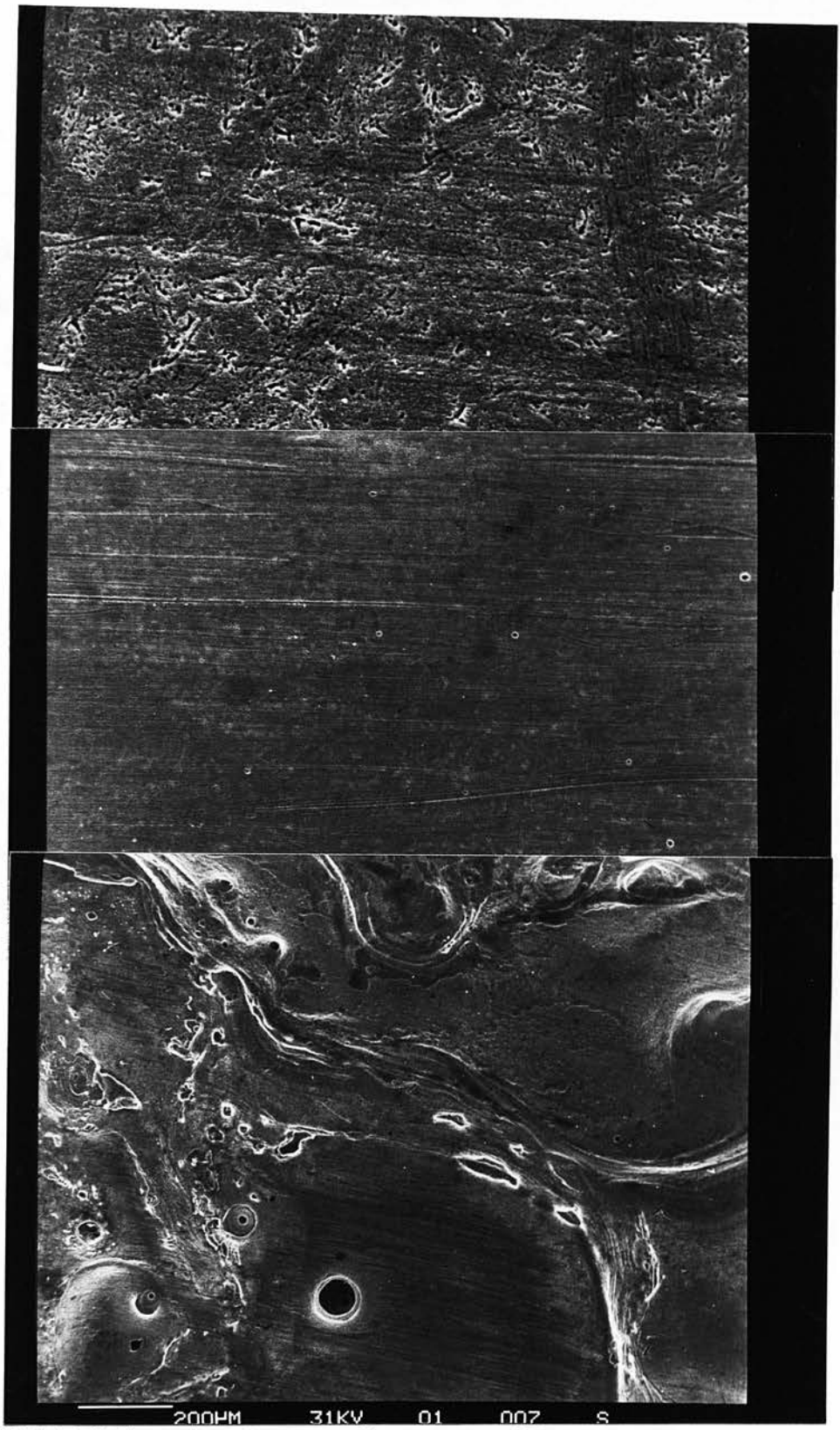

FIGURE 3.8 Scanning electron micrographs of Rex 535 specimens showing the drilled surface along the hole. (a)near drill entry × 500, (b) middle × 100, (c) near exit × 100

3.6.3 Low Alloy Steel

Surface effects revealed in optical micrographs of low alloy steel specimens in Figure 3.9 show tendencies very similar to that of Jethete (low carbon chrome steel) and Rex 535 (cobalt steel). The near-surface region along the hole exhibits no detectable signs of damage whatsoever except for last few millimetres, where typical EDM surface characteristics are apparent. The heat affected zone near the exit consists of several sub-surface layers, totalling a depth of about 50 μm. The substrate appears to have a much finer grain structure than the matrix, which can be attributed to melting and rapid resolidification. There is also evidence of a dark etched band.

Scanning electron micrographs of the drilled surface in Figure 3.10 substantiate the evidence that electrochemical dissolution occurring along the side gap has effectively eliminated any damage due to electric discharges along the hole except for the exit end. However, some preferential grain boundary attack was noted in some areas. Once again, no hardened layers can be detected from the microhardness values in Table 3.1.

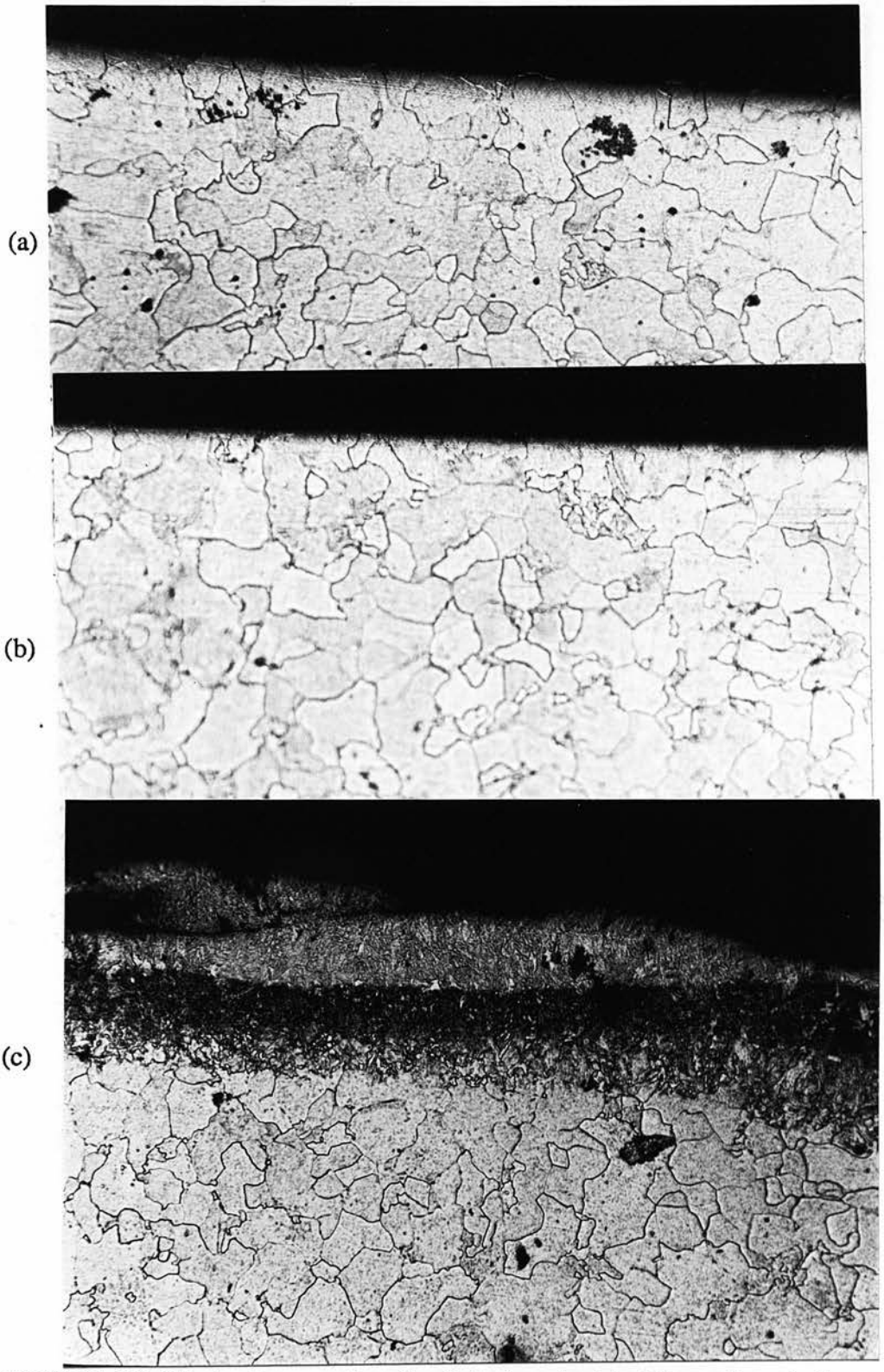

FIGURE 3.9 Photomicrographs of polished and etched low alloy steel specimens showing the subsurface region along the hole. (a)near drill entry × 640, (b) middle × 640, (c) near exit × 640

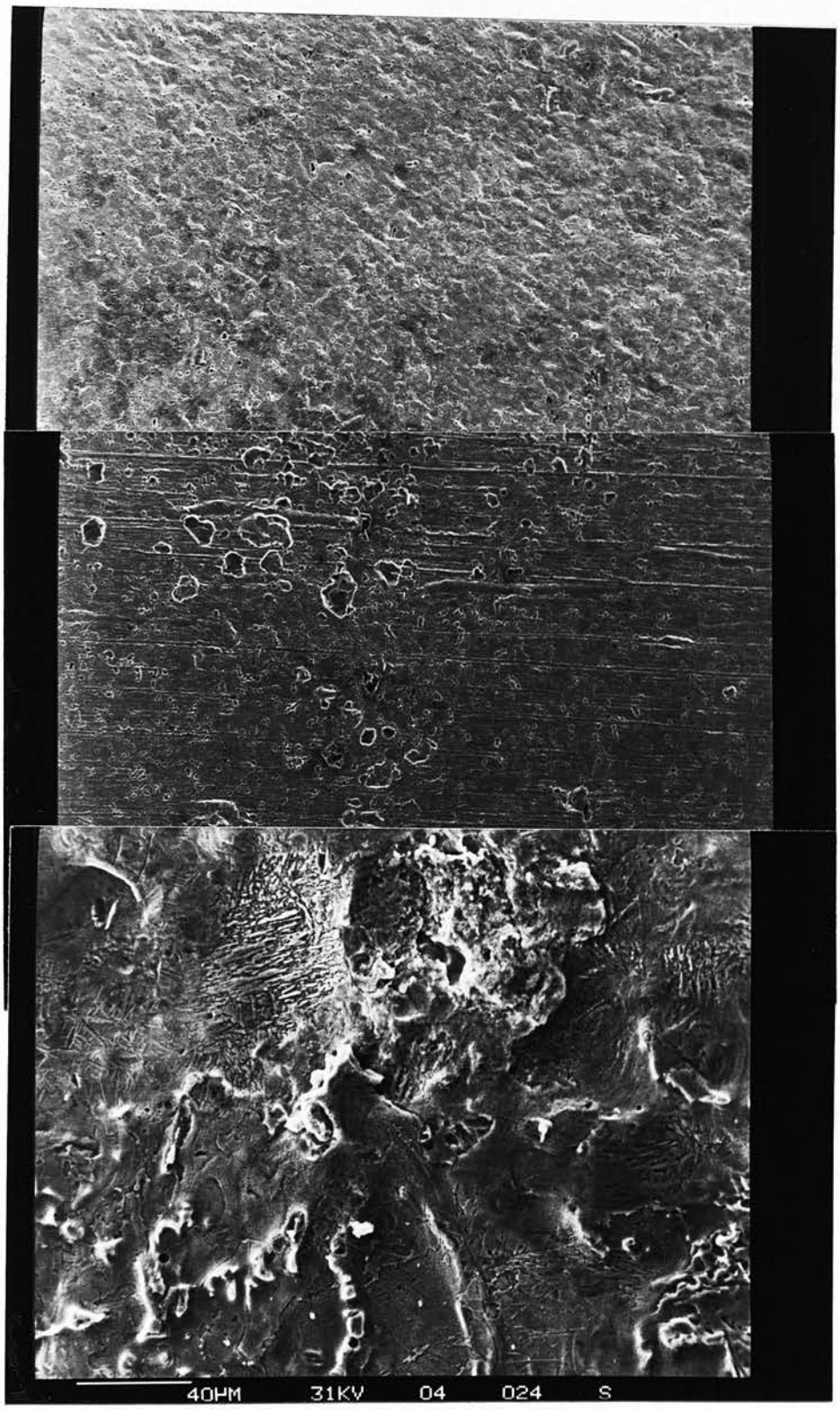

FIGURE 3.10 Scanning electron micrographs of low alloy steel specimens showing the drilled surface along the hole. (a)near drill entry × 100, (b) middle × 100, (c) near exit × 100

3.6.4 Nickel Alloy (Incoloy 901)

As the photomicrographs in Figure 3.11 show, the sub-surface region exhibits virtually no alterations except for a slight undulation, along most of the hole. Neither grain recrystalisation nor precipitation can be found. However, towards the exit some damage to the near surface region can clearly be seen (Figure 3.12). A fused-redeposited layer of about 20 μm average thickness, with heavy microcracking was also observed. The microcracking has penetrated through the substrate layer to the grain boundaries thus causing grain boundary cracking. The damage was not confined to the exit end but spread almost from the middle of the hole. This form of damage is attributed to prolonged, stationary arc discharges occurring at the side gap. The damage caused by the severity of these discharges is too intense for the electrochemical phase to "cure". From microhardness readings given in Table 3 no evidence of hardened layers can be detected.

Scanning electron micrographs of the actual surface in Figure 3.13 shows that preferential grain boundary attacks have occurred at some areas near the entry. At the exit, the surface appears to have typical electrodischarge induced surface characteristics, such as melted and resolidified layers, with overlapping craters.

The undulations may be due to an enhanced crevice corrosion, possibly due to stray current attack, more than off-setting the smoothing effect usually associated with the electrochemical process. Other factors which may influence the roughness of the electrochemically machined surface include the varying dissolution rates of the different phases present.

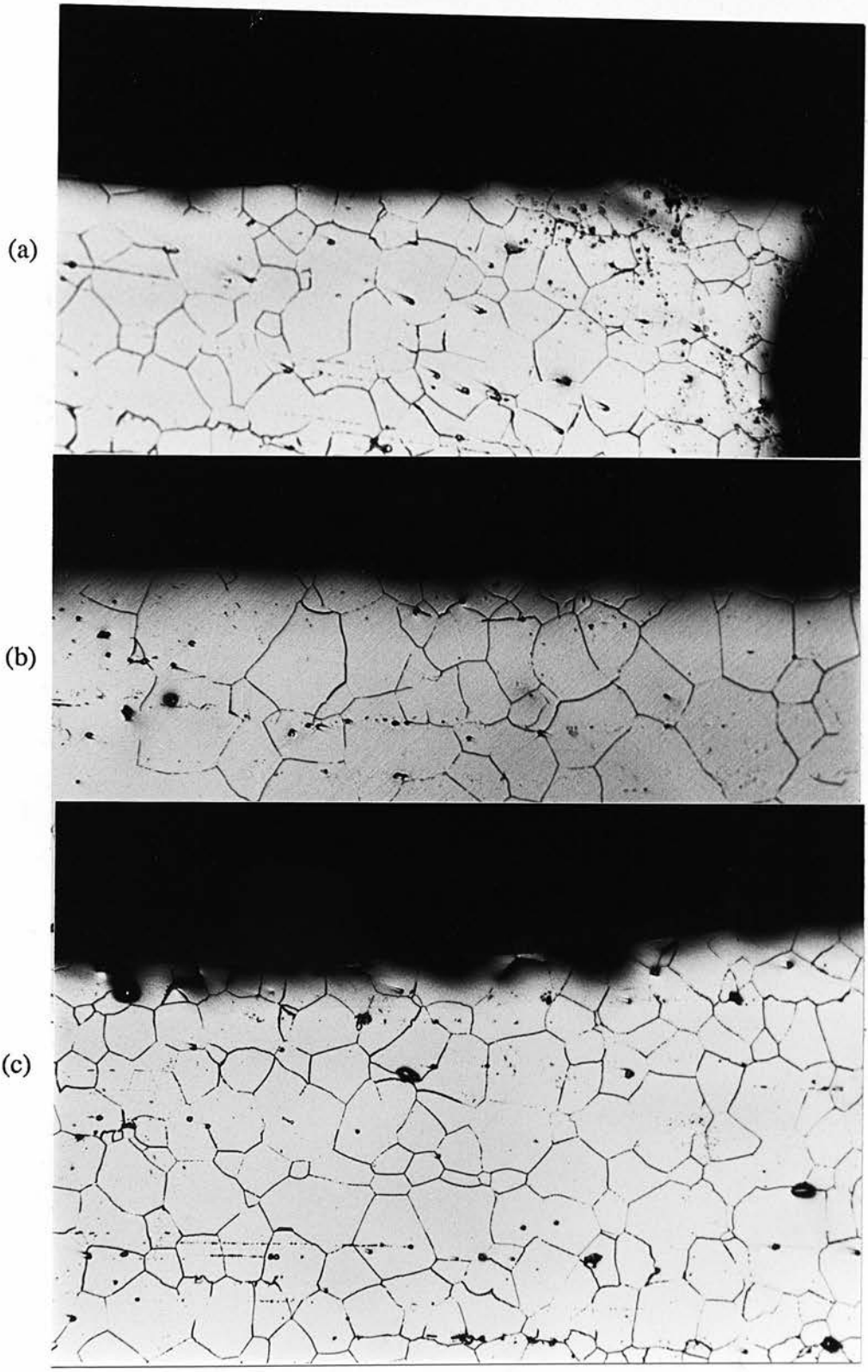

FIGURE 3.11 Photomicrographs of polished and etched Incoloy 901 specimens showing the subsurface region along the hole. (a)near drill entry × 320, (b) middle × 320, (c) near exit × 320

(a)

(b)

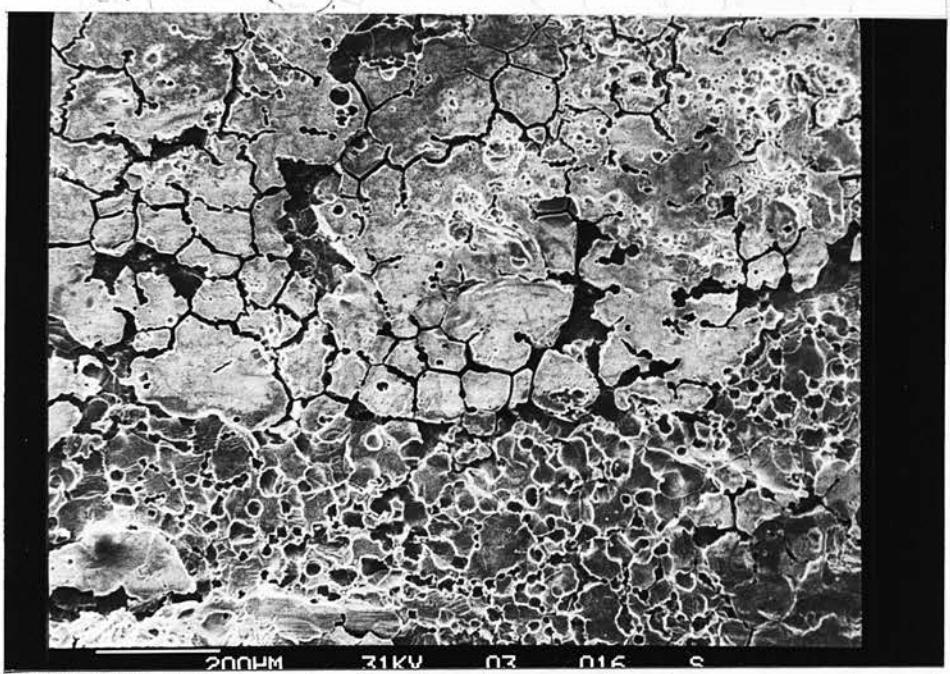

FIGURE 3.12 Micrographs showing damage due to severe prolonged arc discharges in Incoloy 901. (a)optical micrograph showing the subsurface region ×320 (b) scanning electron micrograph showing the machined surface × 100

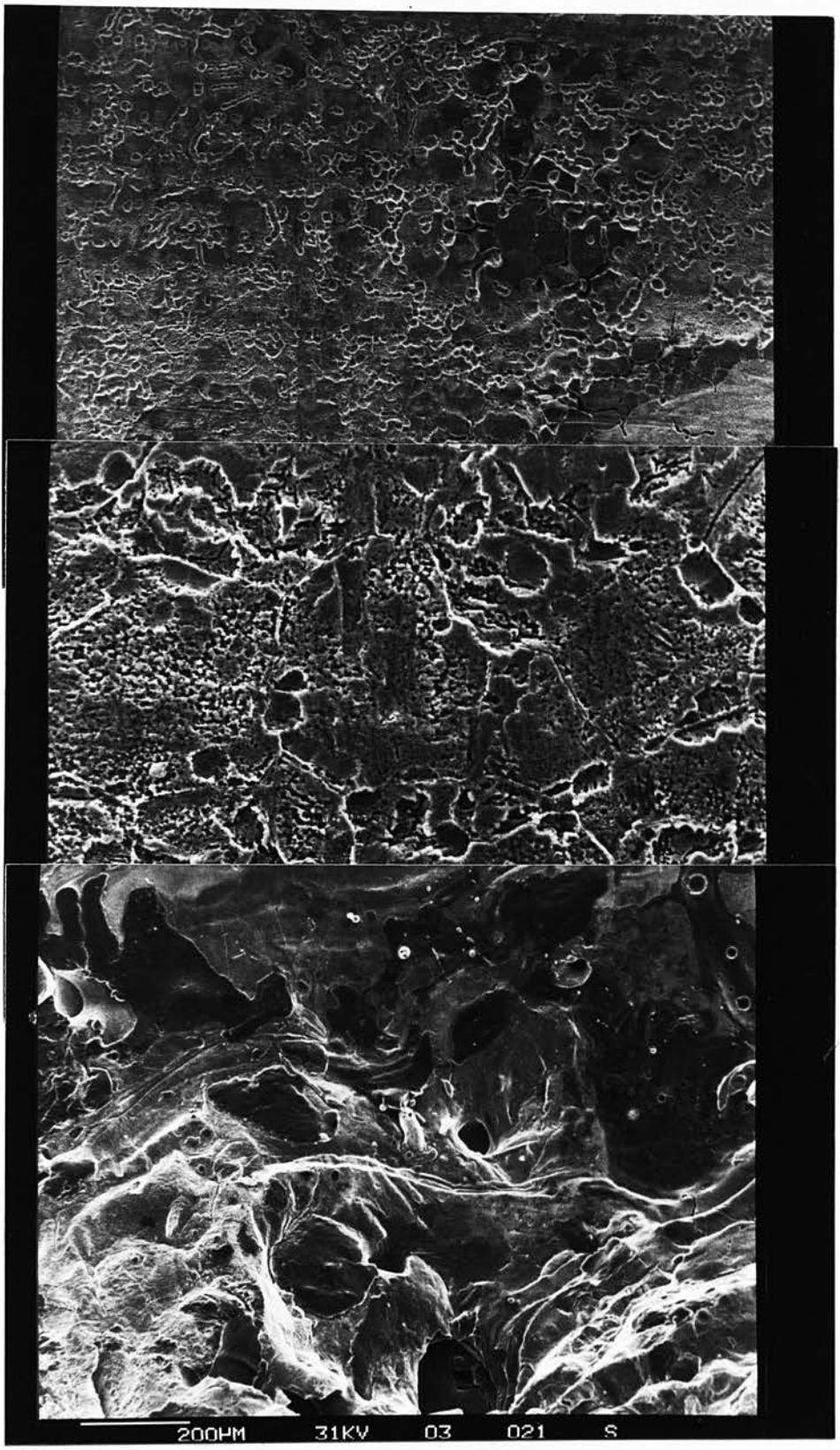

FIGURE 3.13 Scanning electron micrographs of Incoloy 901 specimens showing the drilled surface along the hole. (a)near drill entry × 100, (b) middle × 500, (c) near exit × 100

3.6.5 Titanium

Unlike the other four materials, micrographs of titanium in Figure 3.14 illustrate considerable amount of damage to the surface. The damage is consistent along the entire length of the hole, whereas in the other materials it is confined only to the exit end and to the occasional localised areas where severe, prolonged discharges have occurred. An irregular spattered layer with heavy microcracking can be seen. The surface profile along the hole was very uneven and rough. Further evidence of irregularities can be seen in scanning electron micrographs of the drilled surface (Figure 3.15). Grain boundary cracking, overlapping craters and adhering globular particles are all apparent. It appears that the surface of titanium has undergone a phase transformation from α aligned to α Widmanstatten,[1] has occurred due to the rapid cooling. In effect, the surface integrity of ECAM drilled titanium is very similar to that of EDM. A hardened layer between 100 - 250 μm depth from the drilled surface is evident from microhardness readings in Table 3.1.

All these surface effects in titanium can be attributed to the formation of a tenacious oxide layer in water based electrolytes, which inhibits the electrochemical dissolution of the material. This lack of ECD phase is evident from the reduced current observed. The damage caused by the erosive effect of the discharges thus remains. Successful electrochemical machining of titanium has been achieved using methanoic or formamide based solution of electrolyte by Bannard (**44**). ECAM drilling of titanium using non-aqueous electrolytes may hence yield a better surface finish by improving the ECD at the side gap which would remove the discharge induced damage.

---

[1] A description of the titanium structure and the phases can be found in Driver (**43**).

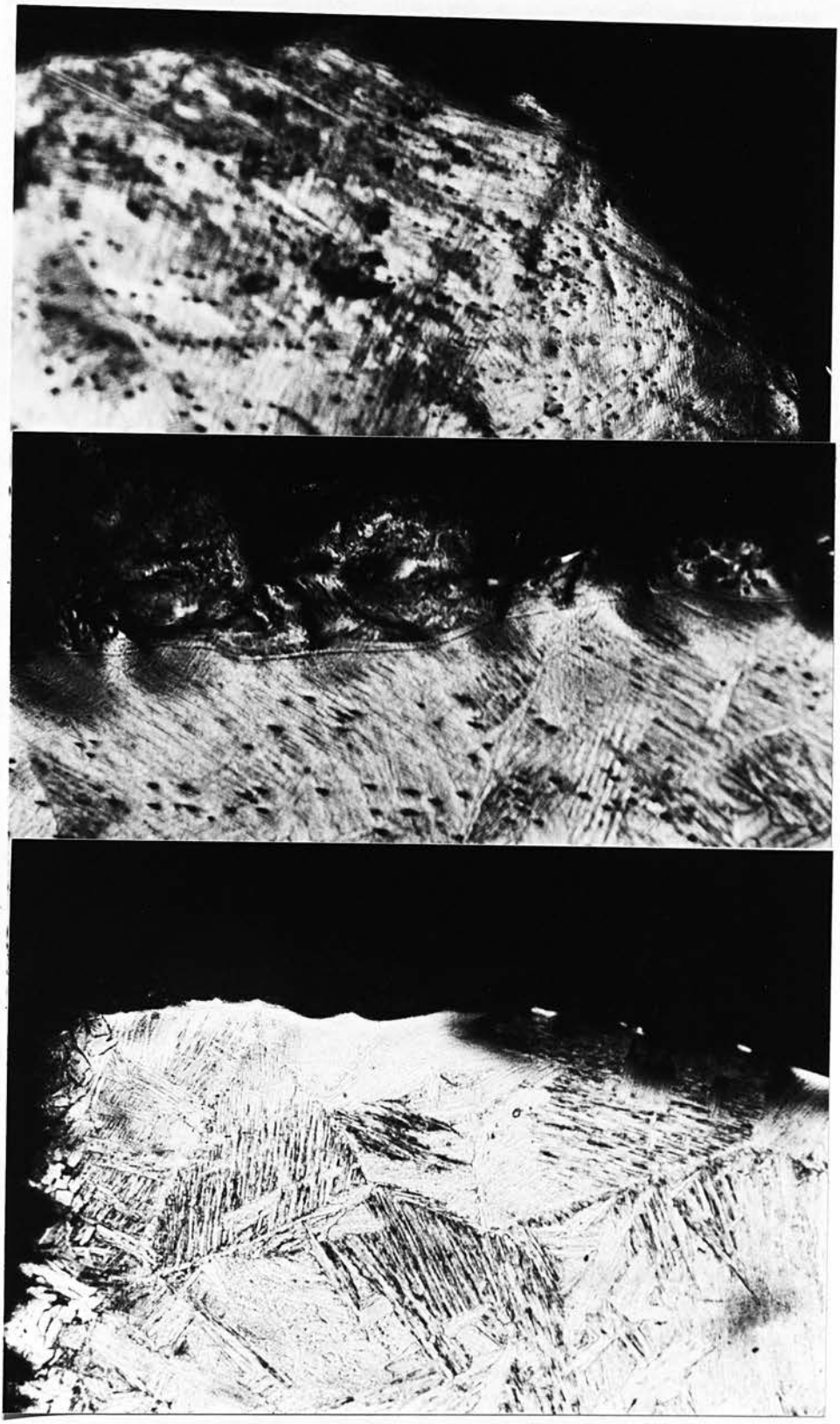

FIGURE 3.14 Photomicrographs of polished and etched titanium specimens showing the subsurface region along the hole. (a)near drill entry × 320, (b) middle × 320, (c) near exit × 320

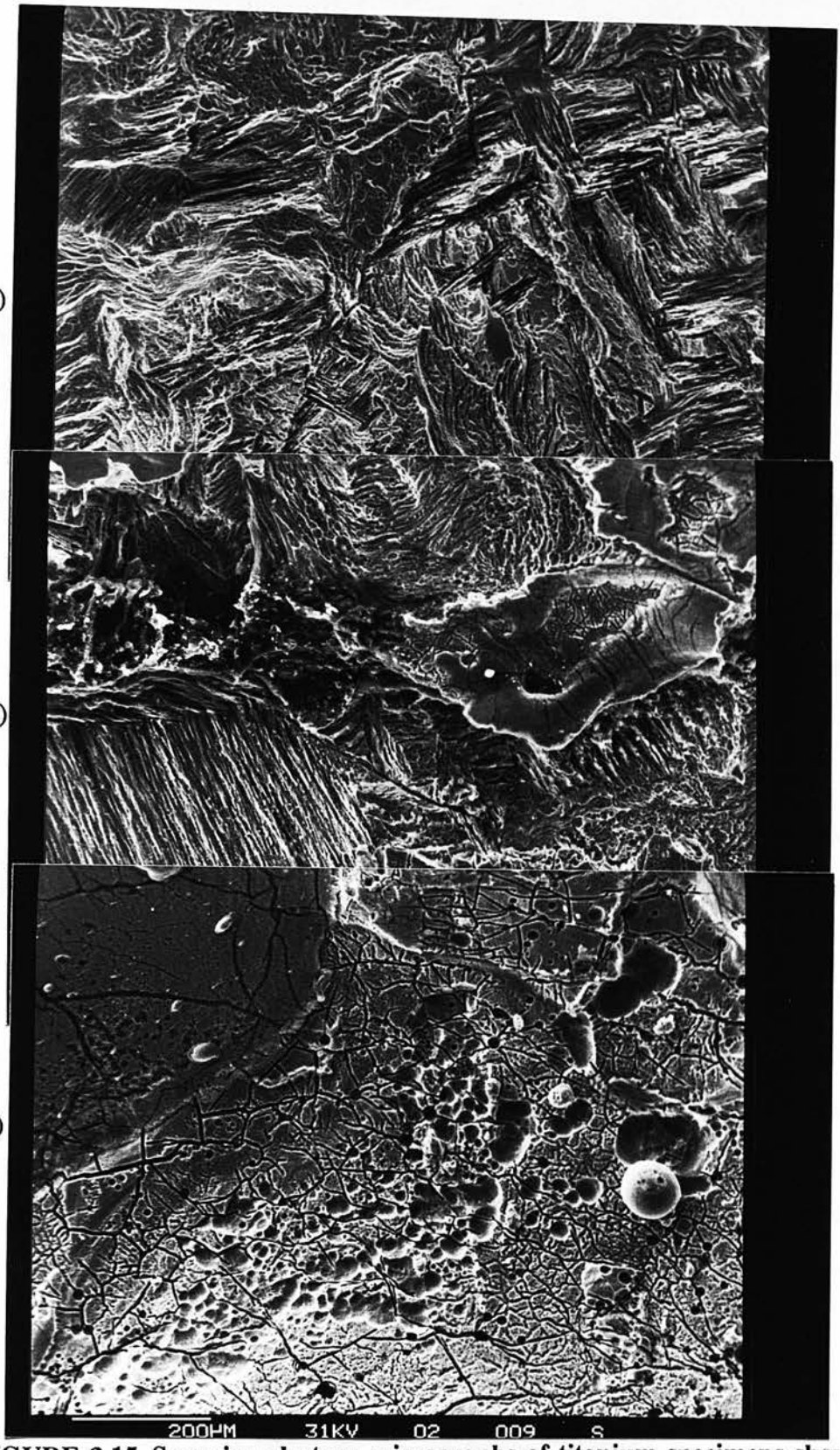

FIGURE 3.15 Scanning electron micrographs of titanium specimens showing the drilled surface along the hole. (a)near drill entry × 100, (b) middle × 100, (c) near exit × 100

3.7 Summary

Microscopic and microhardness examinations were performed to evaluate the surface integrity of electrochemical arc drilling (ECAD) on five different metal alloys.

Optical and scanning electron microscopy revealed similar surface effects in all but titanium. Jethete (Low carbon - high chrome steel), Rex 535 (Cobalt alloy steel), Inco 901 (nimonic alloy) and low alloy steel (1/2% Mo, 1% Cr) exhibited a smooth ECM surface finish along most of the hole. It can be said therefore, that for these four materials, the right balance of EDE to ECD had been achieved to give a smooth, damage free surface finish. However, there were some undesirable effects present at the exit end and also at occasional localised regions.

The damage at the exit, which was due to the lack of ECD there, could have been eliminated completely if an additional metallic extension was used, which would be discarded after the drilling operation. This would have prevented the electrolyte loss there, and enabled the occurrence of ECD.

The damage due to severe prolonged arc discharges appeared in the form of large localised craters, microcracks and recast layers in Incoloy 901. The ECD phase was not sufficient to remove these surface effects. If these localised damaged zones were to be removed by increased ECD action, a reduction in feed rates would be necessary. This in turn would cause large tapers and overcuts giving poor dimensional accuracy. On the other hand, by preventing the formation of these abnormal discharges this type of damage could be avoided. To do this, some form of monitoring and control of the discharges would be necessary.

The surface integrity of ECAD on titanium was very similar to that of EDM. A rough and irregular surface with heavy microcracking, spattered material and recast layers was observed. The surface quality of titanium could possibly be

improved by using non-aqueous electrolytes, thus avoiding the formation of the tenacious oxide layer which prevents the electrochemical dissolution of the damaged layers.

4 : ANALYSIS OF GAP PHENOMENA IN ECAM

4.1 Introduction

This chapter deals with a qualitative analysis of the inter electrode gap phenomena that occurs in ECAM. It explains briefly the fundamental physical characteristics of electric discharges and how they occur in electrolytes. Then it goes on to describe the different discharge types which are possible in ECAM and how to differentiate between them by the radio frequency emission from the gap. The experimental apparatus together with the instrumentation for monitoring the gap situation is described next. Waveforms of voltage, current and the radio frequency signal are presented, which identify the different gap phenomena that occurred in ECAM.

4.2 Electric Discharge Mechanism

Full theoretical analysis of the discharge mechanism involves complicated discharge and plasma physics which is beyond the scope of this thesis. Therefore only a brief outline of the discharge mechanism is given here. The breakdown of a gaseous gap by an electric field is, for moderate and high pressures, usually associated with the appearance of an electric discharge. The essential characteristic of a discharge breakdown is that of a fast, non-steady, irreversible transition from a very low to a very high current state.

On application of an electric field to two metal electrodes separated by an insulating medium, the breakdown of the dielectric would occur if the applied field exceeds the dielectric strength of the medium. It is well known that for a gaseous discharge the breakdown proceeds through the following stages(**45**):

(1) The production of free electrons in the gap, for example, the emission of electrons by the cathode surface known as the cathode phenomena.

(2) The subsequent acceleration of the electrons by the electric field and their retardation by inelastic collisions with atoms.

(3) The multiplication or accumulation of charged particles due to collision ionisation by energetic electrons, resulting in the development of an electron avalanche.

(4) The formation of the plasma channel.

(5) The transition to the visible discharge.

4.2.1 Breakdown Theory of Liquids

The theories dealing with the discharges in liquids are mainly concerned with the dielectric liquids. Even these are still not fully comprehended due to the complex nature of the liquid molecular structure. The theories so far put forward can be divided into two main streams.

a) The first assumes that an avalanche process of ionisation takes place in the liquid medium, as it is known to occur in gases and solids.

b) The second claims that the presence or the creation of agents of another phase - a gaseous one, is necessary for the breakdown to occur.

Both theories have their strong advocates. Watson and Sharbaugh (**46**) proposed that the breakdown resulted from the formation of a vapour bubble, which was extended until the gap was bridged with a vapour channel of low electric strength, since no α-ionisation (electron impact ionisation) process was evident from pulse conduction experiments in hexane at fields up to 1.3×10^8 V/m. The formation of the bubble was considered by them to be due to Joule heating caused by high current densities at the tips of asperities on the cathode. Since

energy densities may be as large as 10^{13} watts/m^3, local vapourisation of the liquid could occur in times as short as a few microseconds.

An alternative theory offered by Kao and Highman (**47**) for gas free liquids suggests that the bubble is formed, not from the gases in solution or adsorbed on the electrode surface, but as a result of the dissociation of the liquid molecules by energetic electrons.

However, Frei et al(**48**) support the breakdown hypothesis based on the electron multiplication process in the liquid phase since no simple explanation of their observed data can be given if breakdown was controlled by the presence of gaseous cavities. Nevertheless, this theory still has to allow for a transition from liquid to gas phase at a given stage of the discharge, since an arc is eventually formed.

Heuvelman et al(**49**) in a study of EDM have considered whether breakdown of a dielectric can be described by a mechanism similar to that for a gaseous breakdown, i.e. by collisional ionisation of the molecules. They suggest that the mean free path in liquids is such that electrons accelerated under the applied field cannot gain sufficient kinetic energy to cause ionisation. The authors conclude that local heating of the liquid causes the vapour bubble to expand rapidly and the breakdown to spread across the whole gap. Furthermore, the pressure dependence of the breakdown mechanism is taken as evidence that transition to a gaseous phase occurs before ionisation begins.

4.2.2 Electric Discharges in Conductive Liquids

Most of the published research involving discharges in conductive fluids has been concerned with avoiding them during ECM. The application of an electric field to a pair of electrodes separated by a conductive fluid would merely result in a

steady flow of current through it. Since the solution is already ionic, no breakdown phenomena leading to electric discharges can be expected. If however, some insulating substance is present in the gap, bridging it, then the formation of electric discharges is possible. The findings of Louterel and Cook(**50**) and Larsson and Baxter(**51**) into discharges during ECM suggest that they occur through the regions of localised gas or vapour produced. This theory is also supported by Kubota(**20**) who investigated the formation of discharges in electrochemical discharge machining (ECDM), a very similar process to ECAM. Further evidence that discharges in electrolytes occur through localised regions of gas bubbles is put forward by Crichton(**24**) in his study of single discharges in ECAM. Both Kubota(**20**) and Crichton(**24**) state that discharges are also possible between the electrode and the electrolyte.

4.3 Gap Phenomena in ECAM

In ECAM, the inter-electrode gap is filled with a highly conductive electrolyte. The gap phenomena which occurs is described below with the aid of illustrations of the gap shown in Figure 4.1.

Initially, a potential difference across the gap would cause an electrochemical cell to be set up. The reaction at the anode would be for the metal to dissolve into the solution as anions, releasing electrons. At the cathode, these electrons combine with the hydroxide ions which exist in the aqueous solution to generate hydrogen gas (Figure 4.1(a)). If the volume of gas generated is sufficient and is not flushed away from the gap, then it can form an insulating bridge between the anode and the cathode (Figure 4.1(b)). The Joule heating effect would cause the elongation of this gas bridge.

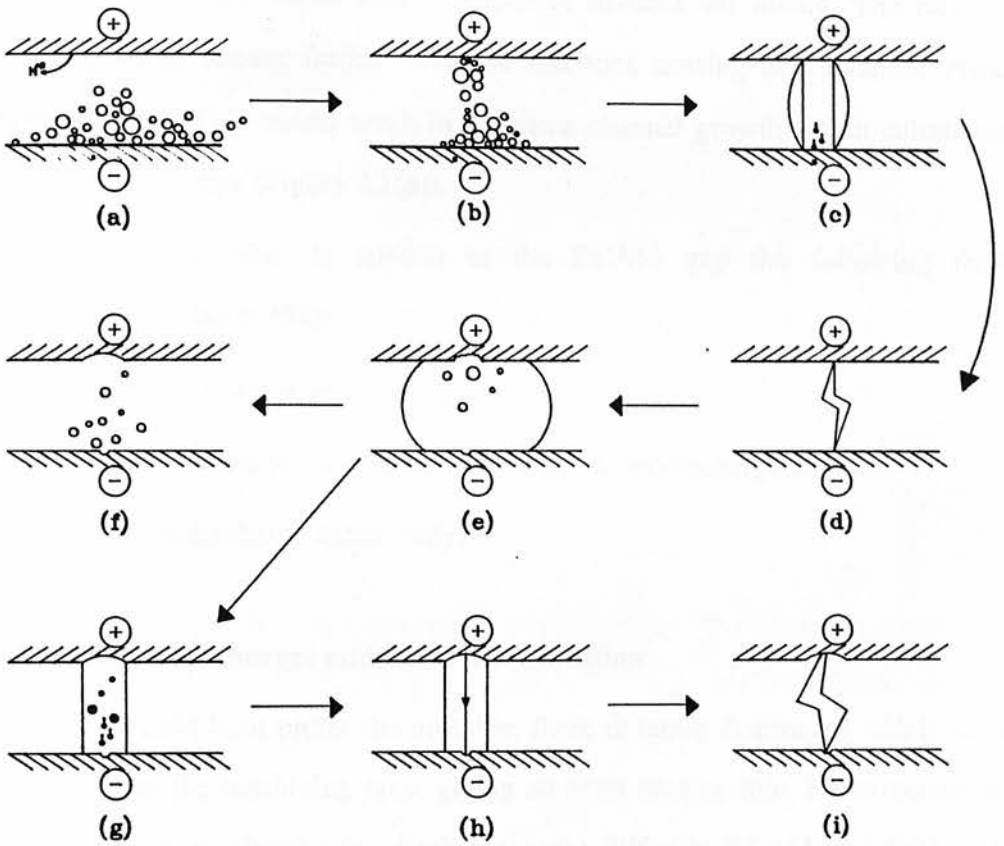

(a) metal dissolution at anode and hydrogen evolution at cathode
(b) gas bubbles bridging the gap
(c) elongation of the gas bubble and the electron emission from the cathode, leading to an electron avalanche
(d) occurrence of a visible discharge
(e) melting and evaporation of metal with explosive collapsing of the the vapour channel
(f) complete deionisation of the channel
(g) plasma channel not fully deionised
(h) Next current pulse flows along the same path.
(i) Stationary, abnormal arc.

FIGURE 4.1 Gap phenomena in ECAM

If the applied electric field across this gas channel is large enough, the breakdown process leading to an electric discharge would then occur. Firstly, the cathode would emit electrons which start accelerating towards the anode. The electron collisions would release further electrons and ions causing an avalanche effect (Figure 4.1(c)). This would result in a plasma channel growth which culminates in a visible discharge (Figure 4.1(d)).

When a voltage pulse is applied to the ECAM gap the following three phenomena may occur (**52**):

a) electrochemical reaction only.

b) electrochemical reaction followed by electrodischarge action.

c) electrodischarge action only.

4.3.1 Types of Discharges and Their Classification

ECAM and EDM both prefer the unstable, finite duration discharges which occur randomly over the machining area, giving an even erosion rate. Nevertheless the definitions used to classify the discharge types differ in ECAM and EDM. In EDM, the preferred discharges are normally referred to as "*sparks*". The energy of the EDM sparks is limited by the considerations towards the surface integrity because the surface roughness and the heat affected zone increase with increasing discharge energy. However, in ECAM one can afford to use much higher energy discharges (longer duration and higher current) than EDM. This is made feasible by the electrochemical dissolution action which smoothes out the craters and reduces the heat affected zone formed by the discharge erosion mechanism. Since ECAM discharges are of much higher energy than EDM ones, they are normally referred to as "*arcs*".

The characteristics of EDM sparks and ECAM arcs are similar nonetheless. One essential characteristic being that of a fast, non-steady, irreversible transition from a very low to a very high current state. The external circuit, i.e. the pulse generator, does not usually allow this discharge to achieve its quasi-stable state. Therefore the life of a discharge is curtailed after a certain period (determined by the pulse on time).

When a discharge extinguishes, the conducting channel begins to deionise by recombination of the charged particles until a complete insulating bridge is formed (Figure 4.1(f)). This should be achieved before the start of the next voltage pulse. Then the next pulse would cause a discharge at a different location. If however, the channel is not fully deionised (Figure 4.1(g)), the current of the next pulse would preferably flow along the same path. This leads to a stationary discharge occurring in the same spot. These stationary discharges commonly known in EDM as "*arcs*", are defined in ECAM as "*abnormal arcs or discharges*". The characteristic of this stationary discharge is that it is a current maintained plasma.

These abnormal arcs are clearly very undesirable since they occur in the same spot causing severe damage to both tool and workpiece. This has already been demonstrated to be the case in Chapter 3. In order to prevent the abnormal discharges from occurring, they have to be distinguished from the normal ones. The obvious choice would be to monitor the voltage or the current waveforms. This has been done for EDM by several researchers (**53,54**). Snoey et al(**53**) have developed a pulse discriminator on the basis of voltage level and pulse duration. However, the difference between a normal and an abnormal arc is not very easily recognised by their voltage and current waveforms. This is because there are so many forms of normal discharges, some of which are quite close to abnormal

arcs(29). In ECAM the identification is made even more difficult because of the ECM element.

Bhattacharyya and El Menshawy (55) have found that the radio frequency noise emitted by the gap was significantly different for arcs and sparks in EDM. Their work revealed that when good machining was in progress, a very intense RF signal was recorded at about 30 MHz. However, when the process deteriorated due to continuous arcing, the RF level dropped considerably. This has enabled them to develop an adaptive control system for EDM machines which has been quite successful in preventing process deterioration due to continuous arcing. Xi et al (56) have used the RF emission from the EDM gap to monitor the performance of several machines simultaneously by utilising different bandwidths of the radiated spectrum. More recently, the RF monitoring technique has been used to optimise an EDM texturing process(57).

The RF monitoring technique has been applied to ECAM in order to identify the different discharge types by Wood(58). He demonstrated that the RF level was higher for sparks than it is for arcs in single pulse experiments. However, his findings cannot be extrapolated to multi pulse ECAM machining as the gap situation in multi-pulse machining is far more complicated than that of a single pulse.

4.3.3 RF Emission by Discharges

The following section analyses why and how normal discharges tend to emit much higher radio frequency noise levels than the abnormal, stationary discharges.

When a normal discharge is formed, it implies the formation of a high density plasma - which is the result of the ionisation of materials by blow-off electrons. It is well known that this type of nonequilibrium plasma tends to equilibrate by emitting electromagnetic radiation at the local plasma frequencies (59).

The collisions which occur in partially ionised gases involve relatively low densities of charged particles and low particle energies. The forces exerted between the colliding particles are short range forces. With increasing degree of ionisation, however, these short range forces are replaced by the long range electrostatic forces between ions and electrons. In these circumstances an electron may be deviated from its original path and accelerated, releasing a pulse of electromagnetic radiation. For the electron the collision has resulted in transition between two unquantised or free states and is known as a free-free transition being essentially an inelastic collision, the loss of energy appearing as loss of radiation.

Since the electrons move at random, energy is radiated continuously and over a wide band of frequencies and therefore is incoherent. In addition to this "bremsstrahlung", radiative collisions may occur following capture of an electron into a bound state.

In the case of an abnormal arc, very little ionisation results as the arc occurs along the previous plasma channel which is not fully deionised. In this context, abnormal discharge means steady current flow through a low impedance conducting path which has developed between the electrodes. Because the current path is continuous, the phenomena which would accompany a normal discharge are absent, and very little radiation is detected.

Abnormal discharges can be thought of as current maintained plasma, since they are maintained in existence by the passage of a steady current through them. In contrast to metallic or liquid conductors, such plasmas remain conducting solely by virtue of the current which is passed through them. If the current ceases for a long enough period the conductivity falls to zero because of loss of charge carriers by diffusion or recombination.

4.4 Experimental Apparatus & Procedure

For the reasons given below, it was decided to use a modified EDM machine for the purpose of monitoring and correlating the ECAM gap situation with RF emission.

1. The previous research in ECAM used a full wave rectified single phase power source. Each voltage pulse is of fixed duration (0.01 sec) and within it, several discharges may result. The duration of each individual discharge is very difficult to estimate. Therefore, the correlation of each discharge with either the voltage, the current or the RF emission is difficult. In square pulse power, the pulse duration is relatively short and can be set to any desired value 0 - 5 ms. Each pulse will result in one discharge only, making it very easy to monitor the discharges and correlate with RF emission.
2. Another reason for using an EDM machine was that it was capable of using a wide variety of workpiece and tool shapes. Since the abnormal arcing becomes more of a problem when larger surface areas are encountered, plane parallel electrodes of a relatively larger area were chosen for the experiments.

4.4.1 The Basic Apparatus

An EDM machine, "AGEMASPARK 740" was suitably modified as described below to carry out the experiments.

a) A tank made of perspex was incorporated to contain the electrolyte, thereby avoiding corrosion of the work table and the machine parts which was not designed to withstand corrosive fluids.

b) The control system of the EDM machine was altered, in order to machine in electrolyte.

c) At first, no gap-flushing was used. Later on a flushing system for the electrolyte was incorporated.

Figure 4.2 shows the apparatus together with the monitoring set-up.

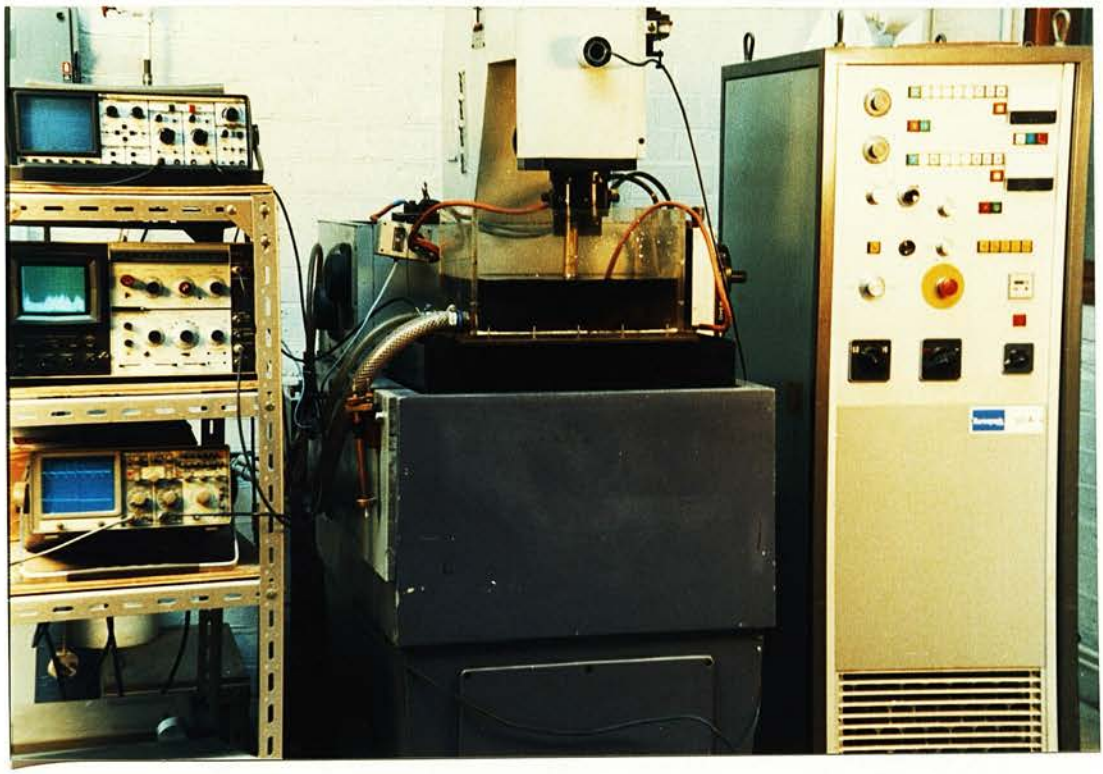

FIGURE 4.2 Experimental Apparatus and Monitoring Instruments

4.4.2 Adaptation of Agemaspark EDM Machine to Produce ECAM

The EDM machine is designed to work with non-conductive fluids such as paraffin, light oil or deionised water. The machining gap width in EDM is proportional to the gap voltage. In order to control the gap, the time averaged gap voltage (V_{gap}) is sensed and compared with a reference value (V_{ref}), the resultant error signal (V_{error}) is then applied to the controller, which is amplified and used to drive the output in a direction to reduce the error to zero. Figure 4.3 shows a schematic diagram of the control system. The operation of the servo control is such that:

1. when $V_{gap} > V_{ref}$ an open circuit is sensed which instructs the servo to feed the tool electrode towards the workpiece.
2. when $V_{gap} < V_{ref}$ a short circuit is sensed and the servo retracts the tool head.
3. when $V_{gap} = V_{ref}$ stable machining is indicated and the servo maintains the gap.

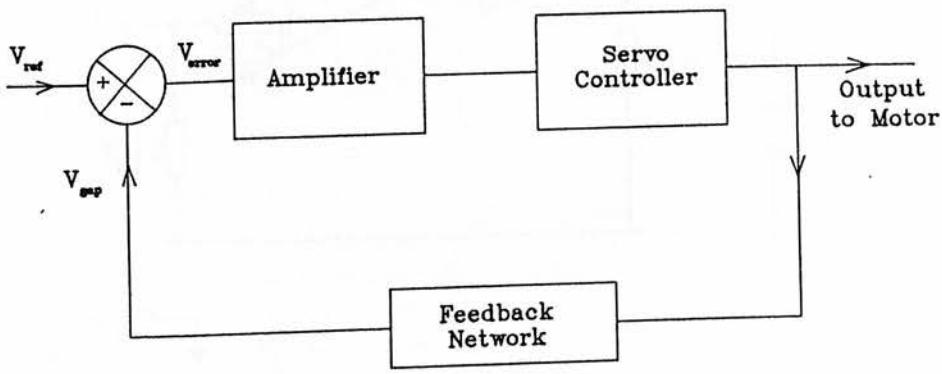

FIGURE 4.3 Schematic diagram of the EDM control system

When electrolyte is used, as soon as the tool touches the electrolyte an electro-chemical current begins to flow reducing the gap voltage below the V_{ref}. This indicates to the servo a short circuit, which then instructs the motor to retract the tool.

In order to machine in electrolyte, the reference voltage to the servo system must be changed. This was achieved by adjusting some variable resistors and also replacing some of the fixed resistors. The circuit diagram of the altered control system is shown in Figure 4.4. The reduction in the reference signal made it possible to achieve a gap width of 0.1 mm in electrolyte.

Some other EDM safety controls such as the limit switches for the dielectric level and the dielectric pump control were also disabled.

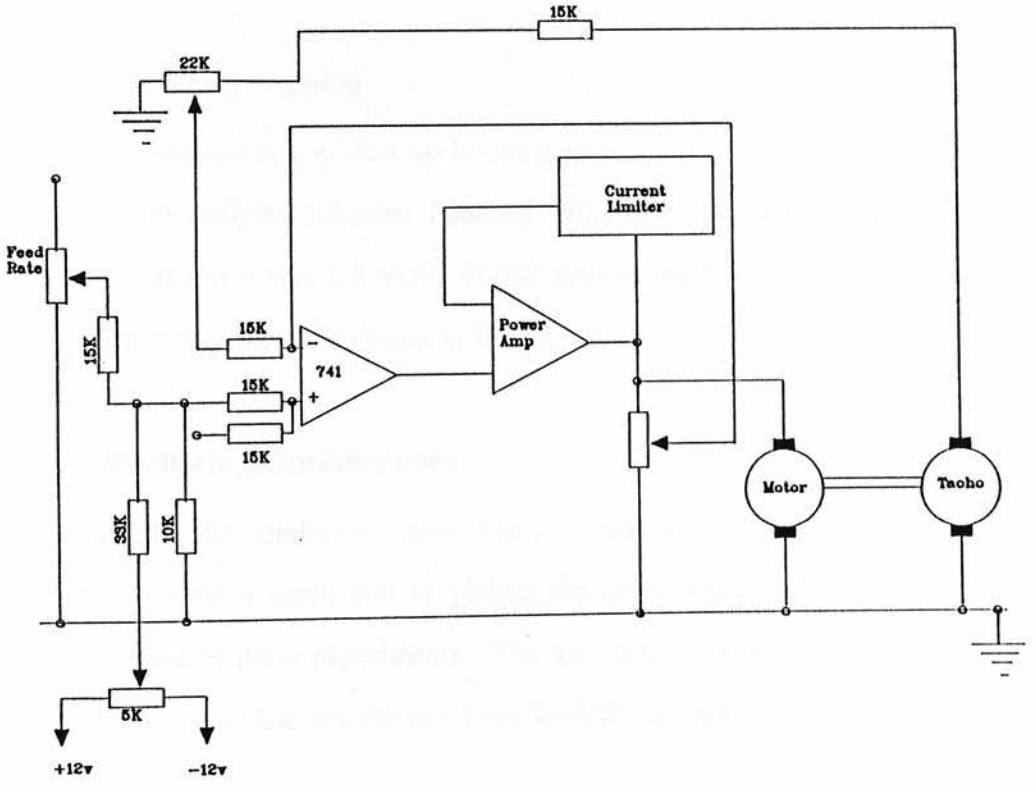

FIGURE 4.4 Circuit diagram of the modified control system

4.4.3 Monitoring & Instrumentation

The three variables monitored were, the gap voltage waveform, the gap current waveform and the RF emission.

1. *Gap Voltage*

   This was measured straight across the gap as shown in Figure 4.5 and observed via a digital storage oscilloscope.

2. *Gap Current*

   At the beginning, a non-inductive shunt similar to the one used by Crichton(**24**), was used to measure the current. However, this shunt proved incapable of handling high currents(50A) for lengthy machining periods. Hence a Hall effect transducer (*Heme 200*) was used as the current measuring device.

3. *Radio Frequency emission*

   The RF emission was picked up by an antenna, which was then received by a spectrum analyser (*Hewlett Packard 140/141*). The video output of the spectrum analyser was fed to the digital storage oscilloscope (*Nicolet 3690*). The monitoring set up is shown in Figure 4.5.

4.4.4 RF Monitoring Considerations

To pick up the RF emission, some form of transducer was necessary. El Menshawy(**54**) used a small coil to pickup the radio signals. Both a coil and dipole were tried in these experiments. The aim was to obtain as clear a signal as possible without undue interference from background sources.

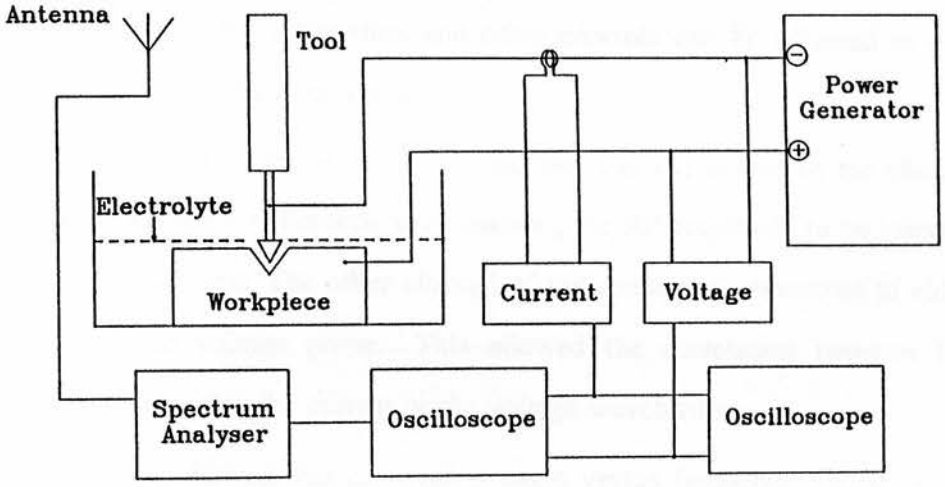

FIGURE 4.5 Gap monitoring set-up

The loop antenna gave better signals up to about 50 MHz. The dipole antenna was used to monitor the signals in the 50 - 110 MHz range. The dipole antenna was constructed using two telescopic radio aerials. This enabled the length of it to be varied to form a half wave element at the monitoring frequency. This facilitated the impedance matching between the antenna and the receiver. The antenna length ranged from 0.2 to 1.5 metres, giving a frequency range of 50 MHz and upwards.

The antenna was directly connected to the spectrum analyser via a short length of coaxial cable. The feeder length was kept short in order to minimise the losses caused by ohmic resistance and dielectric conductance.

The spectrum analyser is a superheterodyne (swept-tuned) receiver which provides a visual display of amplitude versus frequency, displaying the absolute value of Fourier components of a given waveform. The spectrum analyser can be tuned to any frequency in the range 1 - 110 MHz. Its scan rate, scan width, IF bandwidth, gain, RF attenuation and other controls can be adjusted to describe best the signals under observation.

The video output from the spectrum analyser was fed to one of the channels in the digital storage oscilloscope thus enabling the RF amplitude to be viewed as a function of the time. The other channel of the scope was connected to either the current or the voltage probe. This allowed the correlation between the RF waveform and either the current or the voltage waveforms.

Measurements showed that the field strength versus frequency varied depending on the position of the antenna. The electric field at an antenna is a vector sum of the direct field from the emitting source and the other fields which are reflected from nearby objects. If the position of the receiving antenna is changed, these fields arrive at the receiving antenna with phases changed, and the resulting vector is changed.

4.5. Results and Discussion

Initially experiments were conducted in stationary electrolyte (i.e. without gap flushing) to establish the feasibility of ECAM over relatively large areas. Different machining fluids from water to 10% sodium nitrate solution were used to see how the conductivity of the machining fluid affected the metal removal

mechanism. The tools used were 25 mm diameter brass rod and the workpieces were mild steel.

The machining rates for different machining fluids from deionised water to 10% sodium nitrate solution are given in Table 4.1.

TABLE 4.1 Machining rates in different electrolytes

Electrolyte Type	Current Density	Pulse Time On/Off	Metal Removal Rate	Tool Wear
	A cm^{-2}	µs	mm^3 min^{-1}	mm^3 min^{-1}
tap water(Edinburgh)	6.00	250/200	60.92	15.61
2% sodium nitrate	6.00	250/160	23.21	1.56
5% sodium nitrate	6.00	250/160	24.50	1.93
10% sodium nitrate	6.00	250/160	30.25	1.96

4.5.1 Tap Water

Although gas bubbles were observed to be forming around the tool, very little electrochemical dissolution of the anode occurred in tap water. Most of the applied pulses resulted in normal discharges for the conditions given in Table 4.1, indicating optimum machining conditions. It can be said that water (conductivity $0.125m\,\Omega^{-1}cm^{-1}$) acts as a dielectric rather than an electrolyte. After prolonged periods of machining, deterioration of the process occurred. Since no flushing was used this was mainly due to agglomeration of debris which lead to abnormal arcs.

The RF emission at 40 MHz picked up by the loop antenna is shown in Figure

4.6 together with the voltage waveform, when normal discharges were occurring. Figure 4.7 shows the RF level detected at 40 MHz and the voltage waveform when abnormal discharges were occurring. From figures 4.6 and 4.7, it can be seen that, although the voltage is not very different, the RF level detected is significantly different for normal and abnormal discharges. Furthermore, it is apparent from figure 4.8, that the RF level is very much less for a short circuit than for a normal discharge.

In tap water, basically four pulse types occurred : normal discharges, abnormal discharges, short circuits and open circuits.

From the waveforms presented in Figures 4.6 to 4.8, it can be seen that the RF level was considerably higher for the normal discharges than for any other pulse type. Therefore the RF signal can be used to differentiate between the pulse types in tap water.

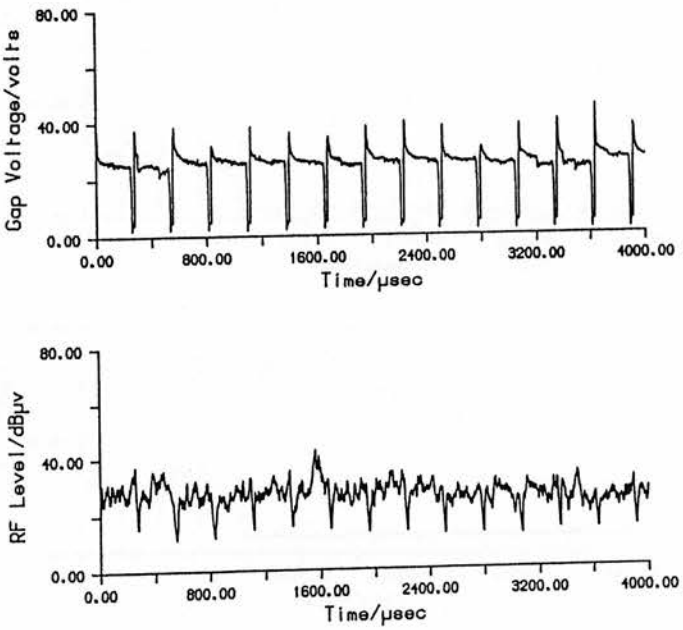

FIGURE 4.6 RF and voltage waveforms for normal discharges

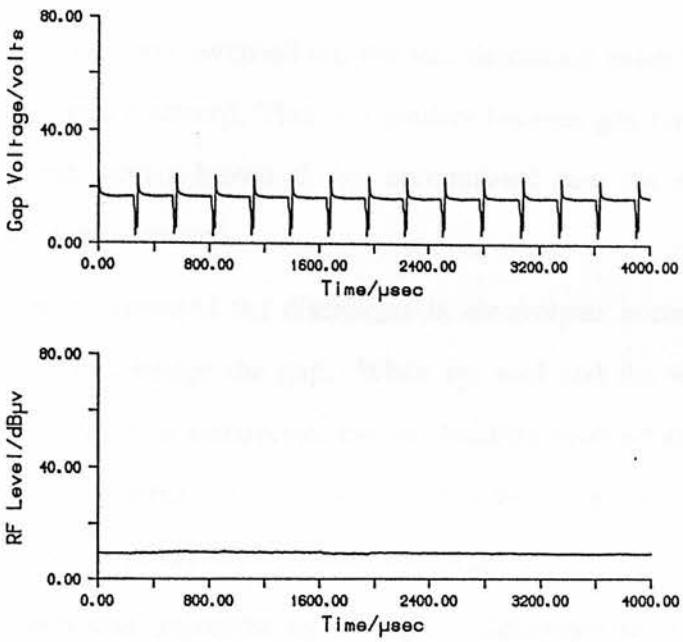

FIGURE 4.7 RF and voltage waveforms for abnormal discharges

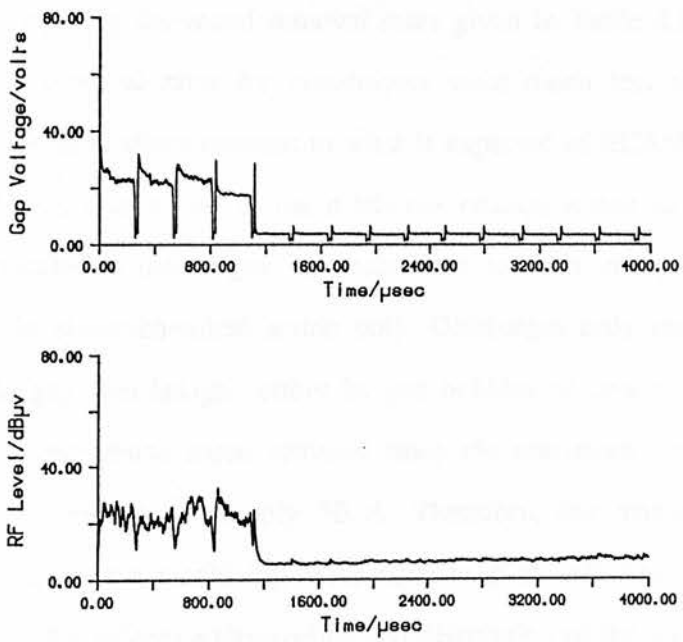

FIGURE 4.8 RF and voltage waveforms for short circuits and normal discharges

4.5.2 Electrolyte

When the power was switched on, the tool descended towards the workpiece and ECD action was observed. This was evident because gas bubbles were generated at the cathode and a brown sludge accumulated near the anode. However, no discharges were observed.

As previously discussed the discharges in electrolytes occur mainly through the gas bubbles that bridge the gap. When the tool and the workpiece were completely submerged in electrolyte, the gas bubbles evolved at the cathode, rose to the surface due to the effects of surface tension acting upon them. Thus, very little gas remained in the gap to cause discharges.

This problem was overcome by having the electrolyte level just above (no more than 2mm) the workpiece surface. This made the bubbles remain in the gap, which in turn, resulted in discharges.

When comparing the metal removal rates given in Table 4.1, it can be seen that the metal removal rates for electrolytes were much less than for ordinary tap water. This is in sharp contrast to what is expected of ECAM. In water the metal removal was totally due to the discharge erosion action as almost all the input pulses resulted in discharges. In electrolytes however, many of the applied pulses resulted in electrochemical action only. Discharges only resulted when the inter electrode gap was bridged either by gas bubbles or debris. The ECD pulses did not yield very much metal removal since the maximum current obtainable with the EDM generator was only 50 A. Therefore, the maximum current density achievable, for the machining areas concerned (5 cm^2), was 10 Acm^{-2}, which was inadequate for effective electrochemical dissolution of the anode.

With increasing electrolyte concentration, the metal removal rate increased slightly (Table 4.1). The higher conductivity resulted in higher current density,

thereby giving increased electrochemical dissolution of the anode. This also lead to more discharges since more gas was generated as a result of the increased ECD rate.

There was a considerable amount of stray electrochemical attack due to the high applied voltage (95 volts). This voltage could not be lowered as the EDM generator had it at a fixed level. The high voltage also resulted in severe sparking giving large craters. Obviously, the EDM power source is not suitable for ECAM. However, it can still be used to observe the ECAM gap phenomena.

The general observations of the ECAM pulse trains suggest that within each applied pulse, any one of the following phenomena may occur:

a) electrochemical action only

b) electrochemical action followed by normal discharges

c) normal discharges

d) abnormal discharges

e) short circuits

Open circuits were absent as some electrochemical current flowed even with larger gaps, although very little metal removal occurred.

At first, only ECD occurred. The waveforms of current and voltage when only ECD was present in the gap are shown in figure 4.9. As the gas bubbles started to accumulate in the gap, the voltage and current waveforms increased and decreased respectively, indicating increased gap impedance. When the voltage had risen sufficiently high, the breakdown of this high impedance gas channel occurred giving normal discharges. Figures 4.10 and 4.11 show the current and voltage waveforms illustrating the above gap condition. Several pulse types (ECD, ECD with normal discharges and normal discharges) which occur in the

ECAM gap can be seen from these figures.

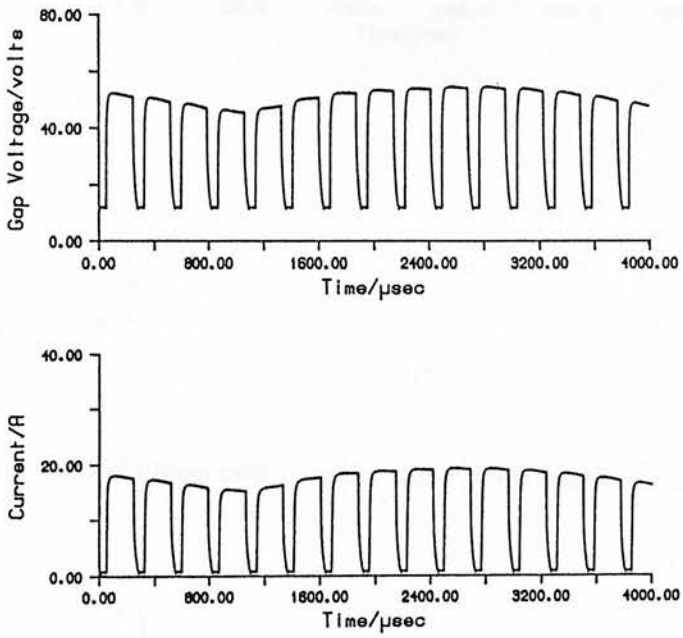

FIGURE 4.9 Voltage and current waveforms of ECD pulses

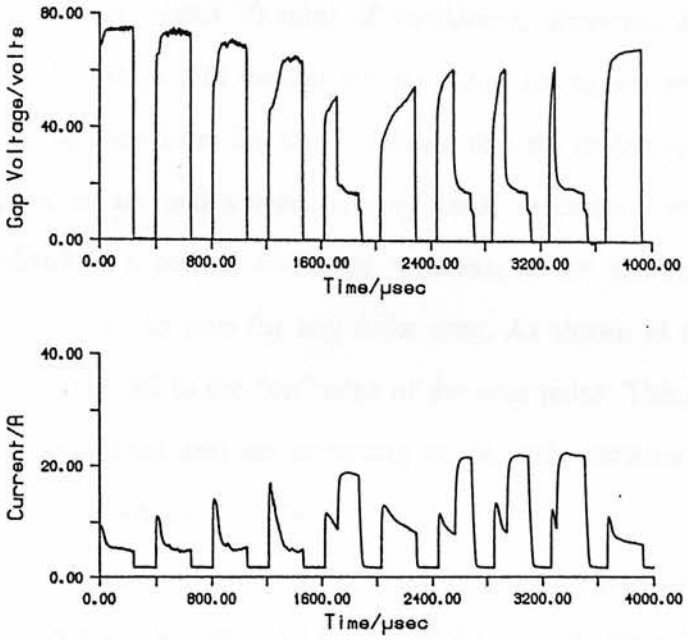

FIGURE 4.10 Voltage and current waveforms for ECD and normal discharges

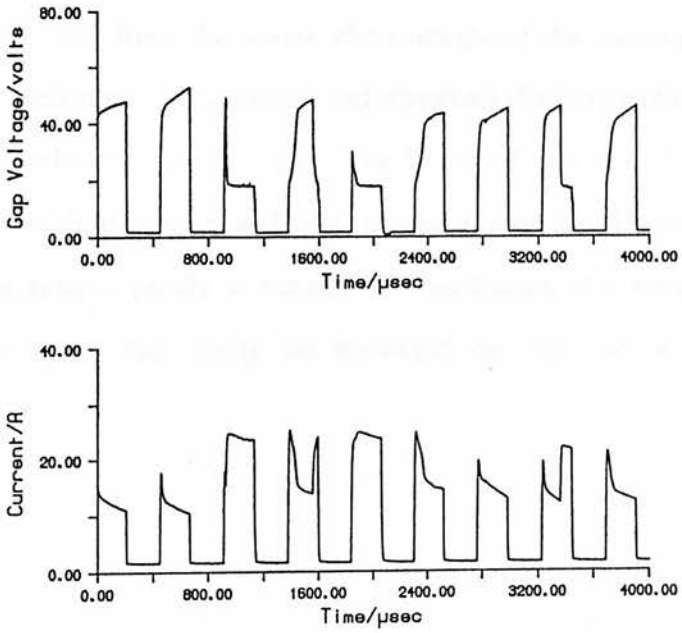

FIGURE 4.11 Voltage and current waveforms for ECD and normal discharges

After long periods (about 30 min) of machining, abnormal arcs occurred. The waveforms of voltage and current for abnormal arcing are presented in Figures 4.12. It can be seen from the above figures, that the difference in current amplitude between an arc and a spark is very small. However, the off-time is quite clearly defined in a normal discharge, whereas, in the abnormal arc the current does not approach the zero for any finite time. As shown in the figure the "off" edge tends to trail off to the "on" edge of the next pulse. This is indicative of the fact that the abnormal arcs are occurring in the same location due to the plasma channel not being deionised fully between the pulses.

The RF level detected at 40 MHz is shown to drop considerably from normal to abnormal discharges in figure 4.13. Figure 4.14 shows the RF level and the voltage waveform observed for abnormal arcs leading to short circuits. Abnormal arcs leading to ECD pulses, can be seen in Figure 4.15. Finally, figure 4.16 gives the current and the RF levels for normal discharges and ECD pulses.

What can be said from the above observations of the current, voltage and RF emission waveforms is that normal and abnormal discharges can be differentiated by the RF emission from the gap. The RF level was also low for other pulse types, such as short circuits and ECD pulses. Hence the RF level can be utilised in a control system, purely to indicate the occurrence of normal discharges. The other pulse types can easily be identified by the current and the voltage waveforms.

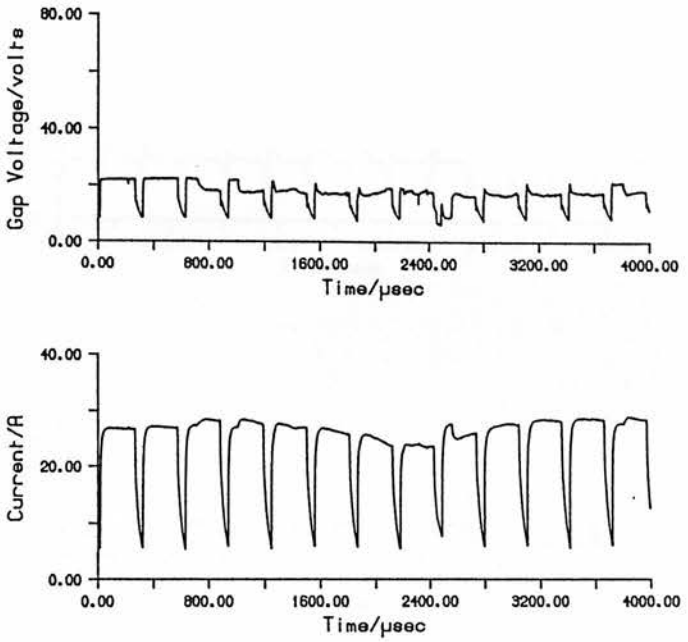

FIGURE 4.12 Voltage and current waveforms for abnormal arcs

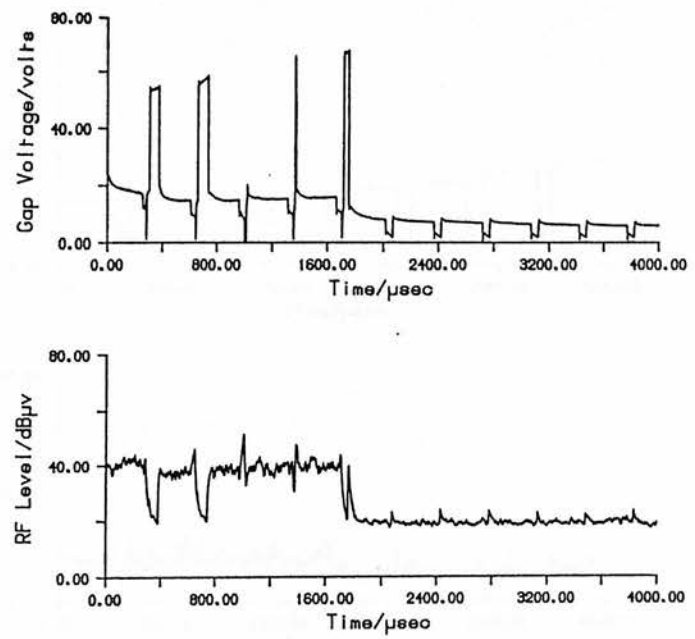

FIGURE 4.13 Voltage and RF waveforms for normal and abnormal arcs

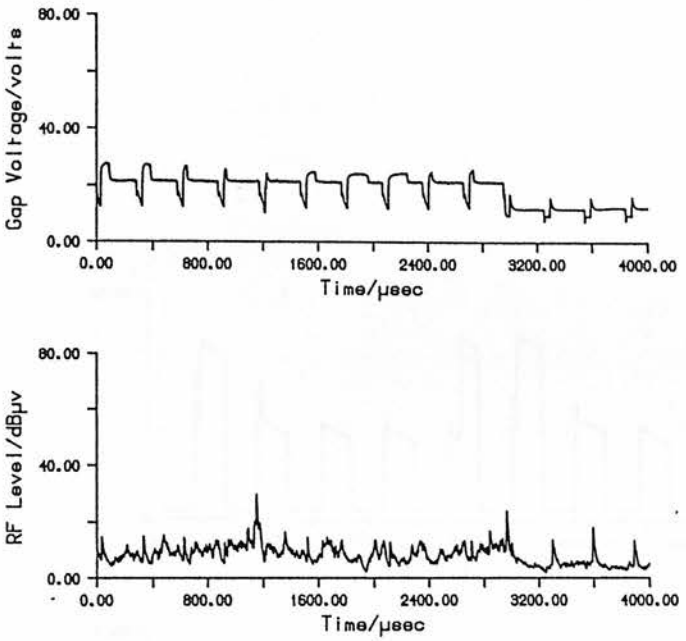

FIGURE 4.14 Voltage and RF waveforms for abnormal arcs and short circuits

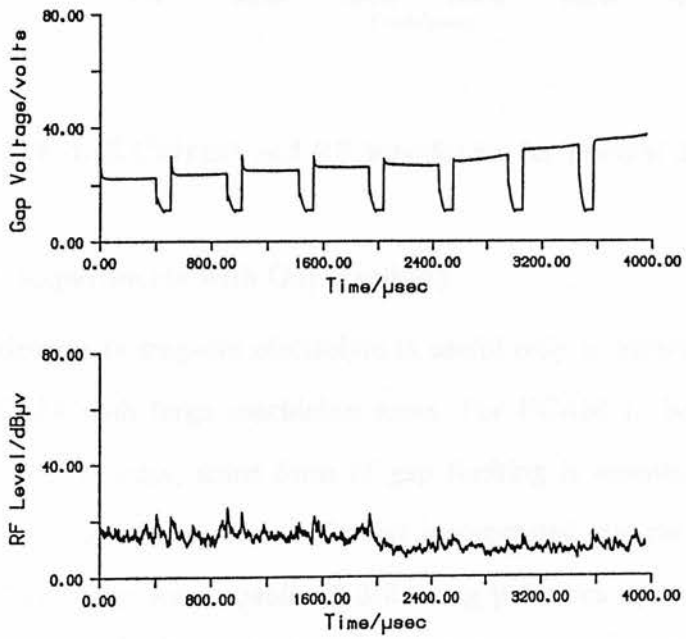

FIGURE 4.15 Voltage and RF waveforms for abnormal arcs and ECD pulses

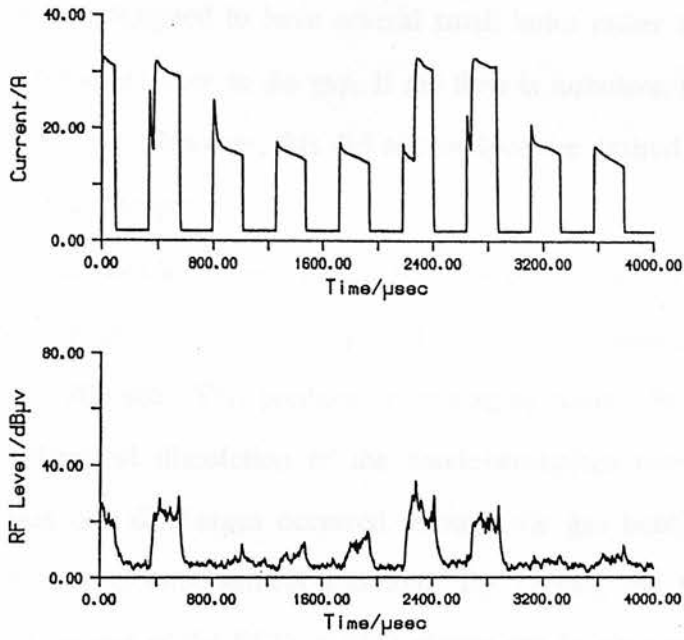

FIGURE 4.16 Current and RF waveforms for normal discharges and ECD pulses

4.5.3 Experiments with Gap Flushing

Experiments in stagnant electrolyte is useful only to ascertain the gap phenomena of ECAM with large machining areas. For ECAM to be a successful practical machining process, some form of gap flushing is essential. To this aim, an air driven pump *(Madan Unicub B)* was incorporated into the electrolyte supply system. The pump was capable of delivering pressures up to 69 bar at flow rate of 1.2 litres min^{-1}. The pulsating effect of the pump was damped with an accumulator.

Originally, the electrolyte was flushed through a center hole in the tube but this proved unsatisfactory as only electrochemical action was present. Due to the removal of gas bubbles from the gap by the flushing action, discharges failed to occur.

The tool was redesigned to have several small holes rather than one center hole to achieve turbulent flow in the gap. If the flow is turbulent, it may help to retain the gas in the gap. However, this did not produce the desired effect - that of having effective discharges.

Finally, it was decided to use pulsed flushing of the gap. A solenoid valve was fitted to the system to achieve the pulsed flushing automatically at intervals ranging from 5 - 200 sec. This produced encouraging results. When the flushing was on electrochemical dissolution of the anode-workpiece occurred and when the flushing was off, discharges occurred through the gas bubbles generated at the cathode by the electrochemical reaction. By varying the flushing on and off times the durations of the ECD to EDE phases can be changed. The pulsed flushing has solved the problem of obtaining discharges in large area ECAM without having to sacrifice the metal removal or the surface finish by having stagnant electrolyte. Further detailed investigation of the pulsed flushing technique is necessary to relate the flushing on/off times with ECD/EDE durations and the metal removal rates. Due to lack of time this has not been done here.

Summary

A qualitative account of the discharge mechanism in large area ECAM was given. The possible gap phenomena in ECAM within a short duration square pulse was found to be: ECD action, ECD and normal discharges, normal discharges, abnormal discharges and short circuits. In order to differentiate

between the normal and abnormal discharges, the RF emission from the gap was monitored. The RF level was found to be considerably higher for a normal discharge than for any other type of gap phenomena above the 12 MHz range. The RF signal, together with the current or the voltage signal, was used to identify the exact gap phenomena in ECAM.

The pulsed flushing of the gap gave encouraging results into how ECAM can be utilised in practical applications of large area machining.

5 : A THEORETICAL MODEL FOR THE RF EMISSION FROM DISCHARGES

5.1 Introduction

This chapter presents the development of a mathematical model relating the charge behaviour within, and radio frequency emission from, ECAM discharges. The existence of such a model, can allow the radio emission patterns already recorded to be interpreted in terms of the high frequency charge behaviour within the ECAM pulses. The mathematical model is based on the assumption that the discharge can be regarded as a short dipole antenna - a Hertzian dipole. It is called a Hertzian dipole as Heinrich Hertz was the first one to investigate the radiation from a small dipole. In fact, Hertz used electric sparks to generate electromagnetic radiation in his experiments(**60**). The electromagnetic field due to the discharges is calculated using Maxwell's equations. The induced electromotive force (emf) on an antenna is then obtained. A comparison with the measured values is made.

5.2 The Field and Particle Equations

The electric and magnetic field vectors **E** and **H**[1] are the basic quantities through which the properties of the electromagnetic field are specified. In general, the two vectors are functions of position **r** and time t. The electromagnetic field is generated by sources: the conduction current density **J** and the space charge density ρ. These two quantities are used in introducing the discharge plasma into Maxwell's equations,

---

[1] The symbols in bold denote vector quantities.

$$\nabla \times \mathbf{E} = -\mu_0 \frac{\partial \mathbf{H}}{\partial t} \quad [5.1]$$

$$\nabla \times \mathbf{H} = \varepsilon_0 \frac{\partial \mathbf{E}}{\partial t} + \mathbf{J} \quad [5.2]$$

$$\nabla \cdot \mathbf{E} = \frac{\rho}{\varepsilon_0} \quad [5.3]$$

$$\nabla \cdot \mathbf{B} = 0 \quad [5.4]$$

where, ε_0 and μ_0 are permittivity and permeability of free space, respectively.

In order to develop a mathematical description of the field of antennae the following equations are used,

$$\mathbf{E} = -\nabla V - \frac{\partial \mathbf{A}}{\partial t} \quad [5.5]$$

and,

$$\mathbf{H} = \frac{1}{\mu_0} \nabla \times \mathbf{A} \quad [5.6]$$

In order to calculate **E** and **H**, the magnetic vector potential **A** and the scalar potential V must be calculated first.

The magnetic vector potential **A** at a point, is related to the source conduction current density **J** by,

$$\mathbf{A} = \frac{\mu}{4\pi} \int_v \frac{\mathbf{J}}{r} \, dv \quad [5.7]$$

and the scalar vector potential V at a point, is related to the charge density ρ by,

$$V = \frac{1}{4\pi\varepsilon_0} \int_v \frac{\rho}{r} \, dv \quad [5.8]$$

For a sinusoidal current, $I = I_0 \cos \omega t$,

$$\mathbf{A} = \frac{\mu}{4\pi} \int_v \frac{J_0 \cos \omega t}{r} \, dv \quad [5.9]$$

Retarded current is used since the effect of the current is not felt at a point r instantaneously, but only after a finite time $\frac{r}{c}$, where c is the speed of light at which the wave propagates.

Hence,

$$I = I_0 \cos \omega \left(t - \frac{r}{c} \right) \qquad [5.10]$$

For simplicity in the expressions,

$$I = I_0 \cos \omega t'$$

where,

$$t' = t - \frac{r}{c}$$

The retarded current density **J** and the retarded charge density ρ can be written as,

$$\mathbf{J} = J_0 \cos \omega t'$$

and

$$\rho = \rho_0 \cos \omega t'$$

Thus, the retarded vector potential can be written as,

$$\mathbf{A} = \frac{\mu_0}{4\pi} \int_v \frac{J_0 \cos \omega t'}{r} \, dv \qquad [5.11]$$

Similarly, the retarded scalar potential V can be written as,

$$V = \frac{1}{4 \pi \varepsilon_0} \int_v \frac{\rho_0 \cos \omega t'}{r} \, dv \qquad [5.12]$$

5.3 Electromagnetic Field Due To Discharges

The discharges are assumed to be short dipoles, in order to calculate the electric and magnetic field strengths in the vicinity of it. The definition of a short dipole is that, the length l is very short in comparison with the wavelength ($l \ll \lambda$). The

two electrodes (tool and workpiece) can be regarded as plates at the end of the discharge which provide capacitive loading. The short length and the presence of these plates result in a uniform current I along the entire length l of the discharge. This is illustrated in Figure 5.1.

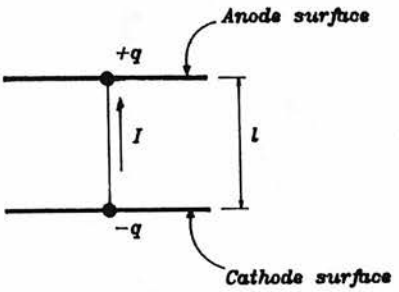

FIGURE 5.1 The discharge current and charge configuration

5.3.1 The Discharge Current

It is very difficult to obtain an exact expression for the discharge current. Nevertheless, the discharge current can be represented by the Fourier series expansion,

$$I(t) = \sum_{n=0}^{\infty} I_n \cos(n\omega t) \qquad [5.13]$$

Only cosine terms are considered, as the current function can be regarded as an even function. For the initial calculation of the field components due to the discharge, however, it is assumed that,

$$I(t) = I_0 \cos \omega t \qquad [5.14]$$

That is, only the fundamental component of the waveform is considered, otherwise, the calculation of the field components becomes very difficult. The fundamental component should give a reasonable approximation as it is the dominant

component.

5.3.2 Calculation of the Field Components

Let the discharge (short dipole) be placed coincident with the z axis and its center at the origin, as shown in Figure 5.2.

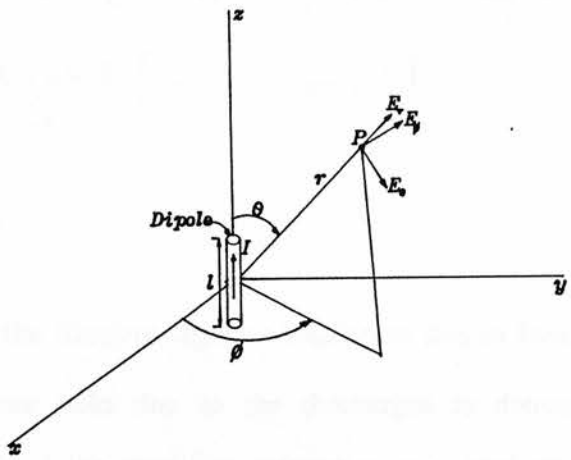

FIGURE 5.2 Relation of dipole antenna to coordinates

The magnetic vector potential has only the z component, A_z which is given by,

$$A_z = \frac{\mu I_0 l \cos \omega t'}{4 \pi r} \qquad [5.15]$$

In polar coordinates,

$$A_r = A_z \cos \theta$$
$$A_\theta = - A_z \sin \theta$$
$$A_\phi = 0$$

The expression for the scalar potential is calculated to be (calculation is not shown here but can be found in most electromagnetic theory text books, for example, Kraus(**61**)),

$$V = \frac{I_0 l \cos \omega t' \cos \theta}{4\pi\varepsilon_0 c} \left[\frac{1}{r} + \frac{c}{j \omega} \cdot \frac{1}{r^2} \right] \qquad [5.16]$$

Substituting these values in equations 5.5 and 5.6, the resulting field components in the spherical polar coordinates are calculated to be,

$$H_\phi = \frac{I_0\, l \sin\theta}{4\pi}\left[-\frac{\omega \sin\omega t'}{rc} + \frac{\cos\omega t'}{r^2}\right] \qquad [5.17]$$

$$E_\theta = \frac{I_0\, l \sin\theta}{4\pi\varepsilon_0}\left[-\frac{\omega \sin\omega t'}{rc^2} + \frac{\cos\omega t'}{r^2 c} + \frac{\sin\omega t'}{\omega r^3}\right] \qquad [5.18]$$

$$E_r = \frac{2\, I_0\, l \cos\theta}{4\pi\varepsilon_0}\left[\frac{\cos\omega t'}{r^2 c} + \frac{\sin\omega t'}{\omega r^3}\right] \qquad [5.19]$$

All the other components are zero.

5.4 Detection of the Electromagnetic Radiation due to Discharges

The electromagnetic field due to the discharges is detected by a receiving antenna. The task of the receiving antenna is to extract energy from the electromagnetic waves generated by the discharges, together with the signals carried by them, and to deliver it to the receiver. The time varying electric field of the wave, in which the antenna is immersed, induces currents and charges in the body of the conducting antenna. A certain voltage is thus developed across the antenna terminals, which varies with time according to the same law as the wave. The electromotive force (emf) induced in the antenna is proportional to the components of the electric field along the antenna.

5.4.1 Emf Induced in a Loop Antenna

The electromotive force $v(t)$ induced in the loop is the line integral along the loop, which is given by,

$$v(t) = \int_{line} \mathbf{E}\, d\mathbf{l} \qquad [5.20]$$

The orientation of the loop in the electromagnetic field is shown in Figure 5.3.

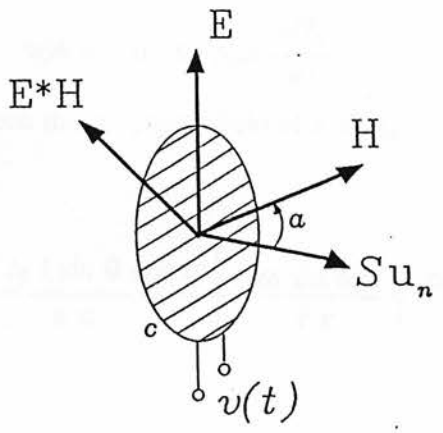

FIGURE 5.3 Orientation of loop in electromagnetic field

Instead of calculating the line integral, by using Stoke's Theorem and the curl equation, $\nabla \times \mathbf{E} = -\frac{\partial \mathbf{B}}{\partial t}$, $v(t)$ can be written as,

$$v(t) = \int_{surface} \nabla \times \mathbf{E} \cdot d\mathbf{S} \qquad [5.21]$$

$$v(t) = -\frac{\partial}{\partial t} \int_{surface} \mathbf{B} \cdot d\mathbf{S} \qquad [5.22]$$

Since the loop is assumed to be small, **B** is practically constant over its area S. Hence $v(t)$ can be expressed as,

$$v(t) = -\mu_0 S u_n \cdot \frac{\partial \mathbf{H}}{\partial t} \qquad [5.23]$$

where $\mathbf{u}_n$ is the unit vector normal to the surface, as shown in Figure 5.3.

The emf is a maximum when the loop is perpendicular to the magnetic field **H** in which case, its plane coincides with the direction of propagation of the wave.

The only component of **H** in the spherical polar coordinates is H_ϕ which is given by the equation 5.17.

Substituting this value of H_ϕ in equation 5.23,

$$v(t) = -\mu_0 S \cos\alpha \frac{\partial H_\phi}{\partial t} \qquad [5.24]$$

where α is the angle between the magnetic field **H** and $\mathbf{u}_n$

This then gives,

$$v(t) = -\frac{\mu_0 S I_0 l \sin\theta \cos\alpha}{4\pi}\left[-\frac{\omega \sin\omega t'}{r c} + \frac{\cos\omega t'}{r^2}\right] \qquad [5.25]$$

5.5 Comparison with the Measured Values

The measured spectrum of the radio frequency emission during normal discharges is shown in Figure 5.4. This was obtained using the loop antenna and displayed on the spectrum analyser screen. From Figure 5.4, it is apparent that the RF emission has a spectrum of frequencies.

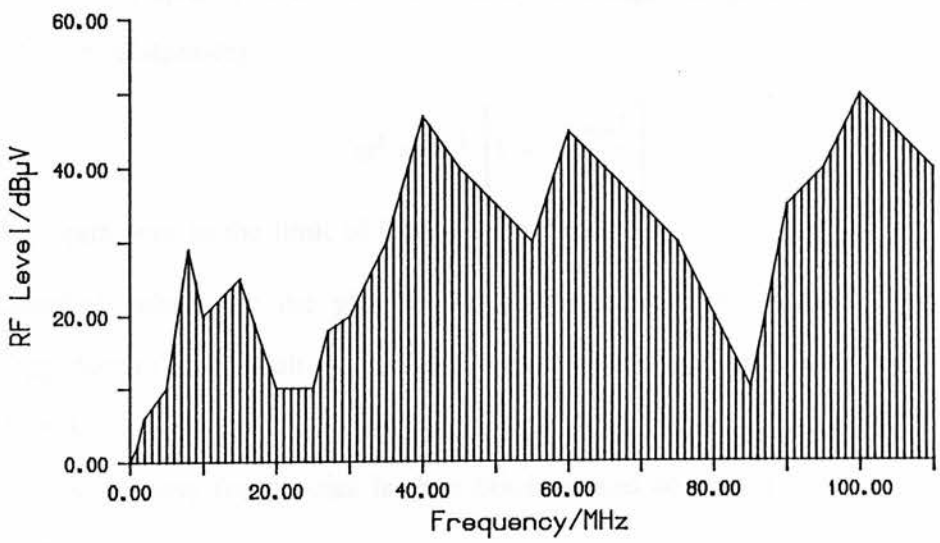

FIGURE 5.4 Measured RF spectrum during normal discharges

5.5.1 Characteristic Frequencies of Radiation

According to Somerville(**62**) and also Bekefi(**59**), the frequencies at which radiation is emitted from plasmas is characterised by the "plasma frequency", ω_p, which is given by,

$$\omega_p = \left[\frac{ne^2}{\varepsilon_0 m_e}\right]^{\frac{1}{2}}$$

where,

n is the electron density

e is the electron charge

m_e is the electron mass

The plasma frequency is a kind of relaxation frequency at which the electrons (or ions) oscillate when the equilibrium distribution has been perturbed(**62**).

If the thermal motion of the electrons is allowed for, instead of a single electron oscillation frequency, a frequency spectrum is obtained. In this frequency spectrum, each frequency is associated with a wavelength of propagation, λ, according to the relationship,

$$\omega^2 = \omega_p{}^2 \left[1 + \frac{12\pi h^2}{\lambda^2}\right]$$

ω_p appears here as the limit of frequency when $\lambda \rightarrow \infty$.

Numerical values for the plasma frequencies cannot be obtained because the charge density is difficult to estimate. From the observed spectrum, however, the values for the characteristic frequencies can be estimated. The electromagnetic radiation at these frequencies is then obtained and compared with the measured spectrum.

5.5.2 Calculation of Emf

The amplitude of the electromagnetic radiation level corresponds to the emf induced in the loop antenna. The value of the emf is given by equation 5.25. From this equation it can be seen that the emf is a maximum when the plane of the loop is perpendicular to the magnetic field (i.e. the angle $\alpha = 0$). Since the loop was positioned to obtain the maximum intensity, it can be assumed that α is 0. Furthermore, the angle θ can also be assumed to be 0 as this is when the maximum intensity is achieved. The other values for the variables used for the calculation is shown in Table 5.1.

TABLE 5.1 Variable values used in the calculation

Variable	Value
Current, I_0	20 A
Length of dipole, l	0.1 mm
Area of loop, S	1257 mm^2
No. of loop turns	1
Distance, r	0.30 m
Permeability, μ_0	400π $nH\ m^{-1}$

These values were substituted in equation 5.25,

$$v(t) = -\frac{\mu_0 S I_0 l \sin\theta \cos\alpha}{4\pi}\left[-\frac{\omega \sin\omega t'}{r c} + \frac{\cos\omega t'}{r^2}\right]$$

to obtain the emf values at the characteristic frequencies of the discharge.

Table 5.2 gives the values of the measured and the calculated values of emf received at the characteristic frequencies.

TABLE 5.2 Calculated and measured values of emf

Frequency MHz	Calculated emf mV max	Calculated emf mV min	Measured emf mV average
40	0.698	0.175	0.223
60	1.047	0.395	0.221
100	1.720	0.975	0.316

From the table, it can be seen that at 40 MHz, the measured signal is well within the calculated range. However, the calculated values at higher frequencies exceed the measured values by significant amounts. This discrepancy at the higher frequency values is due to the inefficiency of a loop antenna to pick up RF emission above 50MHz.

The other factors which have contributed to the high values of the calculated emf are:

a) Neglecting the effects of electrolyte medium, by the assumption that the waves propagate in free space.

b) Not considering the harmonic components of the Fourier expansion of the current waveform in the magnetic vector potential calculation.

c) Assuming the transmission lines to be loss-free.

5.6 Summary

Electromagnetic radiation emitted by electric discharges were mathematically modelled by assuming the discharges to be small Hertzian dipoles. The frequencies at which radiation levels peaked were related to the plasma frequencies of the discharge. The measured values of emf induced in a loop antenna correlated well with the calculated values within its frequency range (0 - 50MHz). This mathematical model gave a reasonable understanding of the charge behaviour

within a discharge by relating it to the RF emission. This model can be regarded as a starter. A more accurate model can be developed by considering all the harmonics of the current waveform. By using a computer package to decompose the current waveform, the mathematical complexity may be reduced.

6 : DEVELOPMENT OF THE PORTABLE ECAM DRILLING MACHINE

6.1 Introduction

Electrochemical arc machining has been proved successful in drilling deep holes with sufficient accuracy in many different metals and metal alloys. So far however, this technique of hole drilling can only be applied to workpieces which are small enough to be mounted on the electrochemical arc drilling apparatus. There are many situations where this is impractical or even impossible. For example, when holes are needed to be drilled in large steel structures. The conventional drilling methods used, although adequate for most purposes, encounter problems such as drill breakage, when holes of high depth to diameter ratio are required. It was felt therefore, that a portable electrochemical arc drilling (ECAD) machine should be developed to tackle the problematic areas of in-situ hole drilling. This portable machine would undoubtedly enhance the application capabilities of ECAM in industry.

One industry which has already expressed a keen interest in the development of this machine is the South of Scotland Electricity Board (SSEB). In fact the machine was specifically developed bearing their requirements in mind. A possible application of the device would be to drill blind holes in large steam boilers for inserting thermocouples. These holes would typically be of 2.5 - 4.5 mm diameter and 100 - 150 mm long.

This chapter describes the design and the construction of the prototype portable ECAM drilling machine.

6.2 Apparatus Specification

1. The main body of the apparatus should contain the following:
   (a) tool holder which also incorporates the means of supplying electrolyte and power to the tool.
   (b) tool feeding mechanism
   (c) tool vibrator
   (d) supporting structure which can be clamped to the work-surface
   (e) provision for electrolyte output and the necessary sealing arrangement to prevent electrolyte spillage.
2. A motion control system is needed to provide the tool feed and vibration.
3. The power supply should be capable of supplying a full-wave rectified unsmoothed voltage which can be varied within the required range.
4. The electrolyte supply and clarifying system should provide fresh and clean electrolyte to the machining gap at the required flow rate and pressure.

6.3 Design and Construction of the Main Body

This is the part which requires to be the most portable. Therefore considerable effort was directed towards keeping the weight and the size of the machine to a minimum. Design considerations were also given to the rigidity of the apparatus and the stiffness of the moving parts in order to obtain consistent accuracy and geometry of the drilled holes. Although no mechanical forces are encountered in the drilling process, electromagnetic, hydrostatic and hydrodynamic forces are induced as shock cycles. These can be attributed to the stochastic generation of discharges, the variation in the flow pattern due to gap oscillations, the explosion of gas bubbles and the unsteady pumping of electrolyte in the gap.

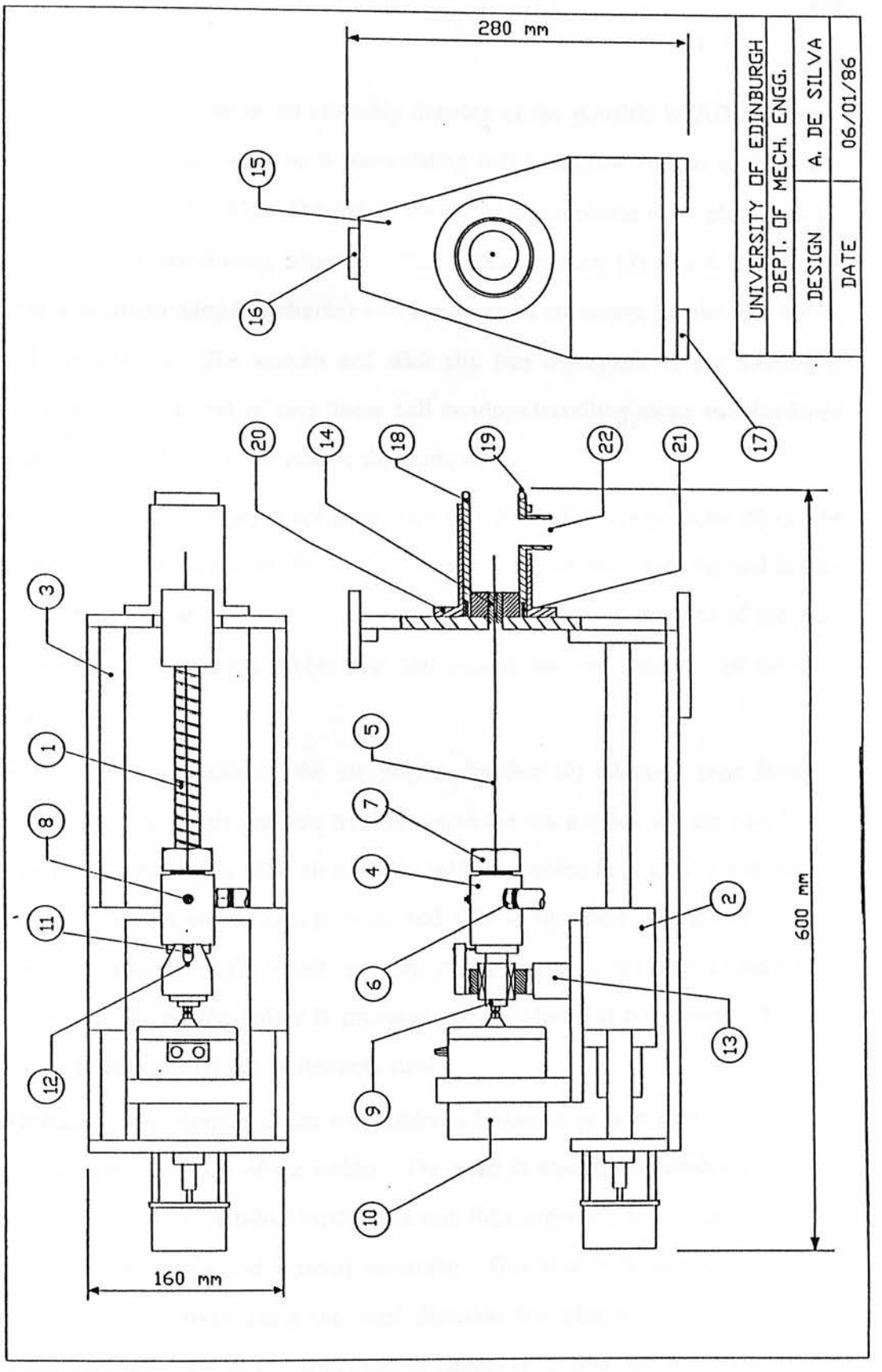

FIGURE 6.1 Sectional assembly drawing of the portable ECAM driller

Figure 6.1 shows a sectional assembly drawing of the portable ECAD apparatus. The feed system is based on a recirculating ball leadscrew and an antibacklash double nut assembly (1). The nut is preloaded to eliminate axial play, thereby increasing the positioning accuracy. The ballnut housing (2) which is made of light aluminium alloy (duralumin) also serves as an anchorage for the tool holder and the vibrator. The smooth and stick slip free movement of the housing is achieved with the aid of two linear ball bearings travelling along two hardened ground shafts (3) on either side of the leadscrew.

The electrode holder (4) is designed such that the hollow copper tube (5) can be pushed into a chamber in the holder through a rubber seal, and the seal is rendered more efficient by the action a spring and also by the pressure of the electrolyte which forces the rubber into and around the circumference of the electrode.

A tapping on the side of the electrolyte chamber (6) admits a pipe fitting to which a flexible high pressure hose is connected via a quick release coupling to supply the electrolyte. The electrode is held in position both axially and radially by a collet and chuck arrangement, and this is tightened around the tube by means of a large nut (7) which holds the chuck captive in the taper of the holder. A tapping (8) on the holder is provided for the electrical connection. The tool holder is constructed out of stainless steel.

To connect the vibrator to the tool holder, a hardened ground steel stub shaft (9) is fitted into the back of the holder. The shaft is electrically insulated from the holder by means of a tufnol bush. The stub then slides inside a linear race acting as a bearing surface and a radial constraint. This allows the electrode holder to move back and forth along the axial direction and also to rotate but does not allow any radial play. The stub shaft is tapped at its free end and is attached to

the armature of a small electrodynamic vibrator(10) via a screw. No rotational movement of the vibrator armature is permitted by the manufacturers, so an additional constraint is required. This takes the form of a small cylindrical roller (11) attached to the tool holder by a pin. This roller guide can move along a slot (12) in a piece of steel fixed to the top of the dural column (13) supporting the stub shaft. This mechanism restricts any rotational play whilst not affecting the axial movement. The finished assembly of this part is photographically illustrated in Figure 6.2.

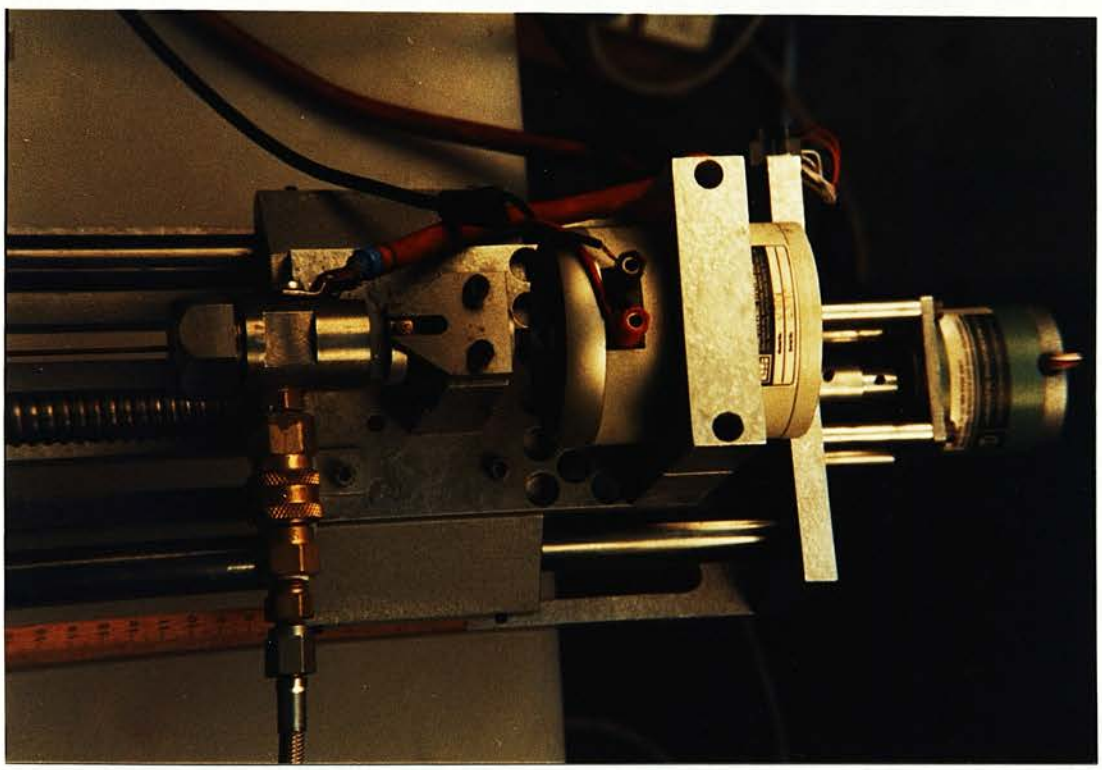

FIGURE 6.2 Vibrator connection to tool holder

To keep the drill straight, it is guided through a P.T.F.E. bush (14) which is embedded in a dural plate (15) attached to the main supporting frame. A slab of mild steel (16) is fixed to the top end of this plate for attaching one of the magnetic clamps. The other two clamps are attached to mild steel slabs (17) located

underneath the base plate.

Figure 6.3 shows the completed apparatus attached to the work by magnetic clamps. The magnetic clamps are *Eclipse Model 922* magnetic positioners. Each comprises of two switchable units which provide infinitely variable power. Each unit has two magnetic faces and accepts either round or flat material. The units are joined by non magnetic steel straps and are simply locked at any angle by a central locking nut. Each magnetic face can exert a pull of about 100 Kg when in contact with mild steel of an adequate thickness and good surface finish. Although each magnetic clamp weighs about 3 Kg, this does not directly add to the weight of the tool head because the magnetic clamps are not permanently fixed to it.

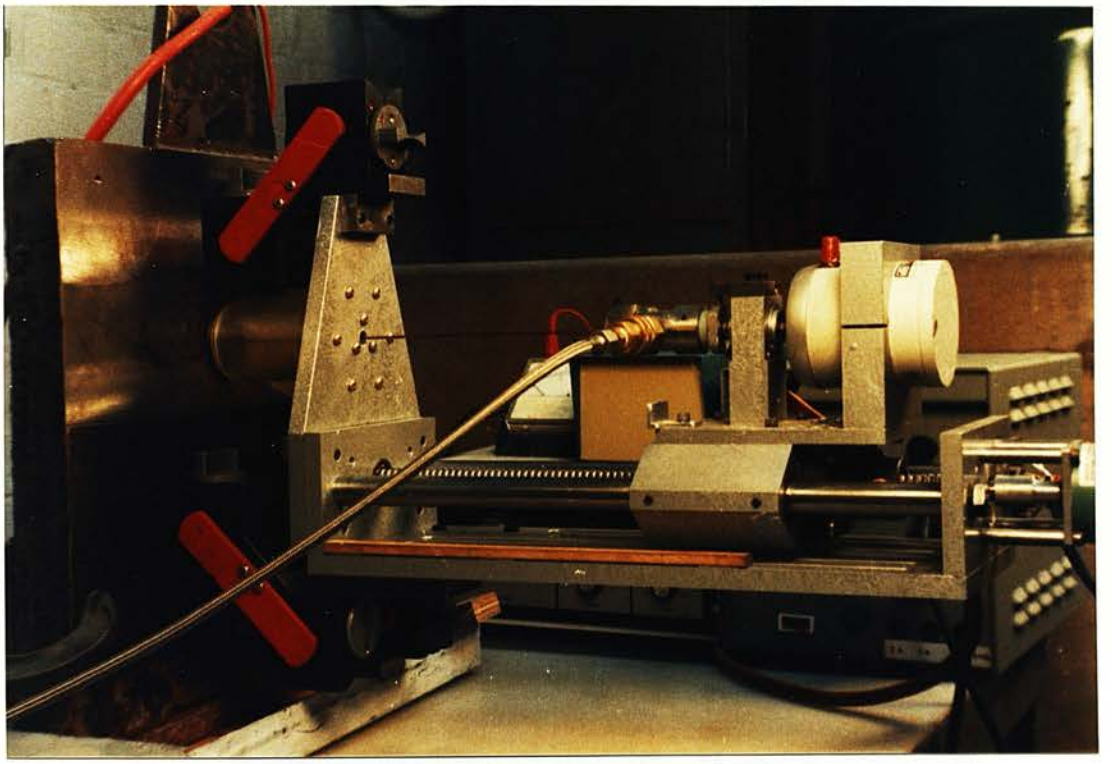

FIGURE 6.3 Drilling apparatus clamped to the workpiece

The apparatus needs to be properly sealed to keep the spent electrolyte to a minimum area. This takes the form of a perspex tube (18) with a rubber O-ring seal (19) which can be pushed against the work-surface by a spring (20) located in the other end of the tube. The tube and the spring are contained by a flanged outer perspex tube (21) attached to the dural plate which houses the drill guide bush. A tapping on the tube provides an outlet for the electrolyte (22). A closer view of the sealing mechanism and the magnetic clamps can be seen in Figure 6.4.

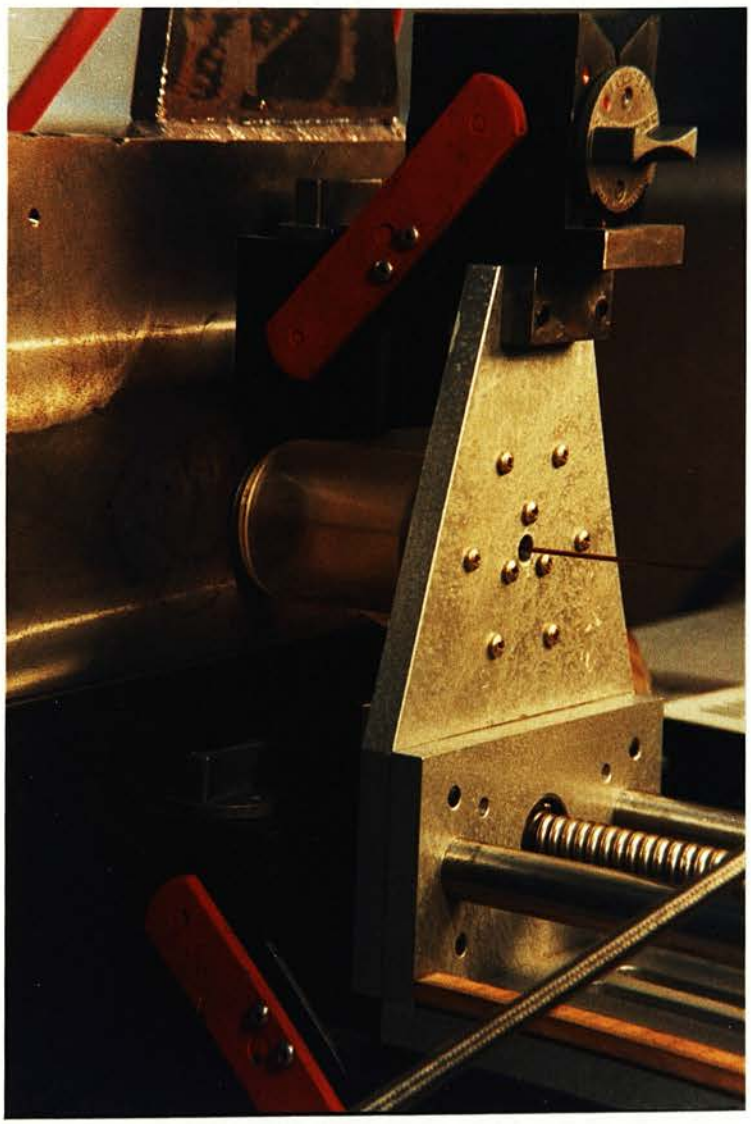

FIGURE 6.4 Sealing arrangement and the magnetic clamps

6.4 Tool Motion Control System

6.4.1 Feed Control Unit

A stepper motor is chosen to drive the ballscrew since it provides a simple open loop control, characterised by a direct input to motor output relationship and reliable motor response without need for a servo-feedback mechanism. Furthermore, the compact size and the ability to provide sufficient torque at low speeds without a reduction gear box make it more suitable than other type of motors. The stepper motor used is *Sigma series 20-22 D200.*

The motor spindle is connected to the ballscrew via a universal coupling. The motor is held in position by four extension rods connected to the back plate of the supporting frame.

The stepper motor control system is based on a *Unimatic UDB053-1 Digicard.* This powered by a 24V power pack generates the step pulses required to drive the motor. The board has a built in wide range oscillator with separate control of fast and slow speeds. This enable the fast control to be used when positioning and retracting the tool and the slow control to be used when feeding the tool.

6.4.2 Feed Rate Calibration

The range of feed rates required is from 5.0 to 40.0 $mm\ \text{min}^{-1}$. Since the ballscrew has a pitch of 5.0 mm, each revolution produces 5.0 mm of linear travel. Therefore the ballscrew should rotate at speeds from 1.0 r.p.m. to 8.0 r.p.m. to achieve the required feed rates. The stepper motor can operate either at 200 or 400 steps per revolution. At 200 steps per revolution, the range of step rates required are from 3 to 30 steps per second. These rates are obtained by adjusting resistor and capacitor values on the board. Thus the stepper motor control system is capable of providing feed rates from 2.5 to 40.0 $mm\ \text{min}^{-1}$ in its

slow mode. In the fast mode it can provide up to 500 *mm* min^{-1}.

6.4.3 Vibration Control Unit

The vibration of the tool electrode has been proved to be an essential part of the ECAD apparatus. This facilitates the clearance of debris from the machining gap and hence prevents short circuits between tool and workpiece. The amplitude and the phase of vibration are quite important process variables which influence the machining parameters. By varying the phase angle between the vibration and voltage waveforms the relative intensity and duration of electrochemical dissolution and electrodischarge erosion phases can be varied (Chapter 2).

A *Ling Dynamic 201* electromagnetic vibrator was selected for its compact size and its ability to provide adequate thrust. The vibrator depends for its operation on the interaction between the steady magnetic field produced by the permanent magnet, and an oscillating current flowing in the moving coil. The drive current for the vibrator is derived from the amplified output from an oscillator *(Ling Dynamic TPO 25)*. The frequency of the movement of the moving coil is the same as the frequency of the oscillator signal. Hence, the load mounted on the armature can be vibrated at the required frequency pre-set on the oscillator.

The model *TPO 25* is a compact combined oscillator/amplifier capable of a power output of 25 watts r.m.s.. A feature of this unit is that it can also be driven from an external signal source.

The amplitude calibration of the vibration was done using a piezo electric accelerometer and a charge amplifier. For sinusoidal motion the amplitude can be calculated from the measured acceleration using the formula given below.

$$a = 0.002 f + 2 d$$

where,

a is the acceleration in g

d is the displacement in mm (peak to peak)

f is the frequency in hertz

6.4.4 Phase Angle Controller

A phase shift controller was designed and built in order to give the required phase angle between the vibration and the voltage waveforms. A schematic diagram of the phase shift controller is shown in Figure 6.5. The basis of the design is that an attenuated signal from the full-wave rectified power supply output is passed through a band-pass filter. This band-pass filter has a centre frequency of 100 Hz and a bandwidth of 10 Hz. The output from this filter has the same frequency as the voltage waveform. This sine wave is then passed through a R-C phase shift network which enabled the phase angle to be set to the required value. This signal is then fed to the external input of the oscillator/amplifier unit which drove the vibrator.

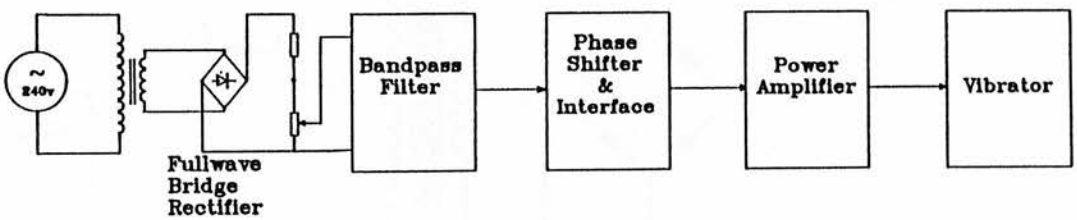

FIGURE 6.5 Schematic diagram of the phase shift controller

6.5 Power Supply System

The power requirement of the machine is a full-wave rectified, unsmoothed voltage which is variable between 0-30 volts r.m.s.. A power rating of 5 KVA at 30 volts should be adequate for most applications.

Figure 6.6 shows a circuit diagram of the basic power system design. This incorporates a variable transformer, a step-down transformer and a full-wave bridge rectifier.

However, difficulties were encountered in obtaining the suitable transformers as they either proved too expensive or too cumbersome. It was decided, therefore, not to manufacture a new power supply but to use one of the existing power supplies for the preliminary experiments.

The power supply used was a Brentford 9 KVA transformer rectifier unit capable of supplying 330 A maximum current. In industrial situations, it is planned to use a suitably adapted, portable welding power unit.

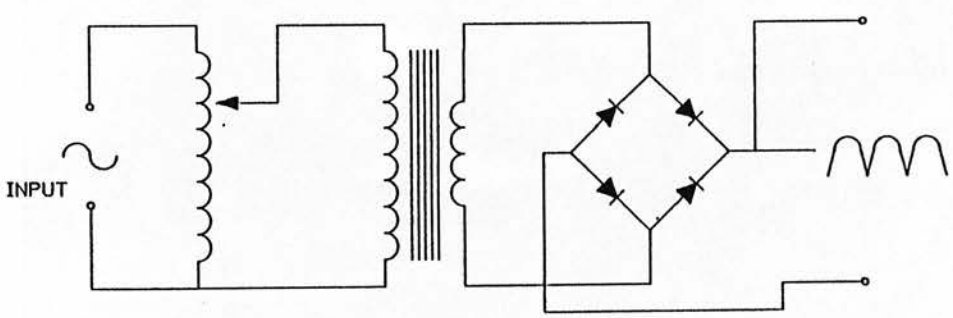

FIGURE 6.6 The basic power supply

6.6 Electrolyte Supply System

The electrolyte supply system consists of a pump *(Gerni 110)* which is capable of delivering up to 5 litres/min at 100 bar. The electrolyte which is stored in a 25 litre plastic tank is pumped via a 10 μm cartridge filter . The pressure of the electrolyte flow is set by a pressure control valve.

The pump is mounted on two rubber tyres, hence its easily movable. However, some situations are envisaged where one would require lengthy hose connections because the portable tool head may be mounted at a place inaccessible to the electrolyte supply system.

An alternative pump *(Madan Unicub Series B)* is also considered when a compressed air supply is available. This is an air driven hydraulic pump which is very compact and easy to maintain, therefore is ideal for the ECAM operation. Figure 6.7 shows this pump and the accessories.

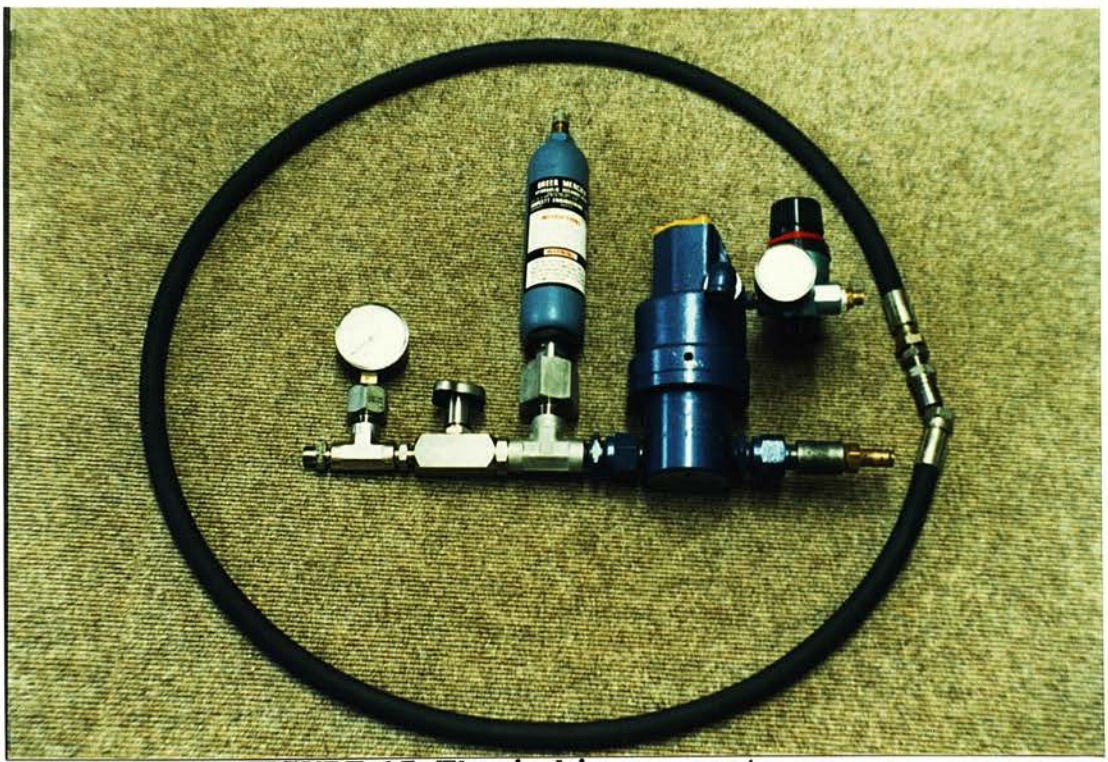

FIGURE 6.7 The air driven compact pump

6.7 Testing of the Portable ECAD Apparatus

Preliminary tests were carried out in the laboratory using a workpiece which is a low alloy steel plate measuring 50 x 50 x 5 cm.. This workpiece was provided by the South of Scotland Electricity Board.

The initial values for the process variables such as feed rate, voltage, electrolyte pressure and vibration amplitude were chosen from the data collected in Chapter 2, using the vertical ECAD apparatus.

6.8 Results and Discussion

The values of process variables used initially are given in table 6.1.

TABLE 6.1 Initial process variables

Machining Variable	Value
average voltage	20 volts
tool feed rate	20 mm/min
electrolyte pressure	30 bar
vibration amplitude	0.1 mm peak to peak
phase angle	0°

Although these values were based on the optimum process variables for the vertical ECAM drilling apparatus, they did not prove to be the optimum values for the portable driller. In fact they gave very poor results. The machining began with severe arcing and ended in a short circuit after few minutes. The process variables were gradually changed until successful drilling of holes was achieved. These values are listed in Table 6.2.

TABLE 6.2 Final process variables

Machining Variable	Value
average voltage	12 volts
tool feed rate	10 mm min^{-1}
electrolyte pressure	30 bar
vibration amplitude	0.25 mm peak to peak
phase angle	0°

Although holes can be drilled satisfactorily using these values, the overcut at the drill entry of 50% and the drill wear of 25% is still too much. Furthermore, the feed rate of 10 *mm* min^{-1} is felt to be too slow as feed rates of 20 *mm* min^{-1} or more have been achieved using the vertical ECAD apparatus. In effect, to optimise the process performance a series of experiments are needed in order to relate the process variables to the machining parameters such as metal removal rate, drill wear, and overcut. From the results of these experiments, the process variables can be chosen to give the desired machining performance.

6.9 Summary

The portable ECAD apparatus can be used satisfactorily to drill holes in large workpieces.

To improve the machining performance, further experimental investigations are necessary in order to relate the process variables to the machining conditions. This would enable one to choose the correct process variables to give the desired machining.

The clamping mechanism was satisfactory. Nevertheless the task of clamping the tool head to the work-surface can be made easier by having a framework with the

three magnetic clamps, which can be attached to the work-surface first. The tool head can then be slotted into this framework.

The sealing arrangement proved to be effective as long as the rubber O-ring seal was flushed right against the workpiece. A softer rubber O-ring would enhance this sealing capability by being more flexible.

7 : CONCLUSIONS AND RECOMMENDATIONS

7.1 Conclusions

7.1.1 ECAM can be used successfully to drill holes in many metals and alloys. For a given material, there exists a set of machining variables which yield the optimum drilling conditions of fastest drill rate, lowest taper and overcut, and lowest tool wear.

For most materials, the optimum conditions are obtained when the energy available to the discharge phase is balanced by the energy available to the electrochemical phase. Since the complex nature of ECAM makes any theoretical prediction of when this occurs difficult, these correct permutations of the machining variables must be gained empirically.

The optimum machining conditions have been established for the five alloys investigated : low carbon chrome steel, cobalt alloy, nickel alloy, low alloy steel and titanium. These conditions can be used as the starting point when drilling other similar materials by ECAM.

For most process variables, common optimum values prevailed for all the materials, indicating that their effect on the machining performance is independent of the material properties. The machining voltage which was the most crucial variable in determining the optimum conditions, differed for each material.

7.1.2 The surface integrity of ECAM drilled alloys can exhibit both ECM and EDM characteristics. The discharges which occur in the frontal gap leave heat induced damage layers which are subsequently removed by the ECD

action occurring along the side gap.

For most of the alloys (iron and nickel based) a smooth damage free surface can be obtained using aqueous sodium nitrate electrolyte. For through holes, some typical electrodischarge induced damage can be present at the exit end, due to the loss of electrolyte which prevents the ECD there. This can be remedied by using a metallic extension piece which can be discarded after the drilling operation.

The surface effects of ECAM on titanium are poor due to lack of electrochemical action. This is a result of the tenacious oxide film which forms on titanium in water based electrolytes, blocking the electrochemical smoothing of the discharge induced damage.

In ECAM the problem of abnormal arcs is also present. These abnormal arcs occur in the same location causing severe damage to both tool and workpiece.

7.1.3 Analysis of the ECAM gap phenomena has given a deeper understanding of the process mechanisms involved in ECAM. When using short duration square pulses instead of the full-wave rectified power, any one of the following gap phenomena can be observed within one pulse:

a) Electrochemical action.

b) Electrochemical action followed by a normal discharge.

c) Normal discharge.

d) Abnormal discharge.

e) Short circuit.

The radio frequency emission from the gap can be used to differentiate between the normal and the abnormal discharges. The RF level detected

during normal discharges is considerably higher than for the abnormal discharges. By monitoring the RF signal together with the voltage or the current clear indication of the ECAM gap situation can be obtained.

7.1.4 The incorporation of pulsed gap flushing has given ECAM the opportunity to machine large flat areas. When flushing is on, only ECD occurs and when the flushing stops EDE occurs. By varying the flushing on and off times the duration of the ECD to EDE phases can be varied to suit the machining requirements.

7.1.5 Further insight into the discharge behaviour can be obtained by theoretically analysing the RF emission from the gap. By making some basic assumptions, the discharge current can be used to evaluate the level of RF emission to a reasonable approximation.

7.1.6 An industrial application of ECAM which arose as a result of this project is the development of a portable device to drill holes in large steel structures for the South of Scotland Electricity Board. The design and the development has been successfully completed. One application of the device is to drill holes in steam boilers to insert thermocouples.

7.2 Further Recommendations

7.2.1 Now that the process mechanisms in ECAM drilling have been further understood, some form of automatic control system can be developed. The gap monitoring signals such as the voltage and the current can be used as the feedback signals. Such closed loop control should ensure a reasonably constant gap. Using the RF emission as a feedback signal, it

should be possible to avoid the abnormal arcs, further enhancing the process performance. Other signals which should be monitored are the electrolyte flow rate /pressure, the vibration amplitude and phase. A microcomputer can be implemented to achieve the autonomy.

7.2.2 Further research is needed in the large area ECAM, in order to establish it as a die producing tool. The results obtained with pulsed flushing are encouraging and should be further investigated. The flushing on and off duration should be correlated with: the EDE duration, the ECD duration, the metal removal rate and the surface finish.

A hybrid ECAM/ECM machine for the production of full die shapes can be developed. The roughing operation can be done using ECAM and the finishing by ECM.

7.2.3 In ECAM discharges can only occur if there is a copious amount of gas bubbles present in the machining gap. Therefore a study into experiments involving gas injection into the machining gap would be useful.

7.2.4 The normal EDM-type power generator has proved to be totally inadequate in its present form when ECAM is to be applied over the large surface areas of many typical dies. In particular, the current generated is not sufficiently high to produce significant electrochemical dissolution. Also, the voltage is too high, resulting in severe discharges and stray electrochemical attack. A new ECAM power supply, in the form of a square pulsed, high current(600A), low voltage (variable between 0-60 V), is recommended. The square pulses will have variable on and off times from 10 - 5000 μsec.

The power supply can be constructed using power MOSFET transistors as the switching elements. The latest developments in these MOSFETs include devices with very low on resistance values, making them ideal for switching high currents. MOSFETs also have several advantages over bipolar transistors:

1) They are voltage controlled devices, enabling them to be driven directly by CMOS or TTL integrated circuit logic, thus simplifying the electronic design of switching circuitry.

2) MOSFETs have outstanding stability with temperature variation, enabling them to be paralleled without danger of thermal runaway.

7.2.5 The theoretical model for the RF emission can be developed further by using a computer subroutine package to give the spectral decomposition of the current waveform. This way all the harmonics of the current waveform can be included in the calculation to give a more accurate model.

BIBLIOGRAPHY

1. Faraday, M, **Experimental Researches in Electricity,** I, II, III, Dover, New York, 1965.

2. DeBarr, A E and P A Oliver, **Electrochemical Machining,** MacDonald and G. Pub. Ltd., 1968.

3. Snoeys, R, F Staelens, and W Dekeyser, "Current Trends in Non Conventional Material Removal Processes," **Annals of the CIRP**, vol. 35 part 2, pp. 467-480, 1986.

4. Lazarenko, B R and N I Lazarenko, **Electrospark Processing of Current carrying Materials,** USSR Academy of Sciences, Moscow, 1958.

5. Weller, E J, **Nontraditional Machining Processes,** Society of Manufacturing Engineers, Dearbon, Michigan, 1984

6. Semon, G, **A Practical Guide to EDM,** Ateliers Des Charmilles S A, Geneva, 1975.

7. Hatschek, R L, "EDM Update '84," **American Machinist,** vol. 128 part 3, pp. 113-124, 1984.

8. Astrop, P, "Seminar reveals some new ideas," **Mach Prod Eng**, vol. 141 p3629, pp. 21-22, 1983.

9. Dobovsek, M and F Roethel, "Contribution to Computer Aided Process Planning of EDM," **Proc. Int. Conf. on Advanced Manufacturing Systems and Technology**, Yugoslavia, October 1987.

10. Drake, T and J A McGeough, "Aspects of Drilling by Electrochemical Arc Machining," **Proc. Machine Tool Design Conference**, pp. 362-369, MacMillan, 1981.

11. Petrow, J N, G H Zajdman, A W Rybalko, and G N Prin, "Pulse Current ECM of Metals," **Int. Symp. Electromachining**, pp. 285-289, Poland, 1980.

12. Inoe, K and I Shibuya , "On the ECDM," **Jap Tool Engineer**, vol. 17, p. 8, 1963.

13. Inoe, K and A Shimizu , "ECD Grinding Machine," **J.S.M.E.**, vol. 71, p. 890, 1968. no 594

14. Kubota, M, "Electrochemical-Discharge Mechanical Grinding with a Graphite Inserted Abrasive Wheel," **Proc of 7th Int Sym on Electromachining (CIRP)**, April 1983.

15. Kimoto, Y, K Tamiya, and K Hirata, "Study on Low Electrode-wear-ratio EDM in water and water solution," **Japan Society of Electrical Machining Engineers**, vol. 1 no 2, p. 45, 1968.

16. Lazarenko, B R and N I Lazarenko, "Mechanism of Passage of Electric Current Through Electrolyte," **Elektronnaya Obrabotka Materialov**, 1977.

17. Glazkov, A V and B R Lazarenko, "Common Problems of Three Dimensional EDM and ECM," **Proc Int Symp for Electromachining (CIRP)**, pp. 7-9, 1977.

18. Kubota, M, "Metal Removal in ECDM," **Proc of ISEM-5**, pp. 217-220, June 1977.

19. Kubota, M, "On the Technological Potentialites of ECDM," **Mechanique**, vol. 303, pp. 15-18, March 1975.

20. Kubota, M, Y Tamura, H Takahashi, and T Sugaya, "Basic Study of ECDM-II," **Jap. Assoc. of Electromachinery**, vol. 26, 1980.

21. Zaytsev, A N and V I Polyanin, "The frequency properties of the interelectrodes gap in spark-electrochemical piercing of small holes," **Electrochemical Ind Proc & Biol**, vol. 5, pp. 16-20, 1978.

22. Saushkin, B P, I Mingazetdinov, V K Sidelnikov, E G Semonov, and V A Gushan, "Special Features of Combined Electrochemical and Electro-Erosion Machining of Elongate Machine Parts," **Electrochemical In Indust Proc & Biol**, vol. 105 part 3, pp. 8-14, 1982.

23. Crichton, I M, J A McGeough, W Munro, and C White, "Comparative Studies of ECM, EDM and ECAM," **Precision Engineering**, 1981.

24. Crichton, I M, "A Computational and Experimental Study of Discharges in Electrolytes," **PhD Thesis**, University of Aberdeen, 1982.

25. Drake, T H, "Aspects of Drilling by Electrochemical Arc Machining," **MSc Thesis**, University of Aberdeen, 1980.

26. Khayry, A B, "Stochastic and Experimental Studies of Drilling by Electrochemical Arc Machining," **PhD Thesis**, University of Aberdeen, 1984.

27. El-Hofy, H, "Stochastic and Experimental Studies of Wire Cutting by Electrochemical Arc Machining," **PhD Thesis**, University of Aberdeen, 1985.

28. Munro, W, "Experimental and Theoretical Studies of the Surface Treatment of Dies and Moulds," **PhD Thesis**, University of Aberdeen, 1983.

29. Snoey, R, D F Dawn, and J P Kruth, "Survey of Adaptive Control in Electro Discharge Maching," **J. of Man. Systems**, vol. 2, No 2, pp. 147-164.

30. Jones, F L, "Electrode Erosion by Spark Discharges," **Brit. Journal of Applied Physics**, vol. 1, no 3, pp. 60-65, March 1950.

31. Van-Dijck, F S and W L Dutre, "Heat Conduction Model for the Calculation of the Volume of Molten Metal in Electric Discharges," **Applied Physics**, vol. 7, pp. 899-910, 1974.

32. Erden, A and B Kafatanoglu, "Heat Transfer Modelling of Electric Discharge Machining," **Proc 21st Int Mach Tool Design and Research Conf**, pp. 351-358.

33. McGeough, J A, **Principles of Electrochemical Machining,** Chapman & Hall, London, 1974.

34. Berghausen, P E, "Electro-Discharge Machining Program," **Final Report ASD-TDR-7-545**, vol. AD 423-199, Defence Document Centre, Arlington Hall Station, Arlington Virginia, July 1963.

35. Crookall, J R and B Khor, "Electrodischarge Machined Surfaces," **Int. J. Mach. Tool Des. Res.**, pp. 373-384, 1975.

36. Bucklow, I A and M Cole, "Spark Machining," **Met. Reviews**, vol. 3 , no. 135 , pp. 103-113., June 1969 .

37. Lloyd, H K and R H Warren, "Metallurgy of Spark Machined Surfaces," **Journal of The Iron and Steel Institute,**, pp. 238-247, March 1965 .

38. Platanik, L S and A A Levechenko, **Kristral-lografiya** , vol. 3 , p. 613., 1958 .

39. Bannard, J, "Fine hole drilling using electrochemical machining," **Int. Machine Tool Des. Res. Conf.**, pp. 503-510, MacMillan Pub. , Manchester, 1978.

40. Cole, R R and Y Hopenfeld, **ASME paper** , no. 62-wa-71 , 1962.

41. Kashthejev, V D, "Processes which control surface microroughness during ECM," **Proc. Int. Symp. for Electromachining**, Poland pp 271-274, June 17-20, 1980.

42. McGeough, J A, A B Khayry, and W Munro, "Theoretical and Experimental Investigation of the Relative Effects of Spark Erosion and Electrochemical Dissolution in Electrochemical Arc Machining," **Annals of the CIRP** , vol. 32, no. 1, pp. 113-118., 1983 .

43. Driver, D, "Developments in Aero Engine Materials," **Metals and Materials**, pp. 345-354, June 1985.

44. Bannard, J E, J R Treble, and P A Brook, "The Electrochemical Machining of Titanium in Non- aqueous Electrolytes," **Int. Symp. for Electromachining**, pp. 121-125., June 1977.

45. Meek, J M and J D Craggs, **Electrical Breakdown of Gases,** pp. 252-256, Clarendon Press, Oxford, 1953.

46. Watson, P K and A H Sharbaugh, **Electrochemical Society**, p. 107, 516, 1960.

47. Kao, K C, **Applied Physics**, vol. 12, p. 629, 1961.

48. Fiei, C, E Perreard, and M Peter, "On the Breakdown Mechanism of Recurring Discharges in Liquid Dielectric," **Helvetica Physica Acta**, vol. 45, 1972.

49. Heuvelman, C J, H J A Horsten, and P C Veenstra, "An Introductory Investigation of Breakdown Mechanism in Electro-Discharge Machining," **Annals of CIRP**, vol. 20, pp. 43-44.

50. Loutrel, S P and N H Cook, "High Rate Electrochemical Machining," **Trans. ASME**, pp. 992-996, Nov 1973.

51. Larsson, C N and E M Baxter, "Tool Damage by Sparking in ECM," **Proc. 18th Int. Mach. Tool Des. Res. Conf**, pp. 499-505, Sept 1977.

52. McGeough, J A and I M Crichton, "Studies of the Discharge Mechanisms in Electrochemical Arc Machining," **Applied Electrochemistry**, pp. 113-119, 1985.

53. Snoeys, R and H Cornelissen, "Correlation Between Electro-Discharge Machinery Data and Machinery Settings.," **Annals of the CIRP**, vol. 24/1, 1975.

54. Snoeys, R, D Dauw, and M Jennes, "Survey of EDM Adaptive Control and Detection Systems," **Annals of the CIRP**, vol. 31/2, pp. 483-489, 1982.

55. Bhahacharyya, S K and M F El-Menshawy, "Monitoring the EDM Process by Radio Signals," **Int. J. Prod. Res.**, vol. 16, pp. 353-363, 1978.

56. Xi, S and L Liming, "Preliminary Investigation on the Radio Frequency Radiation in EDM (in Chinese)," **Electromachinery**, vol. 2, 1984.

57. El-Menshawy, M F and M S Ahmed, "Monitoring and Control of the Electro-Discharge Texturing Process for Steel Cold Mill Work Rolls," **Transfer Technology Ltd**, Birmingham, U.K., 1985.

58. Wood, A N, "Electrochemical Arc Machining - Characteristics, Process Monitoring and Control.," **MSc Thesis**, University of Aberdeen, 1985.

59. Bekefi, G, **Radiation Process in Plasmas,** Wiley, New York, 1980.

60. Phillips, V J, **Early Radio Wave Detectors,** Peter Peregrinus Ltd in association with the Science Museum, London, 1980.

61. Kraus, J, **Electromagentics,** 3rd Edition, McGrawhill, 1984.

62. Somerville, J M, "Some Fundamental Properties of Plasmas," **Discharge and Plasma Physics**, The University of New England, Australia, 1964.

APPENDIX

Surface effects on alloys drilled by electrochemical arc machining

A de Silva, BSc(Eng) and **J A McGeough,** BSc, PhD, DSc, CEng, FIMechE
Department of Mechanical Engineering, University of Edinburgh

Electrochemical arc machining (ECAM) utilizes pulsed power in an electrolyte, in order to remove metal by combined electro-discharge erosion (EDE) and electrochemical dissolution (ECD). In drilling by this technique, EDE occurs at the frontal gap between the cathode–tool and anode–workpiece; in the side gap, ECD is predominant. Machining rates are much greater than those of electrochemical (ECM) and electro-discharge machining (EDM).

This paper is concerned with an investigation of the effects of EDE and ECD on the surface integrity of a range of alloys of industrial interest, drilled by ECAM.

Chrome, cobalt and low-alloy steels and nickel-based (nimonic) alloys all exhibited a smooth surface finish typical of that found with ECM, for most of the length of the drilled hole, except at the exit. There, metallurgical damage due to EDE was apparent. The surface characteristics with titanium were typical of those found in EDM, with virtually no evidence of ECM action. This effect was attributed to the presence of a tenacious oxide film formed on titanium in water-based electrolytes which effectively blocks ECM.

1 INTRODUCTION

Machining of tough, heat and corrosion resistant materials by conventional methods has always presented problems in industry. Alternative methods such as electrochemical (ECM) and electro-discharge machining (EDM) have been developed to overcome the limitations of conventional methods. In ECM, the material removal is by the electrolytic dissolution of an anodic workpiece, the gap between the workpiece and the cathode tool being filled with electrolyte. In EDM, the material is removed by the erosive effect of electric discharges activated across a dielectric fluid.

In recent years, a new process called electrochemical arc machining (ECAM) has been developed, which combines features of both ECM and EDM. This process utilizes a pulsed voltage in an electrolyte, thereby permitting both electrochemical dissolution (ECD) and electro-discharge erosion (EDE) of the workpiece. These combined effects yield higher metal removal rates than ECM or EDM (**1**). As with ECM or EDM, metal removal by ECAM is independent of the mechanical properties of the workpiece material. However, the thermal conductivity and the composition of the material could affect the surface quality and the stock metal removal.

It is of value therefore to investigate the effects of ECAM on different types of materials. The surface characteristics of machined parts are of particular interest for two reasons: firstly, higher surface–volume ratios are encountered as strength–weight ratios are increased and secondly, the extreme environments to which they may be subjected make them inherently more sensitive to their surface conditions.

This paper investigates the surface effects produced by ECAM drilling on different materials, such as high-chrome steels, low-alloy steels, nickel alloy and titanium. The analysis of the surface quality is based on optical and scanning electron microscopic examination and micro-hardness testing.

Surface effects produced by ECAM are expected to have both EDM and ECM surface characteristics.

The MS was received on 17 June 1986 and was accepted for publication on 1 September 1986.

1.1 EDM surface effects

Several publications can be found on surface characteristics of EDM components (**2–4**). It is well known that when a discharge occurs the material is melted, or even evaporated, thus forming craters on the component surface. The heat of the discharge penetrates to the subsurface layers inducing a heat-affected zone. The amount of heat damage is dependent on the thermal conductivity of the material and the intensity of the discharge itself which is governed by the process variables and the gap conditions. The craters produced by EDM are associated with fusion and plastic deformation due to molten liquid solidifying epitaxially when quenched by dielectric. Platanik *et al.* (**5**) have reported that this in turn causes slip, twinning, cleavage and microcracks in the surface depending on the crystal structure, regardless of the ductility of the material. A review on the existing published work on the nature of electro-discharge machined surfaces can be found in Crookall and Khor (**2**).

1.2 Electrochemically machined surfaces

The micro-finish of an ECM surface is governed mainly by the type of electrolyte, the composition of the workpiece material and the machining conditions such as the current density and the electrolyte flowrate.

The main factors resulting in poor surface finish in ECM are pitting, preferential grain boundary attack, surface waviness and formation of oxide layers. Pitting tends to occur in regions of low current density where the passivating layer would slow down dissolution of the majority of the surface. Grain boundary attack is an example of local recession and is very important

0263-7146/86 $2.00 + .05

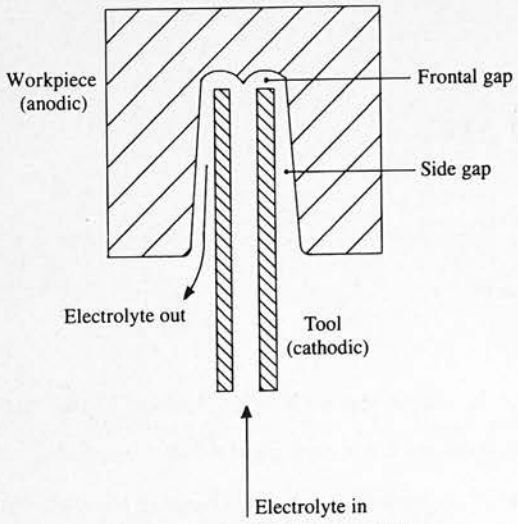

Fig. 1 Electrochemical arc drilling

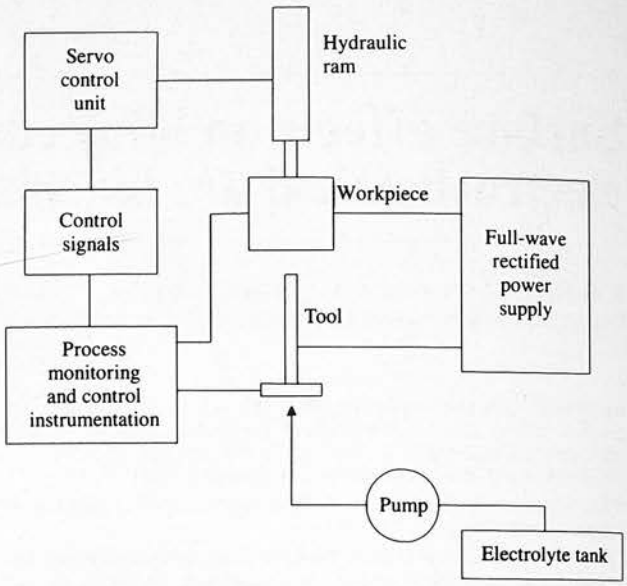

Fig. 2 Block diagram of the basic system in ECAM

because severe attack may reduce fatigue life by as much as 50 per cent.

De Barr and Oliver (**6**) describe how current density, electrode potential and type of electrolyte can result in differential removal rates in inhomogeneous materials. Bannard (**7**) has investigated the surface finish of fine hole drilling using ECM. He has found that electrochemical drilling of multi-phase alloys could present particular problems, where, if the correct dissolution-controlling anodic film is not generated, differential dissolution of the phases would occur resulting in a rough surface. However, Cole (**8**) claims that if the current density is sufficiently large (100 A/cm^2), bright surface finishes could be obtained on many metals and alloys. Kashthejev (**9**) also reports that an increase in the working current density, as a rule, is accompanied by a decrease in surface roughness and by an improvement in reflecting ability. This could be associated with the disappearance of surface etching at high current densities.

Electrochemically machined surfaces are free from residual stresses and also from any heat-affected zones or recast layers. Therefore smooth ECM surfaces are much preferable to EDM surfaces.

1.3 ECAM drilling

In ECAM drilling the main mechanism responsible for material removal at the frontal gap is electro-discharge erosion while at the side gap electrochemical dissolution of the material occurs (Fig. 1). The metallurgically damaged layers caused by the discharge erosion phase are wholly or partially removed by the electrochemical dissolution phase. Therefore, the main factor which determines the ECAM surface integrity is the proportion of EDE to ECD phase.

In McGeough *et al.* (**10**) the factors which affect the surface quality produced by the ECD phase are given as: formation of anodic surface films, non-uniformity of the electrolyte flow pattern, change in bulk conductivity and effects of cathode and anode overpotentials. Likewise, the factors for the EDE phase are given as: the type and duration of the machining voltage, the frequency and distribution of discharges and the effect of electrolyte flowrate.

The proportion of EDE to ECD phase is determined mainly by the machining variables and the gap conditions. Machining voltage is the most crucial process variable where surface quality is concerned. At higher voltages, the intensity of the discharges is greater, thus the craters formed are larger and also the depth of the heat-affected zone is greater. To remove all the damaged layers, prolonged ECD action is required. This invariably means slow feedrates. Prolonged ECD action will also cause larger tapers and overcuts, resulting in poor dimensional accuracy. Another variable which could have a marked effect on the surface quality is the phase angle between vibration and voltage waveforms, which determines the instantaneous relationship between the machining gap and the power transmitted across it. Thus by varying the phase angle the relative intensity and duration of ECD and EDE phases can be changed.

2 EXPERIMENTAL APPARATUS AND PROCEDURE

The salient features of the prototype ECAM drilling apparatus are shown in the schematic diagram in Fig. 2. The cathodic tool is kept stationary with a collet chuck arrangement, while the anodic workpiece, which is located above the tool, is given a linear feed motion using a hydraulic ram. Feedrates of 0 to 50 mm/min can be obtained by using a ramp voltage generator. A vibration frequency 100 Hz and amplitude variable between 0 and 3.00 mm peak-to-peak is superimposed on the feed motion. A power in the form of a full-wave rectified unsmoothed voltage is applied between the electrodes, the average value of which can be varied from 0 to 50 V. The phase angle between the vibration and the voltage waveform is controlled by a variable phase function generator, giving phase differences from 0 to 180°. Electrolyte is pumped through the drill tube into the machining gap at pressures which can be varied from 0 to 40 bar. The electrodes are not submerged and the electrolyte is kept at room temperature.

The tools used were uninsulated copper tubes of outer and inner diameters 1.829 and 0.864 mm respec-

Table 1 Composition of the alloys

Alloy	Composition %											
	Cr	Ni	Mo	V	Co	Ti	C	Si	Mn	Cu	Al	Fe
Jethete	12.00	2.00	2.00	0.30	—	—	0.10	—	—	—	—	bal.
Rex 535	10.00	—	0.08	—	6.00	—	—	—	—	—	—	bal.
Incoloy 901	12.00	42.00	6.00	—	1.00	2.80	0.05	0.40	0.50	—	0.20	bal.
Low-alloy steel	1.08	0.14	0.51	0.02	—	—	0.10	0.28	0.44	0.20	0.15	bal.
Titanium	Commercially pure											

tively. A 20 per cent w/v aqueous solution of sodium nitrate was used as the electrolyte. Workpieces of 32 mm length were obtained from the following five materials: low-carbon chrome steel (Jethete), cobalt alloy steel (Rex 535), nickel alloy (Incoloy 901), titanium and low-alloy steel. The composition of each material is given in Table 1.

Experiments were carried out at a feedrate of 20 mm/min until the drill broke through the specimen. Various combinations of process variables (voltage, electrolyte pressure, amplitude and phase of vibration) were used to establish the optimum machining conditions for each material. The optimum machining conditions gave the highest linear metal removal rate, the least drill wear and the best hole profile in terms of straightness and overcut. The surface effects were analysed for these holes.

2.1 Evaluation of surface integrity

Normal illumination optical microscopy was used to examine the structures in the sub-surface layers of the specimens. Specimens were prepared by taking longitudinal sections through the drilled hole for each material. These were then polished and etched in the following etchants:

low-carbon chrome steel (Jethete)	5 per cent ferric chloride/ nitric acid
cobalt alloy (Rex 535)	5 per cent ferric chloride/ nitric acid
nickel alloy (Incoloy 901)	5 per cent ferric chloride/ nitric acid
low-alloy steel	5 per cent Nital
titanium	10 per cent hydrofluoric acid/ 5 per cent nitric acid

The micro-structure along the drilled hole was examined and photographed on a Zeiz photomicroscope. Micro-hardness readings were taken using a Leitz micro-hardness tester. Scanning electron microscopy was used to examine the ECAM drilled surface. This technique allows the identification of any craters and also gives some indication of the surface roughness due to its relatively high depth of field (1 mm).

3 RESULTS AND DISCUSSION

The relationships between the process variables and the machining parameters were similar for all the materials. Except for the gap voltage, the optimum machining settings for each material were more or less the same. The optimum process variables together with their resulting machining parameters are given in Table 2.

The analysis of the surface integrity along the hole was divided into three areas of significance. The first was the one to two millimetres near drill entry where it generally exhibited rounding-off effects due to stray electrochemical attack. The middle section which consisted of most of the hole length, where actual ECAM (combined ECM and EDM) surface effects were to be found. Finally the last two to three millimetres near the exit where it was expected to have mainly EDM surface effects.

The micro-hardness readings in Table 3 were taken from the middle of the hole as this is where the true ECAM effects are represented.

3.1 Low-carbon chrome steel (Jethete)

Figure 3 shows photomicrographs* of longitudinal sections taken from drill entry, middle and drill exit points

* *Note*: all photomicrographs have been photographically reduced to 65 per cent.

Table 2 Optimum process variables and machining parameters

Material	Average voltage	Average current	Volumetric MRR	Linear MRR	Volumetric tool wear ratio	Hole geometry		
						Entry diameter	Exit diameter	Taper angle
	V	A	mm^3/min	mm/min	%	mm	mm	degrees
Jethete	19.1	66	61.2	16.2	11	2.31	2.12	0.17
Rex 535	22.0	61	63.6	16.7	8	2.45	2.13	0.28
Incoloy 901	17.8	63	76.2	16.7	9.1	2.28	2.02	0.24
Titanium	16.6	29	88.8	17.1	5.2	2.20	2.08	0.10
Low-alloy steel	20.0	68	69.5	16.2	12	2.46	2.11	0.31

Process variables common to all the materials:

Tool feedrate	20 mm/min
Vibration amplitude	0.1 mm peak-to-peak
Phase angle	0°
Electrolyte pressure	30 bar

Table 3 Variation of micro-hardness with depth

Depth from the drilled surface	Micro-hardness kg/mm^2				
μm	Jethete	Rex 535	Low-alloy steel	Incoloy 901	Titanium
70	340	363	147	458	377
170	339	371	151	452	416
270	348	377	145	452	406
370	368	378	155	436	371
570	350	371	150	427	383
1000	357	370	155	433	394

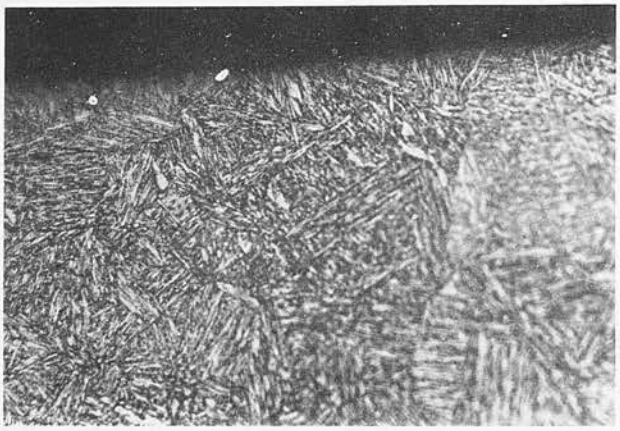

(a)

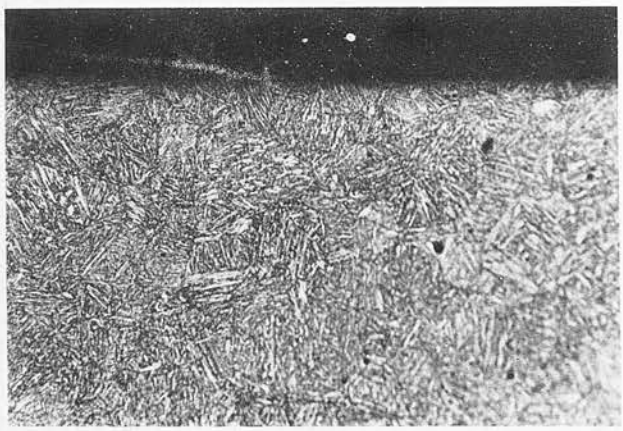

(b)

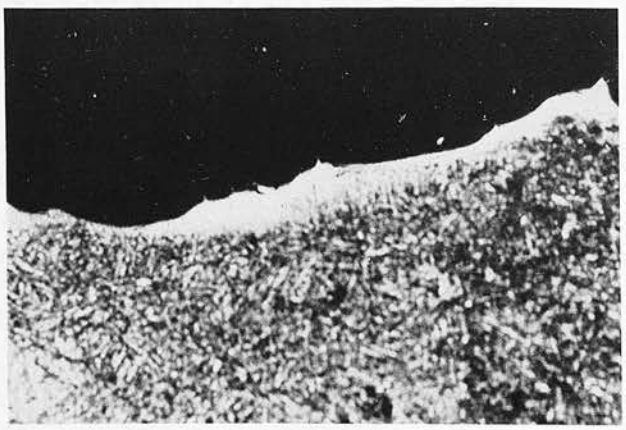

(c)

Fig. 3 Photomicrographs of polished and etched Jethete specimens showing the sub-surface region along the hole: (a) near drill entry (×640), (b) middle (×640), (c) near exit (×640)

(a)

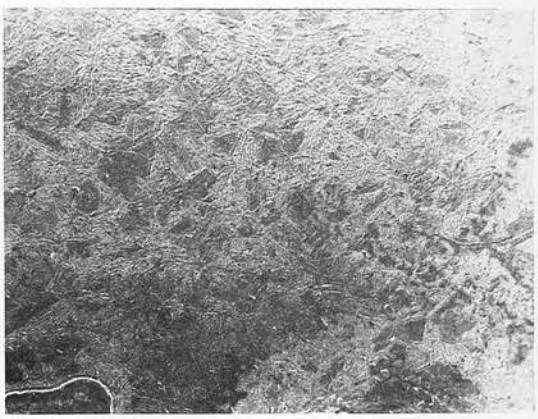

(b)

(c)

Fig. 4 Scanning electron micrographs of Jethete specimens showing the drilled surface along the hole: (a) near drill entry (×100), (b) middle (×100), (c) near exit (×500)

of a typical ECAM specimen. Apart from near the drill exit end, the surface appears to be regular with no sub-surface layers or micro-structural change. At the exit, however, some damage is evident, a white layer of about 10 μm thickness can be seen. This white layer extends to about 1.5 mm from the exit end. Table 3 shows the micro-hardness readings taken at various depths from the drilled surface. No significant variations in these readings can be detected, which indicate that there are no hardened layers left on the surface.

Scanning electron microscope photographs (SEM) of the drilled surface are presented in Fig. 4. Except for the exit end, the surface is smooth and crater-free. However, some surface etching is visible at higher magnification as can be seen from Fig. 5. At the exit, a rough and irregular surface, similar to that of an EDM surface is apparent, with signs of surface melting and resolidification.

The smooth profile and the absence of surface layers up until the last 1–2 mm from the exit end indicate that all the damage induced by the electro-discharge erosion action has been effectively removed by the following electrochemical dissolution action. At the drill exit, electrolyte is lost in the machining gap when the drill breaks through the workpiece. This results in lack of electrochemical dissolution at the exit, thus leaving the damage caused by the discharge erosion action.

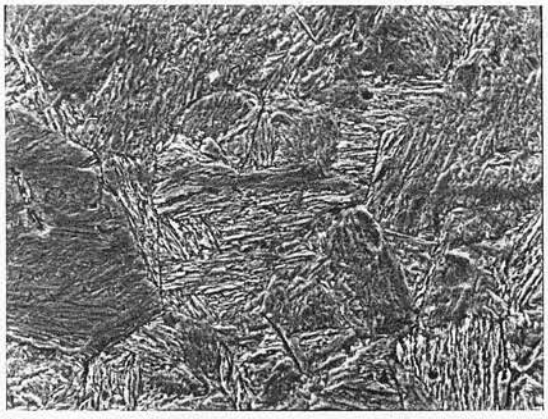

(a)

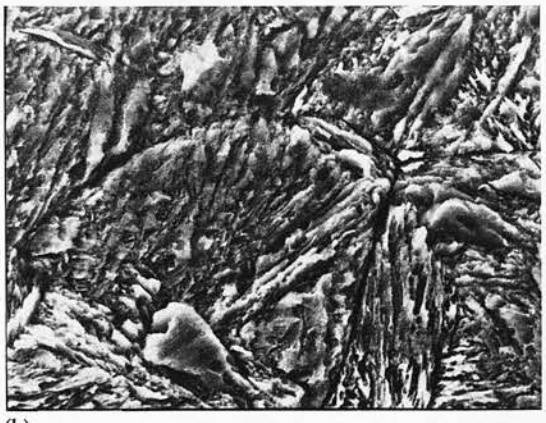

(b)

Fig. 5 Scanning electron micrographs of Jethete specimens showing the drilled surface along the hole: (a) near drill entry (× 500), (b) middle (× 2000)

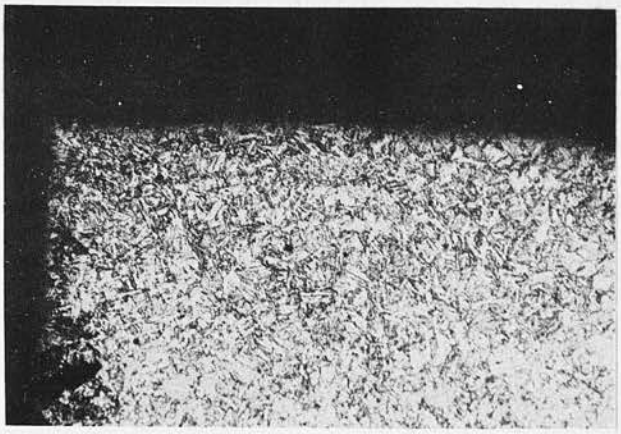

(a)

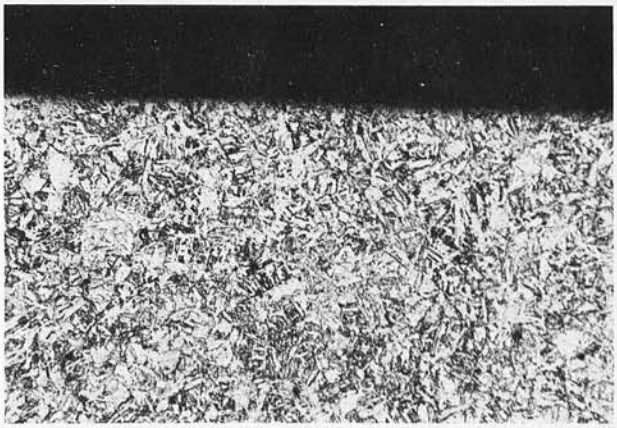

(b)

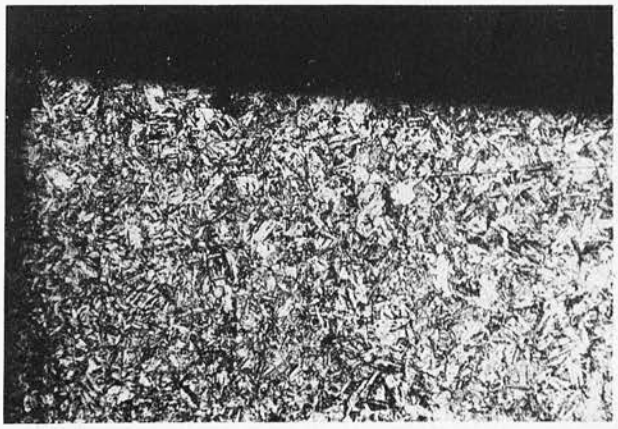

(c)

Fig. 6 Photomicrographs of polished and etched Rex 535 specimens showing the sub-surface region along the hole: (a) near drill entry (× 320), (b) middle (× 320), (c) near exit (× 320)

3.2 Cobalt alloy steel (Rex 535)

As seen from the photomicrographs of Rex 535 in Fig. 6, no significant or measurable effects on the micro-structure can be detected. Even at the exit end the sub-surface region appears to be unaffected. Nevertheless the SEM photograph of the exit end in Fig. 7 shows signs of splashing during the ejection and resolidification. A few pock marks, caused by the entrapped gas bubbles reaching the surface, are also

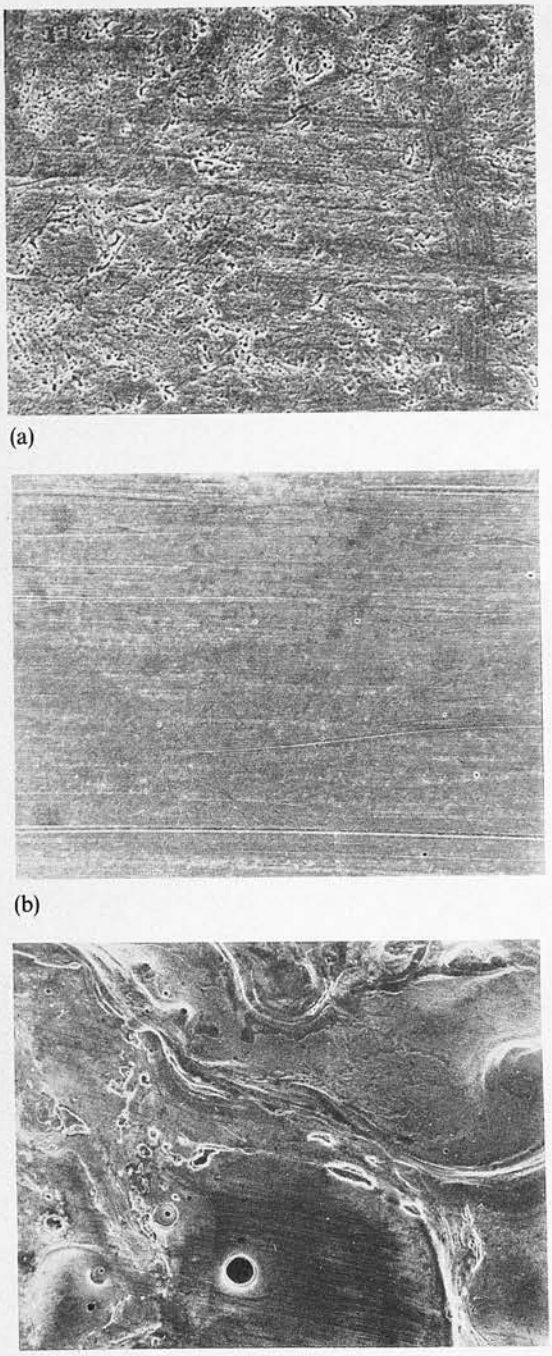

(a)

(b)

(c)

Fig. 7 Scanning electron micrographs of Rex 535 specimens showing the drilled surface along the hole: (a) near drill entry (×500), (b) middle (×100), (c) near exit (×100)

visible. The damage is limited to the final length (last millimetre) of the hole as the SEM photographs on entry and middle sections show a very smooth bright surface. This indicates that ECD occurring along the side gap has effectively removed the surface damage produced by the erosive effects of discharges. In the final millimetre of length of the hole the damage remains because the electrochemical action is lost due to lack of electrolyte. Micro-hardness readings in Table 3 do not vary significantly with depth from the machined surface. This is further evidence that there are no hardened layers left on the surface.

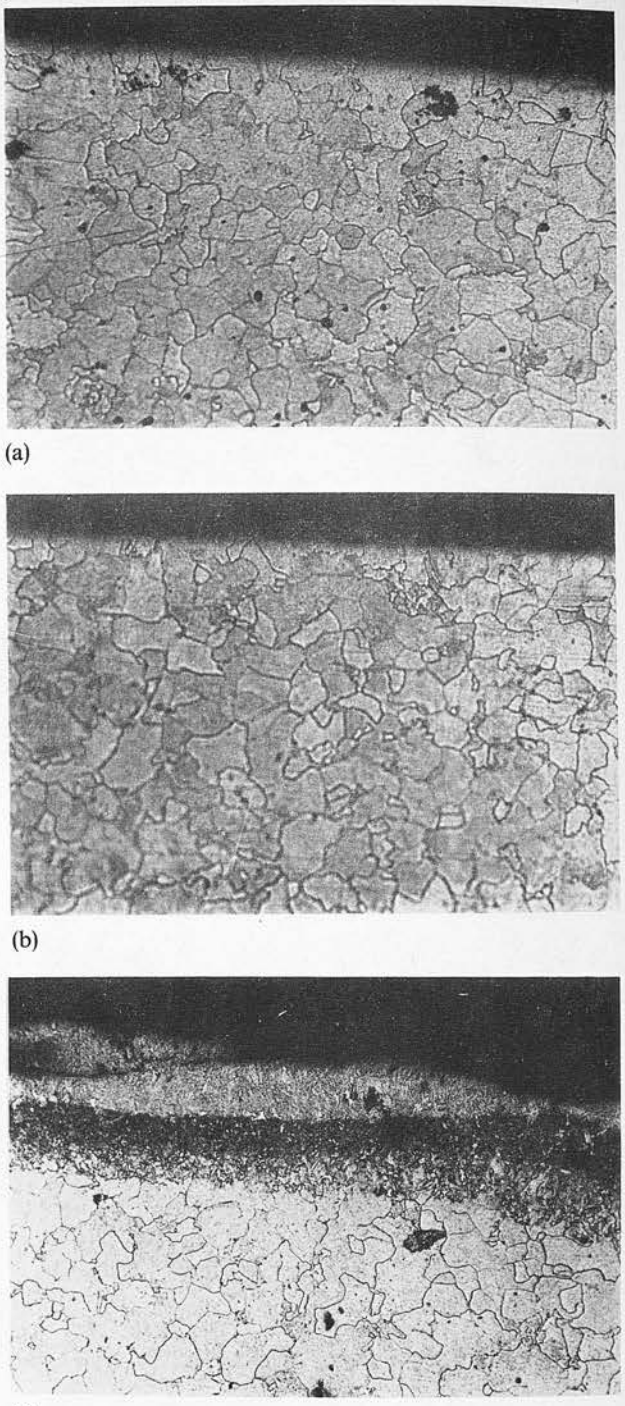

(a)

(b)

(c)

Fig. 8 Photomicrographs of polished and etched low-alloy steel specimens showing the sub-surface region along the hole: (a) near drill entry (×640), (b) middle (×640), (c) near exit (×640)

3.3 Low-alloy steel

Surface effects revealed in optical micrographs of low-alloy steel specimens in Fig. 8 show tendencies very similar to that of Jethete (low-carbon chrome steel) and Rex 535 (cobalt steel). The region near the surface along the hole exhibits no detectable signs of damage whatsoever except for the last few millimetres, where the typical EDM surface characteristics are apparent. The heat-affected zone near the exit consists of several sub-

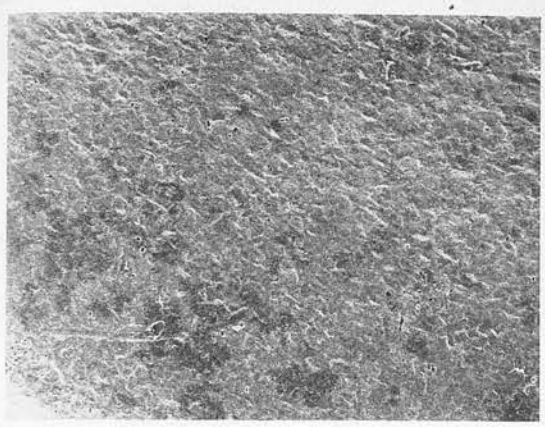

(a)

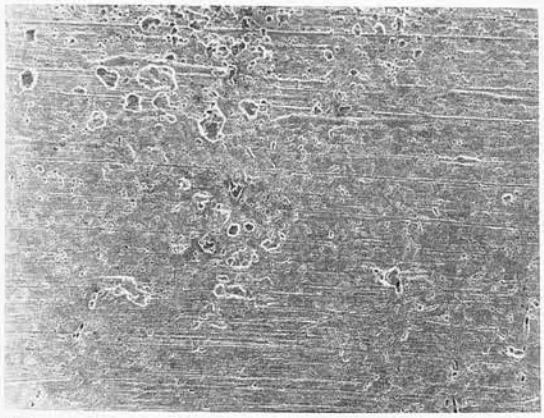

(b)

(c)

Fig. 9 Scanning electron micrographs of low-alloy steel specimens showing the drilled surface along the hole: (a) near drill entry (× 100), (b) middle (× 100), (c) near exit (× 100)

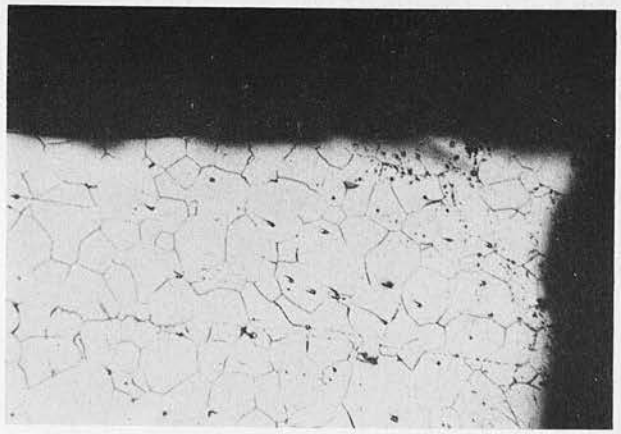

(a)

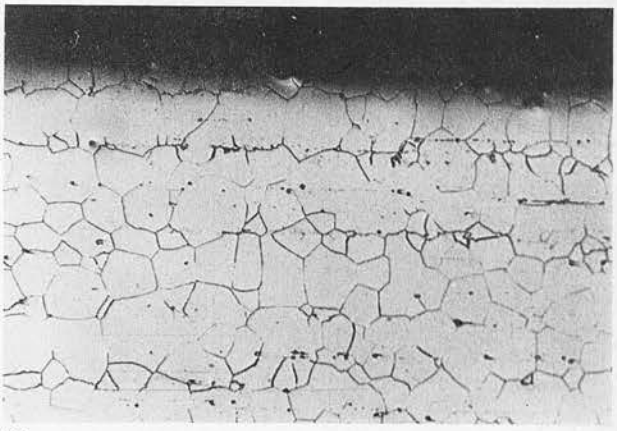

(b)

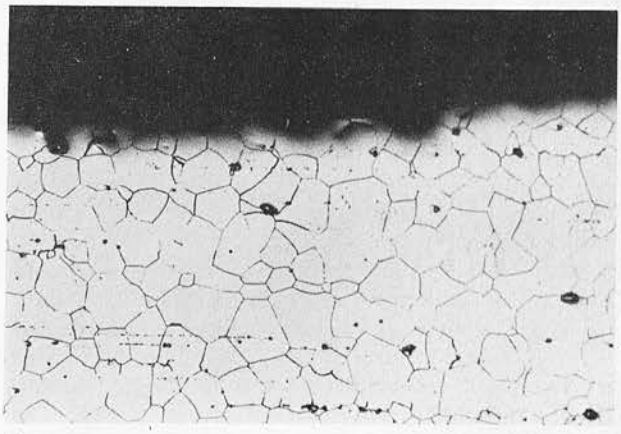

(c)

Fig. 10 Photomicrographs of polished and etched Incoloy 901 specimens showing the sub-surface region along the hole: (a) near drill entry (× 320), (b) middle (× 320), (c) near exit (× 320)

surface layers, totalling a depth of about 50 μm. The substrate appears to have a much finer grain structure than the matrix, which can be attributed to melting and rapid resolidification. There is also evidence of a dark etched band.

Scanning electron micrographs of the drilled surface in Fig. 9 substantiate the evidence that electrochemical dissolution occurring along the side gap has effectively eliminated any damage due to electric discharges along the hole except for the exit end. However, some preferential grain boundary attack was noted in some areas.

Once again, no hardened layers can be detected from the micro-hardness values in Table 3.

3.4 Nickel alloy (Incoloy 901)

As the photomicrographs in Fig. 10 show, the sub-surface region exhibits virtually no alterations except for slight undulation, along most of the hole. Neither grain recrystallization nor precipitation can be found. However, towards the exit some damage to the near-

(a)

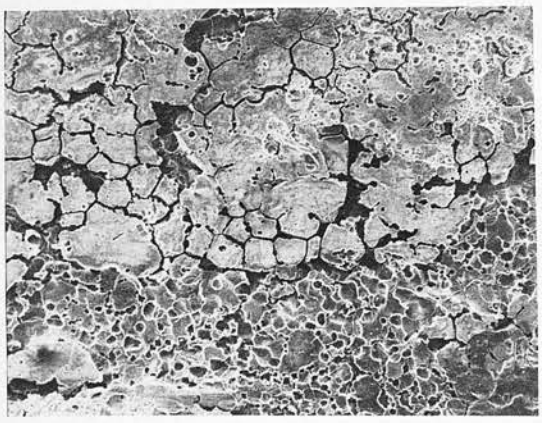

(b)

Fig. 11 Micrographs showing damage due to severe prolonged arc discharges in Incoloy 901: (a) optical micrograph showing the sub-surface region (× 320), (b) scanning electron micrograph showing the machined surface (× 100)

surface region can clearly be seen (Fig. 11). A fused-redeposited layer of about 20 μm average thickness with heavy micro-cracking was also observed. The micro-cracking has penetrated through the substrate layer to the grain boundaries thus causing grain boundary cracking. The damage was not confined to the exit end but spread almost from the middle of the hole. This form of damage can be attributed to prolonged, stationary arc discharges occurring at the side gap. The damage caused by the severity of these discharges is too intense for the electrochemical phase to 'cure'. From micro-hardness readings given in Table 3 no evidence of hardened layers can be detected.

Scanning electron micrographs of the actual surface in Fig. 12 show that preferential grain boundary attacks have occurred at some areas near the entry. At the exit, the surface appears to have typical electro-discharge-induced surface characteristics, such as melted and resolidified layers, with overlapping craters.

The undulations may be due to an enhanced crevice corrosion, possibly due to stray current attack, more than offsetting the smoothing effect usually associated with the electrochemical process. Other factors which may influence the roughness of the electrochemically machined surface include the varying dissolution rates of the different phases present.

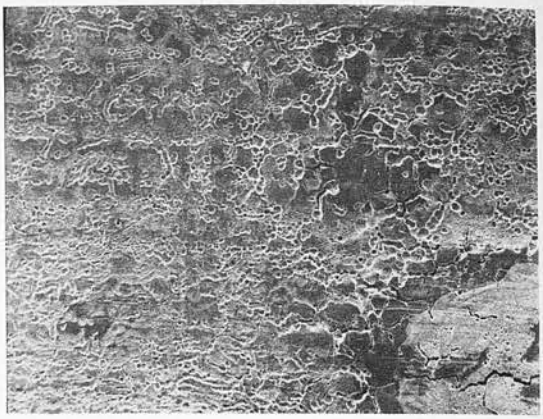

(a)

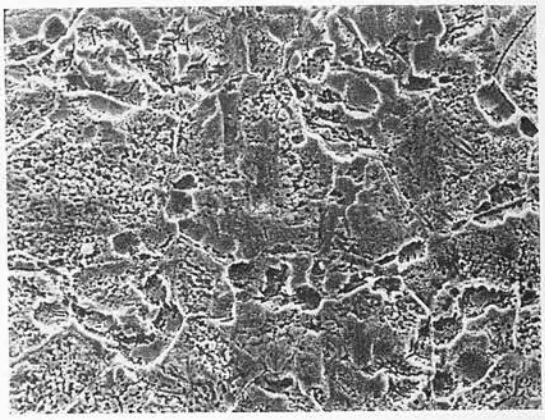

(b)

(c)

Fig. 12 Scanning electron micrographs of Incoloy 901 specimens showing the drilled surface along the hole: (a) near drill entry (× 100), (b) middle (× 500), (c) near exit (× 100)

3.5 Titanium

Unlike the other four materials, micrographs of titanium in Fig. 13 illustrate a considerable amount of damage to the surface. The damage is consistent along the entire length of the hole, whereas in the other materials it is confined only to the exit end and to the occasional localized areas where severe, prolonged discharges have occurred. An irregular spattered layer with heavy micro-cracking can be seen. The surface profile along the hole was very uneven and rough. Further evidence of irregularities can be seen in SEMs of the

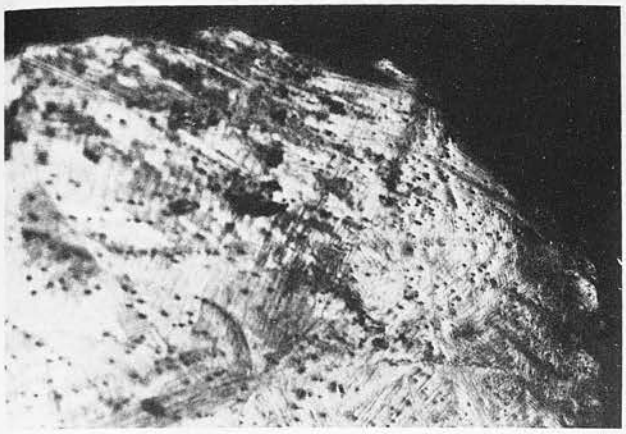

(a)

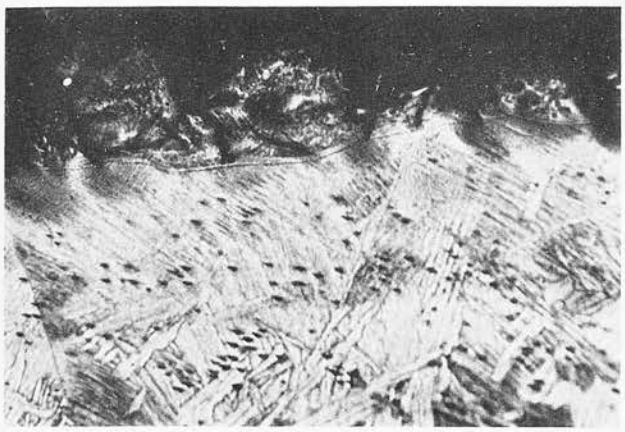

(b)

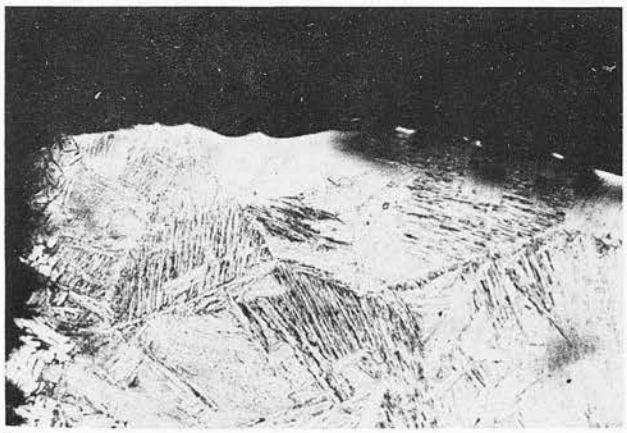

(c)

Fig. 13 Photomicrographs of polished and etched titanium specimens showing the sub-surface region along the hole: (a) near drill entry (× 320), (b) middle (× 320), (c) near exit (× 320)

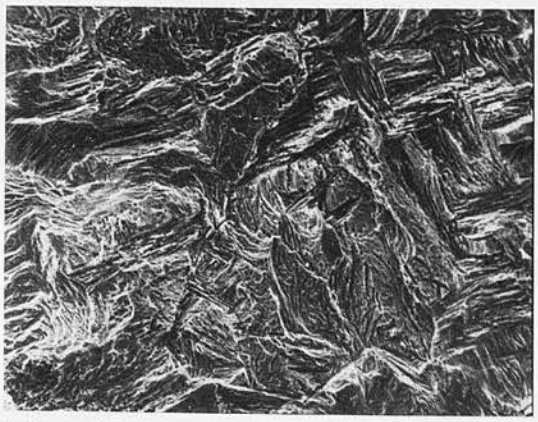

(a)

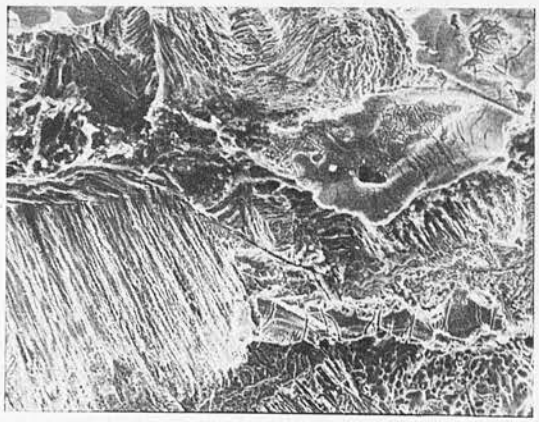

(b)

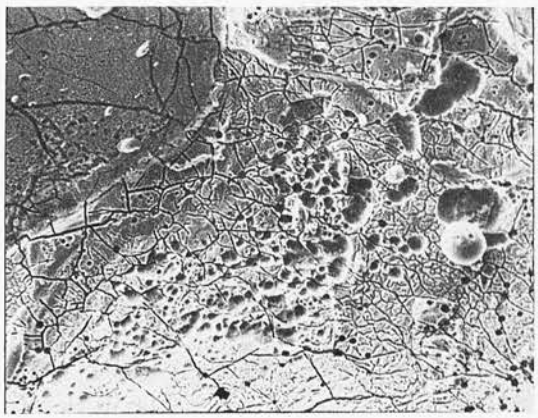

(c)

Fig. 14 Scanning electron micrographs of titanium specimens showing the drilled surface along the hole: (a) near drill entry (× 100), (b) middle (× 100), (c) near exit (× 100)

drilled surface (Fig. 14). Grain boundary cracking, overlapping craters and adhering globular particles are all apparent.

In effect, surface integrity of ECAM drilled titanium is very similar to that of EDM. A hardened layer between 100 and 250 μm depth from the drilled surface is evident from the micro-hardness readings in Table 3.

All these surface effects in titanium can be attributed to the formation of a tenacious oxide layer in water-based electrolytes, which inhibits the electrochemical dissolution of the material. This lack of ECD phase is evident from the reduced current observed. The damage caused by the erosive effect of the discharges thus remains. Successful electrochemical machining of titanium has been achieved using methanoic or formamide-based solution of electrolyte by Bannard (**11**). ECAM drilling of titanium using non-aqueous electrolytes may hence yield a better surface finish by improving the ECD at the side gap to remove the discharge-induced damage.

4 CONCLUSIONS

Microscopic and micro-hardness examinations were performed to evaluate the surface integrity of electrochemical arc drilling (ECAD) on five different metal alloys.

Optical and scanning electron microscopy revealed similar surface effects in all but titanium. Jethete (low-carbon, high-chrome steel), Rex 535 (cobalt alloy steel), Incoloy 901 (nimonic alloy) and low-alloy steel ($\frac{1}{2}$Mo–$\frac{1}{2}$Cr) exhibited a smooth ECM surface finish along most of the hole. However, there were some undesirable effects present at the exit end and also at occasional localized regions. For these four materials, the right balance of EDE to ECD has been achieved to give a smooth, damage-free surface finish without sacrificing the metal removal rate.

The damage at the exit, which is due to the lack of ECD there, can be eliminated completely by utilizing an additional metallic extension which can be discarded after the drilling operation. This would prevent the electrolyte being lost there, thus enabling the occurrence of ECD.

The damage due to severe prolonged arc discharges appeared in the form of large localized craters, microcracks and recast layers in Incoloy 901. The ECD phase was not sufficient to remove these surface effects. If these localized damaged zones were to be removed by increased ECD action, a reduction in feedrates would be necessary. This in turn would cause large tapers and overcuts giving poor dimensional accuracy. On the other hand, by preventing the formation of these abnormal discharges this type of damage could be avoided. To do this, some form of monitoring and control of the discharges are necessary. At present, an investigation into radio-frequency emission from the discharges is being carried out in order to distinguish between the 'normal' (short duration, unstable) discharges and the 'abnormal' (severe, prolonged) discharges.

The surface integrity of ECAD on titanium was very similar to that of EDM. A rough and irregular surface with heavy micro-cracking, spattered material and recast layers was observed. The surface quality of titanium could possibly be improved by using non-aqueous electrolytes, thus avoiding the formation of the tenacious oxide layer which prevents the electrochemical dissolution of the damaged layers.

Finally electrochemical arc drilling with sodium nitrate electrolyte can yield a smooth surface finish with reasonable dimensional accuracy and fast metal removal rates in most iron- and nickel-based alloys. Titanium, however, is likely to require non-aqueous electrolytes to give an acceptable surface finish.

REFERENCES

1 **Drake, T.** and **McGeough, J. A.** Aspects of drilling by electrochemical arc machining. *Proc. Machine Tool Design Conf.*, 1981, pp. 362–369 (MacMillan, London).

2 **Crookall, J. R.** and **Khor, B.** Electrodischarge machined surfaces. *Int J. Mach. Tool Des. Res.*, 1975, 373–384.

3 **Bucklow, I. A.** and **Cole, M.** Spark machining. *Metall. Rev.*, June 1969, 3(135), 103–113.

4 **Lloyd, H. K.** and **Warren, R. H.** Metallurgy of spark machined surfaces. *J. Iron Steel Inst.*, March 1965, 238–247.

5 **Platanik, L. S.** and **Levechenko, A. A.** Electro-spark machining. *Kristral-lografiya*, 1958, **3**, 613.

6 **De Barr, A. E.** and **Oliver, P. A.** *Electrochemical machining*, 1968 (MacDonald and Company, London).

7 **Bannard, J.** Fine hole drilling using electrochemical machining. *Nineteenth Int. Machine Tool Design Research Conf.*, Manchester, 1978, pp. 503–510 (MacMillan, London, 1979).

8 **Cole, R. R.** and **Hopenfeld, Y.** Investigation of electrolytic jet polishing at high current densities. ASME paper 62-WA-71, 1962

9 **Kashthejev, V. D.** Processes which control surface microroughness during ECM. *Proc. Int. Symp. for Electromachining*, June 1980, Poland, pp. 271–274 (CIRP).

10 **McGeough, J. A., Khayry, A. B.** and **Munro, W.** Theoretical and experimental investigation of the relative effects of spark erosion and electrochemical dissolution in electrochemical arc machining. *Ann. CIRP*, 1983, **32**(1), 113–118.

11 **Bannard, J. E., Treble, J. R.** and **Brook, P. A.** The electrochemical machining of titanium in non-aqueous electrolytes. *Proc. Int. Symp. for Electromachining*, June 1977, pp. 121–125 (CIRP).